VIBRATIONAL ANALYSIS OF PDC BITS IN A LABORATORY COMPLIANT DRILLSTRING

By

MOHAMMAD FARAZ MUBARAK HUSSAIN KHAN

Bachelor of Science in Mechanical Engineering

Oklahoma State University

Stillwater, Oklahoma

December, 2020

Submitted to the Faculty of the
Graduate College of the
Oklahoma State University
in partial fulfillment of
the requirements for
the Degree of
MASTER OF SCIENCE
December, 2022

VIBRATIONAL ANALYSIS OF PDC BITS IN A

LABORATORY COMPLIANT DRILLSTRING

Thesis Approved:

Dr. Mohammed F. Al Dushaishi

Thesis Adviser

Dr. Prem Bikkina

Dr. Hunjoo Lee

ACKNOWLEDGEMENTS

I first want to thank my committee members and professors, beginning with my advisor, Dr. Mohammed Al Dushaishi. As well as Dr. Prem Bikkina and Dr. Hunjoo Lee. I would also like to thank my parents for their continued support.

I would like to thank the U.S. Department of Energy, Office of Energy Efficiency & Renewable Energy, under Award Number EE0008603, for supporting this research. I also wish to thank Sandia National Laboratories for allowing the testing to be performed at their Hard Rock Drilling Facility.

Name: MOHAMMAD FARAZ MUBARAK HUSSAIN KHAN

Date of Degree: DECEMBER, 2022

Title of Study: VIBRATIONAL ANALYSIS OF PDC BITS IN A LABORATORY COMPLIANT DRILLSTRING

Major Field: PETROLEUM ENGINEERING

Abstract: Excessive vibrations during drilling operations can shorten the life of downhole equipment and instruments. One of the major contributors to drilling vibrations is bit-rock interaction. Therefore, controlling drillstring vibrations increases the range of drilling operating parameters to maintain a safe drilling operation. The goal of the research is to study the effect of drillstring vibration on drill bit dynamics and to estimate the frictional parameters of various bit-rock interaction models using laboratory testing data. In collaboration with Sandia National Laboratory (SNL), drilling tests in a controlled laboratory environment with multiple drillstring configurations mimicking field drillstring vibrations were performed at the Hard Rock Drilling Facility (HRDF). The rigid configuration was used as a base case to compare the effect of drillstring vibration on drill bit dynamics. The various drillstring configurations were investigated using two 3¾ inches of Polycrystalline Diamond Compact (PDC) bits with 4 and 5-blade designs. Drilling tests were conducted at 500 lb axial load increments up to 5500 lb at three constant rotating speeds of 80, 120, and 160 RPM. The results showed that the flywheel configuration provides a stable torque to the bit, while the torsional compliance configuration produced less torque at the same weight on bit (WOB) compared to the rigid configuration for the 4-bladed bit. The axial compliance configuration increases the WOB variation. The combined axial torsional compliance configuration showed increased fluctuation in WOB, rotational speed, and applied torque. Overall, traditional rigid drillstring experiments overestimate drilling vibrations frequencies by an average of 26.3% in the axial direction and 35% in the torsional direction when compared to the combined axial and torsional compliance for both bit designs. The use of the 5-bladed PDC bit in hard rock reduces axial vibrations by 53.7% in the axial direction and 14.2% in the torsional direction. The drilling test data were compared with one coupled axial and torsional bit-rock interaction model, and three uncoupled torsional bit-rock interaction models to perform a sensitivity analysis and determine the frictional constants for the testing data. The sensitivity of models showed difficulties in predicting actual laboratory conditions where such models are highly dependent on the frictional constants which are difficult to obtain for a certain drilling condition.

TABLE OF CONTENTS

LIST OF TABLES

LIST OF FIGURES

CHAPTER I

1 INTRODUCTION

Drilling is one of the many challenges faced in geothermal drilling and is among the most expensive and dangerous processes in the discovery and development of geothermal reservoirs. Drilling expenses are increased when drilling components, particularly the drillstring, break prematurely. Drillstring failures are often caused by severe vibration waves traveling through the drillstring. Drillstring vibrations have been linked to many sources such as bottom hole assembly (BHA) design, the formation being drilled, trajectory, geometry, drilling mud, and drilling rig equipment (Ritto et al., 2017). Understanding the main source of drillstring vibration provides mitigation strategies to avoid severe vibrations and optimize drilling efficiency. Polycrystalline Diamond Compact (PDC) bits have become more popular because of their high Rate of Penetration (ROP) and drillability (Hareland et al., 2009). PDC bits, however, have a poor track record in hard formations such as those seen in geothermal applications which encounter server drillstring vibrations. Drillstring is subjected to three types of vibrations during drilling, namely axial which causes bit bounce, torsional vibration which may cause stick-slip, and lateral vibration that could produce whirl (Figure 1.1)

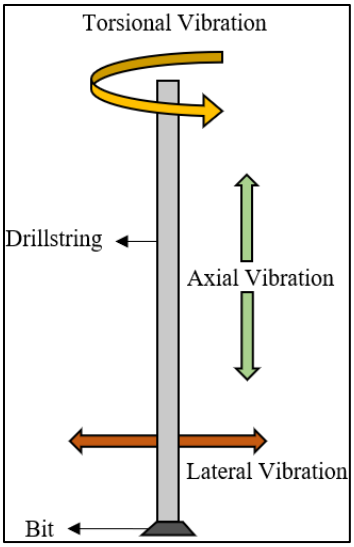

Figure 1.1. Drillstring Vibration Modes

While drilling, the drillstring is subjected to axial, torsional, and lateral vibrations simultaneously, however, one mode will be more dominate. The longitudinal mode is reported to be responsible for 75 percent of drillstring failures among the principal types of vibration (Kriesels et al., 1999; Sotomayor et al., 1997). Bit bounce is considered to be the most severe kind of axial vibration which is caused by the bit–rock contact in which the bit loses contact with the formation. During bit bounce, the downhole weight on bit (WOB) goes to zero for a brief time interval, and later the bit strikes the formation with a WOB value higher than the provided surface WOB, this occurs generally as a result of axial resonance. Axial vibration is the most prevalent type of vibration in vertical wells whilst drilling hard rocks and can be felt at the surface using roller cone bits (Katz & Chilingarian, 1996). Axial vibration and bit bounce can lead to accelerated cutting teeth wear, loss of cutters, accelerated bearing failure, MWD tool failures, and a decrease in ROP (Ashley et al., 2001; Li & Guo, 2007).

Drillstring lateral vibration creates considerable high frequency bending moments, such as lateral vibrations due to mud motor imbalance (Zhu & Liu, 2013). Imbalance mass is a common vibration excitation mechanism that can lead to lateral resonance and have a significant influence on tool life, causing fatigue failure of BHA components, wellbore washout, and stabilizer wear (Zhu &

Liu, 2013). When PDC bits are employed, self-excitation is mostly induced by the bit-rock contact and primarily stimulates torsional oscillations. There are two forms of frequency-induced whirling: forward whirl and backward whirl during drillstring rotation. Forward whirl occurs when the rotation of the deflected drillstring around the borehole axis is in the same direction as the applied rotation (Leine et al., 2002). A backward whirl occurs when the drill collars roll backward over the borehole wall in the opposite direction of rotation. Because of wellbore contact, whirling modes are activated, allowing an over-gauge hole to be drilled in low-strength rocks (Leine et al., 2002).

Torsion vibration is one of the most common and harmful types of vibration (Ritto et al., 2017), which is known as stick-slip in its most extreme form. It can cause catastrophic failures in BHA components, rotary steerable systems, measuring while drilling and logging while drilling equipment (MWD/LWD). Stick-slip can drastically raise drilling costs because downhole vibration can dramatically reduce the rate of penetration (ROP).

For many years, it has been well-understood that self-excitation at the bottom induces friction-generated vibration. The study of drillstring stick-slip vibration may be traced back to Belokobyl'skii and Prokopov (1982). The drillstring may be subjected to significant levels of torsional vibrations due to its poor torsional rigidity and the contemporaneous torques applied at the top and bottom extremities (Brett, 1992).

Understanding stick-slip sources, forecasting their creation, and knowing how to suppress them are critical. A variety of strategies have been suggested to reduce the drillstring stick-slip vibration. It is difficult to conclude that one strategy is better than the others because each has advantages in certain drilling conditions. Stick-slip behavior is often measured using rotational speed since the accompanying tangential acceleration measurements are relatively low due to the low frequency associated with stick-slip (Hohl et al., 2020). The ideal operating condition was found to minimize the mean deviation of the drill-bit angular velocity compared to the target one. Furthermore, the incorporation of a controlled dynamic WOB was recommended, resulting in lower levels of mean

deviation of angular velocity and, as a result, improved drilling stability zones (Monteiro & Trindade, 2017).

According to numerical models, the frequency of stick-slip and the severity of bit bounce are decreasing in lockstep with the applied rotational speed and WOB. As a result, increasing these two settings helps in reducing stick-slip and bit bounce during practical drilling (Kamel & Yigit, 2014). It has been experimentally observed that the drop in resultant torque with rotational velocity is a manifestation of the system reaction, rather than an inherent rate dependency of the interface laws between the rock and the drill bit, as is often supposed (Richard et al., 2007).

The drillstring may also experience lateral (bending) and axial (longitudinal) vibrations, depending on the operational circumstances (Spanos et al., 2003). These vibrations are intimately coupled together and can occur simultaneously. The excessive bit wear caused by lateral and torsional motion can affect ROP and lead to bit bounce (Aldred & Sheppard, 1992).

The scope of this research is centered around the drill bit dynamics and its interaction with the formation rock. Specifically, this work is aimed at understanding the effect of drillstring vibration on drill bit dynamics and understanding the physical law of bit-rock interaction during drilling with PDC bits.

CHAPTER II

2 LITERATURE REVIEW

The bottomhole assembly (BHA) design and the numerous forces acting on the drillstring such as drillstring contact with the wellbore wall and drill bit interaction with the formation rock, make drillstring vibrations complicated. Such elements have an impact on drilling performance, notably drill bit contact, which is determined by bit design and formation lithology as a result, modeling bit-rock interaction is critical for gaining a better understanding of how vibrations react to various bit designs and drillstring operational parameters. The following study of the literature explores prior laboratory research addressing compliant and noncompliant drillstring testing, drillstring vibration, and its influence including bit-rock interaction modeling.

2.1 Laboratory Evaluation of Drillstring and Drill Bits

Laboratory experiments addressing drillstring and drill bit designs are common methods to evaluate bit performance and the effect of drillstring vibrations. Commonly, laboratory evaluation of drill bits neglects the effect of drillstring vibrations and if considered, only drilling-induced vibrations are analyzed without considering the drillstring effect. For instance, Glowka (1987) used single cutters experimental setup to develop a model to estimate PDC wear based on cutting forces, critical cutter temperature, and PDC cutter wear status. By introducing a low-pressure cell, Garcia-Gavito and Azar (1994) simulated field drillstring conditions in a laboratory setting (Figure 2.1). The experimental investigation examined the impact of PDC bit design characteristics on the dynamic

pressure distribution at the bit-rock interface on a cement rock sample utilizing 6 ¾ inches and 8 ½ inches PDC bits.

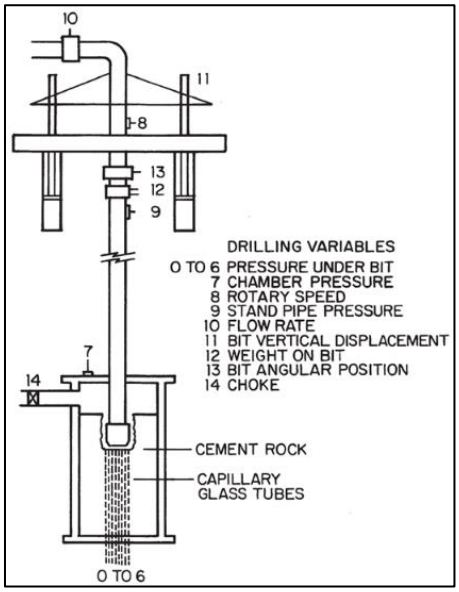

Figure 2.1. Schematic Illustration of Drilling Setup (Garcia-Gavito & Azar, 1994)

In a more recent study, Miyazaki et al. (2019) evaluated PDC bit performance in geothermal applications that focuses on PDC bit wear. Their laboratory testing facility (Figure 2.2) was capable of testing large PDC bits with a diameter of 6.25 inches. The bit consisted of 10 nozzles and 8 blades with a total of 42 cutters, drilling through three types of andesite rocks and one granite type. The wear progress of PDC cutters was quantitatively monitored and shown to be related to several rock abrasivity indicators. Their study showed that PDC cutter wear is highly affected by the rock unconfined compressive strength (UCS).

Figure 2.2. Laboratory Drillstring Overview (Miyazaki et al., 2019)

Due to the dynamic complexity of drillstring vibrations, laboratory scale investigations provide an economical and efficient controlled environment for studying drillstring vibrations. Extensive laboratory scale investigations were performed previously to address specific drillstring phenomena. Srivastava and Teodoriu (2019) performed a literature review addressing laboratory scale drillstring vibration experiments and outlining the different approaches that have been used for such investigations. Due to the difficulties of replicating all drillstring vibration phenomena seen in the field on a laboratory scale, drillstring vibration experiments are built to investigate one or two specific vibration phenomena. For example, Kapitaniak et al. (2018) used a laboratory-scale experiment to investigate the drillstring forward and backward whirls. Their drilling rig consisted of a flexible shaft to simulate the drillstring dynamics and the whirling motion as seen in Figure 2.3. Their experimental investigation included a commercial PDC bit to simulate the bit-rock interaction. Besides replicating forward and backward whirl motion on a laboratory scale,

Kapitaniak et al. (2018) investigated the effect of rotational speed on the co-existence of forward and backward BHA whirl which was used to calibrate a model.

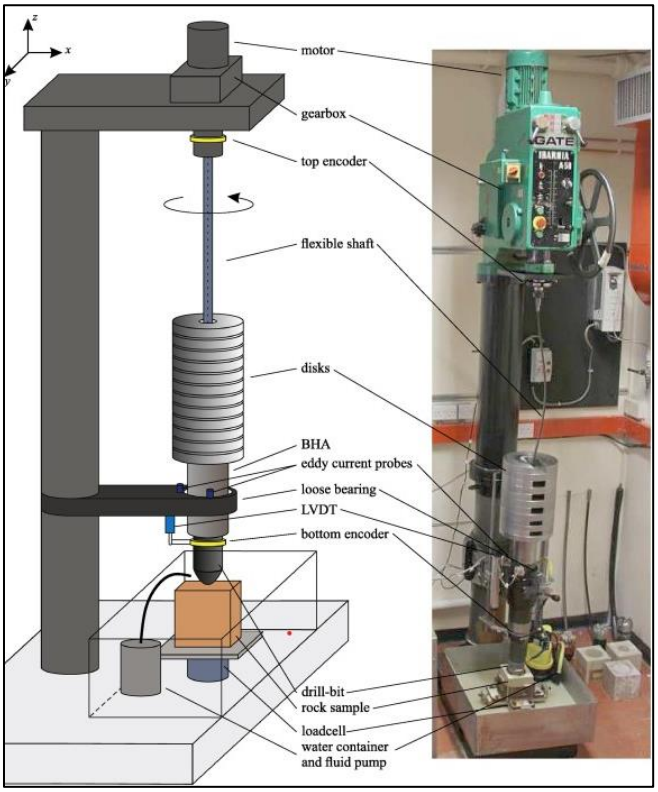

Figure 2.3. Schematic and Pictorial Laboratory Drillstring Design (Kapitaniak et al., 2018)

In previous work using the same experimental setup as Kapitaniak et al. (2018), Wiercigroch et al. (2017) replaced the flexible shaft with a rigid shaft to investigate the bit-rock interaction, i.e., coupled axial and torsional vibrations. They developed a bit interaction model based on state-dependent delay interaction for nonuniform PDC bits. Their experimental results showed the torque on bit (TOB) decreases as the rotational speed increases up to a certain thrust hold value, where TOB starts to increase beyond this point.

Using the mechanical similarity method, Westermann et al. (2015) developed a laboratory-scale drillstring setup (Figure 2.4) to reproduce torsional and lateral vibration on a laboratory drillstring setup. A torsional spring is used to simulate the torsional rigidity of the drill pipes, while the shaft is compressed with an axial force that corresponds to the applied WOB. The goal of this research

is to compare the new laboratory-scaled rig to previous test rigs and identify variations in the vibration while measuring contact forces.

Figure 2.4. Scaled Laboratory Rig (Westermann et al., 2015)

Investigations of drillstring vibrations on a laboratory scale require compliance mechanisms to compensate for drillstring slenderness in the field. A facility that incorporates drillstring compliance while still allowing for genuine bit-rock interaction would give a sophisticated, practical knowledge of the impact of drillstring dynamics on bit life and performance. Elsayed and Raymond (1999) developed a compliant laboratory drillstring setup equipped with a PDC bit to investigate PDC bit chatter. To introduce compliance in the axial direction, a set of springs were used between the hydraulic cylinders and the strengthened beam. The drillstring is coupled to the drive motor through two counter-wound power springs, resulting in rotational compliance similar to that of a field drillstring. Compression springs are also used to support the drillstring in the longitudinal direction. This design generates a spring-mass system that simulates drillstring field conditions. The study demonstrates that including compliance in laboratory testing settings improves the replication of actual field conditions. It has been demonstrated using such a method, bit chatter may be severe and particularly damaging to cutters in harder rock such as Sierra white granite (Elsayed & Raymond, 1999). Elsayed and Raymond (2002), found that at lower speeds and higher WOB, the effect of stick-slip can be noticed. It is also observed that torsional compliance is seen as side bands in the axial frequency spectrum at reduced WOB intervals. The presence of these

sidebands is caused by a combination of frequency and amplitude modulation. At higher WOB, axial vibrations are limited due to the fact that the drillstring is constrained in both axial and torsional directions which makes the drillstring torsionally rigid because of the reduced impact of torsional compliance on axial vibrations. Raymond et al. (2005) quantified the influence of axial and torsional compliances on drillstring stability in a laboratory-scaled setup. The setup consisted of a hydraulic motor that rotates a short drillstring with a 3.25-inch diameter coring bit. The findings indicate that an adjustable damper has been shown to improve the stability of PDC bits in hard rock such as geothermal deposits.

Another study conducted by Raymond et al. (2008), was to correctly mimic the dynamic motion of the drillstring in a controlled laboratory setting so that the bit response could be examined before field drilling operations. The drillstring laboratory setting consisted of a mechanical analog approach and a model-based approach (Figure 2.5). Simulations using model-based control have shown to be capable of generating realistic drill bit dynamics in the laboratory, outperforming simulations with basic mechanical analogs.

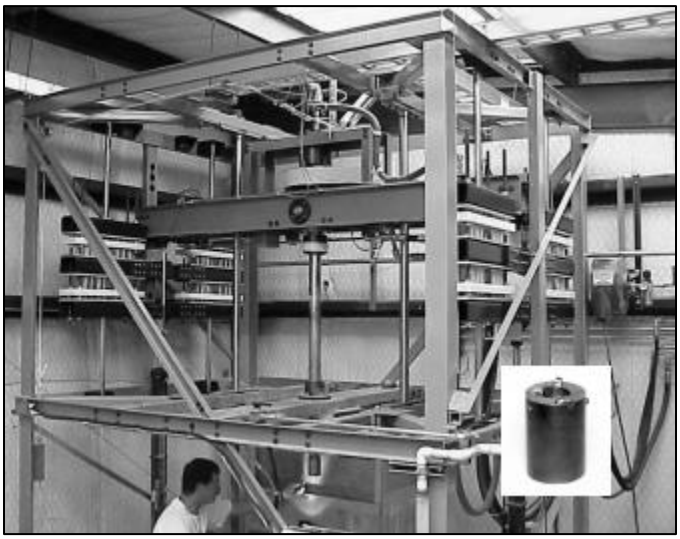

Figure 2.5. SNL Mechanical Analog Drillstring (Raymond et al., 2008)

2.2 Bit-Rock Interaction Modelling

Vibration modeling of the drillstring is required for predicting troublesome vibration patterns and creating mitigation methods. Drillstring vibration models have progressed over time from simple static models to complex dynamic models for predicting drillstring movements downhole. The reaction of the rotary drilling machine is greatly influenced by the bit-rock interaction model (Mendil et al., 2021). Early studies focused on the excitation mechanisms of several types of vibrations. All models are constrained by certain assumptions and simplifications due to the intricacy of the drillstring and its interactions with its surroundings

One of the major contributors to drillstring vibrations is the bit-rock interaction. In drillstring vibrations, the bit-rock interaction is treated as an external force or boundary condition at the end of the bit. The main reason for modeling the bit-rock interaction is to model or simulate the stick-slip vibrations seen while drilling to establish a safe drilling operating window. Other phenomena can occur at the bit including bit-bounce where several models were established to simulate such events (Yigit & Christoforou, 2006).

The drillstring dynamic motion can be modeled using lumped mass parameter approach, where the equation of motion in the torsional direction may be written as (Yigit & Christoforou, 2000):

$$J\ddot{\phi} + c_v\dot{\phi} + K_T\left(\phi - \dot{\phi}_{rt} \times t\right) = -TOB \qquad (1)$$

where J represents the drillstring mass moment of inertia in $\mathrm{kg.m^2}$, c_v is the viscous damping coefficient ($\mathrm{N.m.s}$) and K_T is the torsional stiffness in $\mathrm{N.m/rad}$. The torque on bit (TOB) is the bit-rock interaction force, which depending on the modeling assumption might be coupled with axial displacement or uncoupled as a function of angular velocity and displacement. Using the lumped parameters approach, the equation of motion of the drillstring axial vibration is:

$$m_a\ddot{x} + c_a\dot{x} + k_a x = F_a \qquad (2)$$

where m_a is the effective drillstring mass in kg, c_a is the axial effective damping in $\mathrm{N.s/m}$, and k_a axial effective stiffness having a unit of $\mathrm{N/m}$. The effective drillstring mass accounts for the drillstring and drilling fluid masses. The axial force F_a accounts for the static applied axial load and the dynamic WOB variation due to drilling written as:

$$F_a = F_0 - WOB \tag{3}$$

where the static load F_0 is defined in terms of the drillstring weight and the applied hook load, $F_0 = W_{ds} - HL$ where W_{ds} is the weight of the drillstring and HL is the hook load.

2.2.1 Uncoupled bit-rock interaction models

Some of the early work addressing stick-slip with simplified bit-rock interaction (BRI) was using a single torsional vibration model with assumed Coulomb friction for the drag torque (Belokobyl'skii & Prokopov, 1982). Navarro-López and Cortés (2007); Navarro-Lopez and Suarez (2004) investigated the effect of self-excited stick-slip and the effect of operating parameters during sliding motion using a variation of the Stribeck and dry friction model. The total torque on bit (TOB), $T_b(\mathrm{x})$ in Equation 4, was represented by the summation of the frictional bit-rock interaction torque $\mathrm{T_{fb}}$ and viscous damping torque $\mathrm{T_{ab}}$ associated with bit contact with the formation.

$$\mathrm{TOB} = T_{ab}(\omega_b) + T_{fb}(x) \tag{4}$$

The term x is the system state vector. The viscous damping torque is defined as $T_{ab} = c_b \times \omega_b$. The frictional BRI torque was defined as a piecewise function accounting for stick, sliding, and transition between stick to slip mode written as:

$$T_{fb}(x) = \begin{cases} T_{eb}(x), & if\ |\dot{\varphi}| < D_v, |T_{eb}| \le T_{sb}\ (stick), \\ T_{sb} sgn\big(T_{eb}(x)\big), & if\ |\dot{\varphi}| < D_v, |T_{eb}| > T_{sb}\ (stick-slip), \\ f_b(\omega_b) sgn(\omega_b), & if\ |\dot{\varphi}| \ge D_v\ (sliding) \end{cases} \tag{5}$$

where $\mathrm{D_v}$ has a value larger than 0 and represents the zero-velocity band, $\mathrm{T_{eb}}$ is the required static reaction torque to move the bit, $\mathrm{T_{sb}}$ is the drilling torque defined in terms of static friction μ_{sb}, bit radius $\mathrm{R_b}$, and applied WOB as:

$$T_{sb} = \mu_{sb} \times WOB \times R_b \quad (6)$$

For the sliding mode, a combination of static and Coulomb friction was adopted with a velocity decaying function in the form of:

$$f_b(\omega_b) = R_b \times WOB \times \mu_b(\omega_b) \quad (7)$$

where μ_b is defined as dry friction given by,

$$\mu_b = [\mu_{cb} + (\mu_{sb} - \mu_{cb})e^{-\frac{\gamma_b}{\upsilon_f|\omega_b|}}] \quad (8)$$

In the above equation, γ_b is the friction model parameter and υ_f is a velocity constant with a value of 1 used for unit consistency. The required static reaction torque to move the bit is defined as a function of the bit and drillstring motion following:

$$T_{eb}(x) = c_t(\omega_r - \omega_b) + k_t(\varphi_r - \varphi_b) - T_{ab}(\omega_b) \quad (9)$$

Navarro-López and Cortés (2007) BRI model requires several constants such as the velocity band D_v and friction model parameter γ_b where no elaboration on how to obtain these constants for field applications.

A similar BRI formulation was proposed by Huang et al. (2018), with similar friction torque as (Navarro-López & Cortés, 2007) for PDC bits, where the only difference in Navarro-López and Hunags model is the cutting process in the TOB equation. The TOB equation of Huang et al. (2018) model is shown in Equation 10, where T_{fb} is the friction contact defined in Navarro-López and Cortés (2007) model (Equation 6).

$$T_b = T_{bc} + T_{fb} \quad (10)$$

The torque due to the cutting action in terms of the intrinsic specific energy of rock ϵ was defined as:

$$T_{bc} = \frac{1}{2} \times \epsilon \times \bar{R}_b^2 \times n \times d \quad (11)$$

where *n* is the number of blades of the PDC bit, d is the depth of cut and $\bar{\mathrm{R}}_b$ is the equivalent radius of the PDC bit given by:

$$\bar{\mathrm{R}}_b = \int_0^{R_b} \frac{2\pi r}{\pi R_b^2} \times r \times dr = \frac{2}{3} \times R_b \tag{12}$$

Sampaio et al. (2007) developed a different uncoupled bit-rock interaction model (Equation 13), where the TOB is defined as a function of the applied rotational speed ω_{bit}, bit cutting characteristics μ_{bit}, and rock property constants α_1, and α_2.

$$\mathrm{TOB} = \mu_{\mathrm{bit}} \times WOB \left(\tanh\left(\omega_{\mathrm{b}}\right) + \frac{\alpha_1\, \omega_{\mathrm{bit}}}{1 + \alpha_2\, \omega_{\mathrm{bit}}^2} \right) \tag{13}$$

A comparison of three different bit-rock interaction models was presented by Mendil et al. (2021). The results showed that the Stribeck model (Equation 14) has considerably increased system dependability which gives a better estimate of the dynamic of the field conditions.

$$\mathrm{TOB} = \mathrm{T}\frac{2}{\pi}\left(\alpha_1 \mathrm{x}_3 \mathrm{e}^{-\alpha_2 |x_3|} + \tan^{-1}(\alpha_3 x_3)\right) \tag{14}$$

In the above equation, α_i, x_i are friction parameters, and T is the torque provided by the top drive.

Manzatto and Trindade (2011) used a similar BRI model as in Navarro-López and Cortés (2007), where the torque on bit was defined as a piecewise function following:

$$TOB = T, \qquad |\omega_b| \leq \delta\ e, |T| \leq a_2 F_b; \tag{15}$$

$$TOB = a_2 WOB \times sign(T), \qquad |\omega_b| \leq \delta\ e, |T| > a_2 F_b; \tag{16}$$

$$TOB = [a_1 + a_2 - a_1) e^{-\beta|\omega_b|}] WOB \times sign(\omega_b), \ \ |\omega_b| > \delta. \tag{17}$$

Equation 17 is the condition when the drilling operation is in the stick phase, T is the applied torque and $a_1, a_2\ and\ \beta$ are the friction model parameters, and δ represents the zero-velocity band to balance the units which have a value greater than 0.

2.2.2 Coupled bit-rock interaction models

Bit stability due to induced torsional and lateral vibrations using a linear stability approach was addressed by Dunayevsky and Abbassian (1998). The BRI for the torsional mode, i.e., torque, was modeled as a function of applied WOB, bit constants f_0 and f_1, and an exponentially decaying parameter γ (Equation 18). The coupling between the torsional and lateral modes was achieved using a bit side force, which is a function of bit speed and motion.

$$TOB = WOB \times (f_0 + f_1 \times e^{\gamma \times \omega_b}) \tag{18}$$

Christoforou and Yigit (2003) defined the bit rock interaction as a function of WOB and cutting conditions. The cutting process includes the cutting action and friction between the bit and the formation:

$$\mathrm{TOB} = \mathrm{WOB} \times \left[\mu f(\omega_b) + \zeta \sqrt{\mathrm{R_b} \times DOC}\right] \tag{19}$$

where μ and ζ are constants for the friction process and the cutting process at the bit. The dynamic WOB is a piece-wise function consisting of contact stiffness k_c and formation surface elevation *s* during contact given by,

$$WOB = \begin{cases} k_c(x - s) & if\ x \geq s, \\ 0 & if\ x < s, \end{cases} \tag{20}$$

There are no developed or refined procedures for obtaining these constants for field case studies. The formation surface elevation is modeled as a sinusoidal function according $s = s_0 sin(n_b \phi)$. Where n_b is the bit factor and ϕ is the drill collar angular displacement in radians. The depth of cut (DOC) is defined as a function of ROP and average bit speed in radians/ per second as:

$$\mathrm{DOC} = \frac{2\pi ROP}{\omega_b} \tag{21}$$

where ROP is a function of applied WOB given by,

$$ROP = c_1 \times \mathrm{WOB} \times \sqrt{\omega_b} + c_2 \tag{22}$$

Where $f(\omega_b)$ is a continuous function used to represent the effect of bit speed on TOB as shown below,

$$f(\omega_b) = tanh(\omega_b) + \frac{\alpha_1 \omega_b}{1 + \alpha_2 {\omega_b}^2} \tag{23}$$

Where α_1 and α_2 are friction model parameters. There are no methods derived or elaborated on how to obtain these constants for field cases (Christoforou & Yigit, 2003; Yigit & Christoforou, 2006).

Yigit and Christoforou (2006) used a similar model for the BRI, the difference can be seen in the TOB equation, where a continuous function was used to represent the effect of bit speed on TOB.

$$\mathrm{TOB} = WOB \times R_b \left(\mu(\omega_b) + \xi \sqrt{\frac{\mathrm{R_b}}{\mathrm{DOC}}} \right) \tag{24}$$

$$\mu(\omega_b) = \mu_0 (tanh\phi + \frac{\alpha \omega_b}{1 + \beta {\omega_b}^{2\gamma}} + \nu \omega_b) \tag{25}$$

Where μ_0, α, β, γ, ξ and ν are all friction model parameters and no methods were derived or elaborated on to obtain these constants for field cases.

Yigit and Christoforou (1998) defined the BRI forces as a function of the drill collar angular speed (ω_b), a bit factor n which depends on the type of bit being used. The TOB and WOB were as:

$$TOB = T_0 + T_f \sin n\phi f(\omega_b) \tag{26}$$

$$WOB = F_0 + F_f \sin n\phi \tag{27}$$

The subscripts 0 and f signify the mean and amplitude values for the TOB and WOB respectively. Later, Yigit and Christoforou (2000) modified the equation to include a continuous function $f(\omega_b)$ which is used to represent the effect of bit speed on TOB as follows,

$$TOB = (T_0 + T_f \sin n\phi) f(\omega_b) \tag{28}$$

Aarsnes and Van De Wouw (2019) represented their BRI model, for the coupled axial-torsional model, in terms of friction and cutting components, where the axial force seen at the bit was modeled as:

$$\omega_b = R_b \zeta \varepsilon N \times DOC + w_f g(v_b) \tag{29}$$

The first term in Equation 29, $R_b \zeta \varepsilon N \times DOC$ represents the cutting force with ε being the intrinsic specific energy, N is the number of cutter blades, v_b is the axial bit velocity, ζ is the cutter sharpness coefficient. The second term represents the wear flat force component, where w_f is the normal force that must be overcome before axial cutting can begin. The non-linear term $g(v_b)$ is given as,

$$g(v_b) = \frac{1 - Sign(v_b)}{2} = \begin{cases} 0, & v_b < 0 \\ [0,1], & v_b = 0 \\ 1, & v_b > 0 \end{cases} \tag{30}$$

The TOB is given by,

$$T_b = R_b^2 \varepsilon N \times DOC + T_f \tilde{g}(\omega_b) \tag{31}$$

Where $\tilde{g}(w_b)$ is the torsional stick force if the force delivered to the bit by the drill string is insufficient to counteract the torque caused by the bit-rock interaction, if it exceeds that torque-on-bit, the bit begins to slide torsionally.

Leine et al. (2002) developed a coupled torsional-lateral model, where the TOB was defined as:

$$\text{TOB} = -\frac{sgn\phi \times \text{T}}{1 + \delta|\omega_b|} \tag{32}$$

The TOB on the bit-rock interaction model by Tucker and Wang (2003) was defined as a function of bit axial velocity, depth of cut, and WOB as shown below,

$$\text{TOB} = \text{a}_4 DOC + a_5, DOC = \frac{ROP}{\Omega}, ROP = -a_1 + a_2 WOB + a_3 RPM \tag{33}$$

Where a_1, a_2, a_3, a_4, and a_5 are friction constants where no elaboration on how to obtain these constants for field cases. This relationship can be combined and the TOB can be directly expressed in terms of bit angular velocity and WOB as,

$$\text{TOB} = \frac{(-a_1 + a_2 WOB)a_4}{RPM} + a_3 a_4 + a_5 \tag{34}$$

Ritto et al. (2009) used a similar model to Tucker and Wang (2003) with the addition of a regularization function (Equation 35-36). The regularization function is used to describe Coulomb's frictional effects, where the frictional torque and rate of penetration are regularized so that they diminish when the drill-bit rotational velocity approaches zero from both positive and negative values.

$$\text{WOB} = -\frac{ROP}{a_2 Z(\omega_b)^2} + \frac{a_3 \omega_b}{a_2 Z(\omega_b)} - \frac{a_1}{a_2} \tag{35}$$

$$\text{TOB} = -\frac{ROP a_4 Z(\omega_b)^2}{\omega_b} + a_5 Z(\omega_b) \tag{36}$$

The regularization function is denoted by $Z(\omega_b) = \omega_b / \sqrt{(\omega_b)^2 + e^2}$. In a different study, Trindade and Sampaio (2005) treated the regularization of TOB using a nonlinear equation, as shown in Equation (37)

$$TOB = (-a_1 + a_2 WOB)a_4 \frac{\text{RPM}^3}{(RPM^2 + \epsilon^2)^2} + a_3 a_4 \frac{RPM^3}{(RPM^2 + \epsilon^2)^{\frac{3}{2}}} + a_5 \frac{RPM}{(RPM^2 + \epsilon^2)^{\frac{1}{2}}} \tag{37}$$

Here, the coulomb friction is represented by ϵ. Based on the model formulation, the model is characterized by uncoupled rather than coupled as mentioned by the author.

Richard et al. (2004) define the bit-rock interaction in terms of cutting and friction components. The TOB model was defined as the sum of cutting and frictional processes, the same goes for WOB

given as, $T = T_c + T_f$ and $W = W_c + W_f$. The cutting process occurs in front of each blade, and a frictional process occurs along the worn flats are defined as follows,

$$T_c = \frac{R_b^2}{2}\varepsilon DOC, T_f = \frac{R_b^2}{2}\gamma\mu l\sigma, W_c = R_b^2\varepsilon\zeta DOC \text{ and } W_f = R_b^2 l\sigma \quad (38)$$

Here, l is the wear flat of width, ε is the intrinsic specific energy, ζ describes the angle of the cutting force on the cutting face which is typically from $0.6 \leq \zeta \leq 0.8$ and σ is the stress magnitude acting across the worn flat interface. The spatial alignment (γ) and arrangement of the wear flats, for bits with flat bottoms, the number is between 1 and 4/3.

Khulief et al. (2007) accounted for the WOB fluctuation by considering the stiffness of the rock being drilled to model the coupled axial-torsional stick-slip vibrations. Their model assumes that the bit never loses contact with the formation and the bit is restricted in the lateral direction. The initial value of friction mechanism is indicated by, $W_0 + k_f DOC$, which after one revolution is reduced to its constant value W_0 which is the mean WOB when the expression $k_f x_0$ disappears.

$$WOB = W_0 + k_r DOC(1 - \sin 2\pi ft) \quad (39)$$

where f denotes the frequency of the fluctuations and DOC denotes the depth of cut in one revolution. The rate of penetration (ROP) and the depth of cut is linked to the frequency f as $f = \frac{ROP}{DOC}$. The amplitude of the oscillating period is proportional to the depth of cut, whereas the frequency f of a bit spinning at an angular velocity ω_b and RPM may be computed from,

$$\frac{2\pi}{\omega_b} = \frac{DOC}{RPM} \quad (40)$$

The TOB, of Khulief et al. (2007) model, is given by:

$$TOB = \mu_k WOB \times \xi(\omega_b) \quad (41)$$

Here μ_k is the coefficient of kinetic friction, the function $\xi(\omega_b)$ is related to the bit's angular velocity and frictional constants α_1 and α_2 given by,

$$\xi(\omega_b) = \tanh(\omega_b) + \frac{\alpha_1 \omega_b}{1 + \alpha_2 \omega_b^2} \quad (42)$$

A non-linear reversible bit-rock interaction model coupling the axial and torsional vibration was developed by Ritto and Sampaio (2012). The TOB for this model was defined as:

$$TOB[\omega_b(t)] = \mu_{bit} WOB(t)[\tanh[\omega_b(t)] + \frac{\alpha_1 \omega_b(t)}{1 + \alpha_2 \omega_b^2(t)}] \quad (43)$$

Where $\alpha_1 \; and \; \alpha_2$ are parameters that depend on rock properties, the WOB, which is the sum of the constant reaction force at the bit f_c and a time-dependent force $f_a(t) = f_0 \sin(\omega_0) + 0.01 f_0$, μ_{bit} is the friction coefficient. The model has a few weak points: first, it is not flexible enough to fit well for both lower and higher bit velocities, and second, it cannot induce hysteresis effects to differentiate forward and backward behaviors (Real et al., 2018). Real et al. (2018) suggested some improvements to Ritto and Sampaio (2012) model by including these constraints as shown in the equation below,

$$TOB\left[\omega_b, \ddot{\theta}_b\right] = b_0[\tanh(b_1 \omega_b) + \frac{b_2 |\omega_b|^{b_4} sign(\omega_b)}{1 + b_3 |\omega_b|^{b_5}} (1 + H\left(\omega_b, \ddot{\theta}_b\right))] \quad (44)$$

The parameters $b_1, b_2, b_3, b_4 and \; b_5$ depend on the rock properties and $b_0 = R_b \mu WOB$, where R_b indicates the bit radius and μ is the frictional coefficient. The hysteretic function H is equal to 0 if the model is reversible and has no hysteretic cycles. If H is greater than zero, the hysteretic model is triggered by approximating the Heaviside function as:

$$H\left(\omega_b, \ddot{\theta}_b\right) = \beta_1 \tanh\left(\beta_2 \ddot{\theta}_b\right) sign(\omega_b) \quad (45)$$

Ren and Wang (2017) defined WOB as follows,

$$WOB = k_R[x - s_0 \sin(n_{bit} \phi)] \quad (46)$$

Where, n_{bit} is the coefficient of bit, ϕ is the angular displacement of bit, k_R is the rock stiffness and s_0 is the amplitude of the formation surface profile. The TOB of their model was given by,

$$T_{bit} = \left[\frac{a^2 \varepsilon d}{2} H(\dot{\phi}) + \frac{\mu \gamma a w_c}{2} sign(\dot{\phi}) H(\dot{x})\right] H(d) \quad (47)$$

Here a is the bit radius, μ is the bit-rock interaction parameter, ε is the intrinsic specific energy, H is the Heaviside step function, w_c is the normal contact force and γ is a bit parameter.

A summary of the bit-rock interaction models is shown in Table 2.1. For each model, the vibration mode includes either coupled or uncoupled models. Friction models are identified as state-dependent, rate-dependent, or regenerative effects. State-dependent is when friction is a function of axial or torsional displacement. On the other hand, rate dependence is a function of axial or torsional velocity, The regenerative effect model is a function of time delay. The bit-rock interaction, depending on the coupling behavior, consists of TOB and WOB which are a function of torsional/axial velocities, torsional/axial displacements, axial displacement, and depth of cut. For uncoupled models, the WOB is mostly defined as a constant force. The differential equation type includes ordinary differential equation (ODE), partial differential equation (PDE), and dynamic delay differential equations (DDE).

Table 2.1. Summary of Bit-Rock Interaction Models

Author	**Vibration mode**	**Friction Model dependents**	**Bit-rock interaction (State/Rate)**		
			TOB Type	**WOB Type**	**Diff Eq. Type**
Belokobyl'skii and Prokopov (1982)	Torsional	Rate dependent	$\dot{\theta}$	-	ODE
Dunayevsky and Abbassian (1998)	Torsional Lateral	Rate dependent	$\dot{\theta}$	Constant	ODE
Navarro-López and Cortés (2007)	Torsional	Rate-State dependent	$\dot{\theta}$, θ	Constant	ODE
Huang et al. (2018)	Torsional	Rate dependent	$\dot{\theta}$	Constant	ODE
Christoforou and Yigit (2003)	Axial Torsional	Rate-State dependent	$\dot{\theta}$, θ, u	u	ODE
Al Sairafi et al. (2016)	Axial Torsional	Rate-State dependent	$\dot{\theta}$, θ, u	u	ODE

Mendil et al. (2021)	Torsional	Regenerative	$\dot{\theta}$	Constant	DDE
Aarsnes and Van De Wouw (2019)	Axial Torsional	Regenerative	$\dot{\theta}, d(t)$	$\dot{\theta}, d(t)$	PDE
Leine et al. (2002)	Torsional Lateral	Rate dependent	$\dot{\theta}$	Contact	ODE
Yigit and Christoforou (2000)	Torsional Lateral	Rate dependent	$\dot{\theta},\ \theta$	$\dot{\theta}$	ODE
Manzatto and Trindade (2011)	Torsional	Rate-State dependent	$\dot{\theta},\ \theta$	$\dot{\theta}$	ODE
Trindade and Sampaio (2005)	Axial Torsional	Rate dependent	$\dot{\theta}, d(t)$	Constant	ODE
Richard et al. (2007)	Torsional	Regenerative	$d(t)$	$d(t)$	DDE
Yigit and Christoforou (1998)	Torsional Lateral	Rate dependent	$\dot{\theta}$	$\dot{\theta}$	ODE
Navarro-Lopez and Suarez (2004)	Torsional	Rate-State dependent	$\dot{\theta},\ \theta$	Constant	ODE
Khulief et al. (2007)	Axial Torsional	Rate-State dependent	$\dot{\theta}, \theta, d(t)$	$d(t)$	ODE
Ritto and Sampaio (2012)	Axial Torsional	Rate dependent	$\dot{\theta}$	Constant	ODE
Real et al. (2018)	Axial Torsional	Rate dependent & Regenerative	$\dot{\theta}$	Constant	ODE
Tucker and Wang (2003)	Axial Torsional	Rate dependent	$\dot{\theta}, d(t)$	Constant	ODE
Ritto et al. (2009)	Axial Torsional	Rate dependent	$\dot{u}, \dot{\theta}$	$\dot{u}, \dot{\theta}$	ODE
Sampaio et al. (2007)	Torsional	Rate-State dependent	$\dot{\theta}$	Constant	ODE
Ren and Wang (2017)	Axial Torsional	Regenerative	$\dot{\theta},\ \theta$	θ	PDE
Yigit and Christoforou (2006)	Axial Torsional	Rate-State dependent	$\dot{\theta}, \theta,$ u	u	ODE

2.3 Literature Gap

Drillstring vibrations are difficult to replicate in a laboratory environment as it requires large space and are economically not feasible. Thus, scaled laboratory testing is often used to study drillstring vibrations. Typical laboratory scale experiments consist of stiff drillstring hindering the ability to replicate field drillstring vibrations (Garcia-Gavito & Azar, 1994; Glowka, 1987; Miyazaki et al., 2019). In practice, the field drillstring is slender with low rigidity which is not easy to replicate in laboratory settings.

Compliant laboratory configurations are used to address the slenderness and rigidity similarity of field investigations. Kapitaniak et al. (2015) and Wiercigroch et al. (2017) used a drilling compliant configuration with a flexible shaft to generate torsional and lateral vibration. Their setup considered torsional compliance without accounting for axial vibrations. Axial and torsional drillstring compliance configuration was used by several researchers to investigate different bit dynamic phenomena (Elsayed & Raymond, 1999; Elsayed & Raymond, 2002; Raymond et al., 2008). Their experiments consisted of PDC cutters mounted into a coring bit to investigate the effect of drilling compliance. The use of a full-scale PDC bit in drilling compliance configuration has not been fully investigated.

The interaction between the bit and the rock during drilling is affected by the bit type and design and the formation being drilled. In general, bit-rock interaction is modeled in static conditions, i.e., non-temporal, to analyze the bit performance and model ROP for a given drill bit. For vibration analysis, the bit-rock interaction is temporal and state-dependent which complicates the dynamics of drill bits (Depouhon et al., 2015; Mendil et al., 2021). The majority of the bit-rock interaction models lack validation with experimental and field data and methods of estimating empirical frictional constants of such models (Al Sairafi et al., 2016; Christoforou & Yigit, 2003; Huang et

al., 2018; Khulief et al., 2007; Navarro-Lopez & Suarez, 2004; Ren & Wang, 2017; Yigit & Christoforou, 2006).

2.4 Research Objectives

The objective of this research is to perform frequency analysis to fully understand the effect of compliant drillstring vibration in the torsional and axial directions on bit dynamics using two industrial scale PDC bits which include four and five blade designs. The drillstring testing configurations include Rigid (R), Flywheel (F), Torsional Compliance (TC), Axial Compliance (AC) and Combined Axial and Torsional Compliance (CAT), a detailed explanation of the configuration is provided in Chapter 3.

To understand bit-rock interaction law, a few of the existing bit-rock interaction models which include Navarro-Lopez and Suarez (2004), Yigit and Christoforou (2006), Huang et al. (2018) and Ritto et al. (2009) are compared, contoured, and analyzed with the laboratory Rigid testing data for the 4-bladed PDC bit.

CHAPTER III

3 METHODOLOGY

3.1 Drillstring Vibration Effect on Drill Bit Dynamics

To address the effect of drillstring vibrations on drill bit dynamics, a unique indoor laboratory-based drilling rig was used. The rig is a part of the Hard Rock Drilling Facility (HRDF) at Sandia National Laboratories, which is capable of replicating field-drilling conditions using advanced controlled, axial, and torsional compliance mimicking field vibrations (Raymond et al., 2008). The rig is made up of a drillstring that is supported by a vertically traversing hydraulically driven frame that houses a rotating top drive mechanism (Figure 3.1).

Figure 3.1. SNL Hard Rock Drilling Facility (Barnett et al., 2022)

The experimental rig consists of a fixed-displacement hydraulic motor that rotates the drillstring, while hydraulic cylinders apply axial stress to the drillstring. A swivel feeds water as the drilling fluid above the top drive. The rig is equipped to monitor and regulate the drilling operation as well as the bit interaction. A central computer control collects drilling data such as WOB, torque, RPM, drillstring position, acceleration, and downhole data labeled as VRS. A centrally positioned displacement transducer (CPDT) is used to monitor the location of the drillstring with respect to the frame and provide means of evaluating the axial vibrations, the torsional position displacement transducer (TPDT) is used to monitor the torsional vibration of the drillstring in relation to the drillstring's supporting structure. On the drillstring support fixture, an accelerometer is attached at the centerline. A drill bit is mounted at the end of the drillstring, where a 3 ft cube rock sample is placed under the rig allowing bit-rock interaction and rock penetration (Figure 3.2).

Figure 3.2. HRDF Platform with Rock Sample (Barnett et al., 2022)

3.1.1 Experimental setup and configuration

The HRDF has several test configurations to reproduce drillstring vibrations seen in the field in a laboratory scale setting. Each configuration is independent and tested separately or combined. In this investigation, five test configurations are tested including rigid (R), flywheel (FW), torsional compliance (TC), axial compliance (AC), and combined axial and torsional compliance (CAT)

configuration. Figure 3.3 shows a representative schematic of the drilling setup of HRDF with all the configurations at once, which is for illustration purposes.

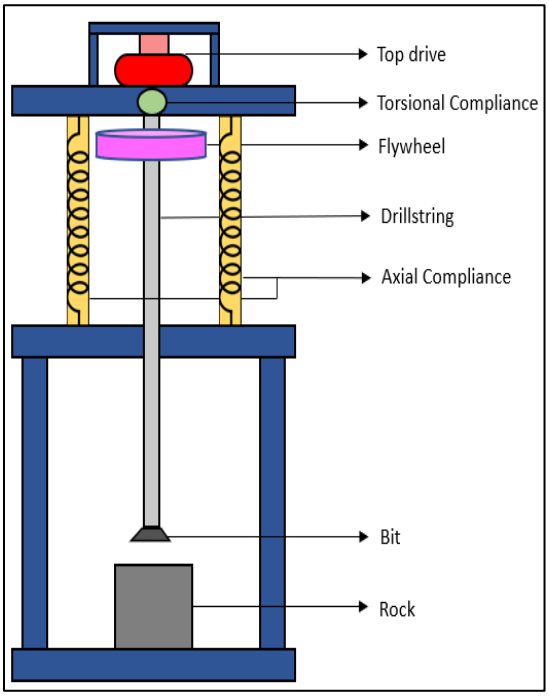

Figure 3.3. SNL HRDF Schematic Illustration

The rigid configuration without induced vibration is frequently used as the testing standard for drilling bit performance tests in laboratories.

The flywheel design consists of a 24-inch diameter A-34 steel plate mounted on the drillstring. The drillstring natural frequencies are extremely low under field settings due to the drillstring slenderness ratio (Elsayed & Raymond, 2002; Raymond et al., 2008). Typical laboratory rigs are stiff and have a significantly larger frequency range than the real drillstring employed in the field, making it difficult to investigate dynamic phenomena like bit chatter. To overcome this issue, the flywheel configuration is implemented to increase the rotating mass moment of inertia, lowering the drillstring frequency to within the field condition range.

The torsional compliance configuration addresses field drillstring flexibility in the torsional direction. Two counter-wound springs aid the HRDF drillstring's torsional compliance. To assure

non-zero torque during winding and unwinding during drilling, the springs are pre-loaded (Elsayed & Raymond, 2002). The effective torsional springs' torque (T) in lb-in and angular deflection (θ) in degrees relationship is represented as:

$$T = 123.13 \times \theta + 85.507 \quad (48)$$

The axial compliance configuration is applied using servo-hydraulic actuators which control the damper consisting of springs and a damping system. Compression springs are also employed to provide longitudinal support for the drillstring. The last testing configuration, integrated testing with both axial and torsionally compliance configuration.

Each test configuration, i.e., five different configurations, was tested with two distinct designs of PDC bits having a diameter of 3.75 inches. The first 4-balded PDC bit consists of a total of 15 primary cutters with a 13 mm diameter (Figure 3.4). The second bit is a 5-bladed design with 19 primary cutters of 11 mm in diameter (Figure 3.5).

To mimic geothermal hard rock, Sierra White Granite was used for all tests. The rock sample of the Sierra White Granite has an unconfined compressive strength of 28,000 psi, a bulk density of 2.65 g/cc, and an unconfined Youngs modulus of 6×10^6 psi. A constant flow rate of 15 gallons per minute was used for all tests with water as drilling fluid to normalize the effect of drill bit hydraulics. The goal of using two distinct drill bits is to examine the effect of drillstring dynamics on different bit designs.

Figure 3.4 Profile of the 4-Bladed PDC Bit (Barnett et al., 2022)

Figure 3.5. Profile of the 5-Bladed PDC Bit (Barnett et al., 2022)

3.1.2 Testing matrix

Each test was carried out with a constant rotating speed and an increasing axial load, i.e., WOB. For each test configuration, three constant rotational speeds were tested at 80, 120, and 160 RPM. Due to the different bit designs and rig limitations of each test configuration, the range of the applied WOB differs. A summary of the applied WOB of each test configuration and rotational speed for the 4-blade and 5-blade PDC bits is tabulated in Table 3.1 and Table 3.2, respectively.

Table 3.1. Testing Matrix of the 4-Bladed PDC Bit

Testing Configuration	PDC bit	RPM	WOB (lbs)
Rigid	3 ¾" 4-Blade	80, 120 and 160	1500-5000
Flywheel			1600-5150
Torsional Compliance			1470-4900
Axial Compliance			1500-3100
Combined Axial and Torsional Compliance			1500-3000

Table 3.2. Testing Matrix of the 5-Bladed PDC Bit

Testing Configuration	PDC bit	RPM	WOB (lbs)
Rigid	3 ¾" 5-Blade	80, 120 and 160	1500-5000
Flywheel			1650-5150
Torsional Compliance			1580-5200
Axial Compliance			1450-3400
Combined Axial and Torsional Compliance			1500-3150

3.1.3 Data processing

A sampling frequency of 512 samples per second was used to measure the raw data from the SNL testing, where the raw data was provided in a .txt file as shown in Figure 3.6. Each drillstring configuration test had six large text files averaging 350 megabytes in size. Three text files for four-blade testing with rotational speed range of 80, 120, and 160 RPM, and three more for the five-blade testing with the same RPM range.

```
NOV 4-Blade Bit @ 80 RPM & WOB: 2000-5000 lb
Test # = 1      Hole # = 1      Hole Index = G2 Test Operator = David   Control Mode = Constant WOB
Test Time       Time    Pressure - top left     Pressure - bottom left  Pressure - top right    Pressure
0.0000  10:40:07        8.4902E+1       2.4564E+2       6.6082E+1       2.3352E+2       1.0175E-4
0.0020  10:40:07        8.4902E+1       2.4564E+2       6.6082E+1       2.3352E+2       7.7499E-5
0.0039  10:40:07        8.4902E+1       2.4564E+2       6.6082E+1       2.3352E+2       9.5037E-5
0.0059  10:40:07        8.4902E+1       2.4564E+2       6.6082E+1       2.3352E+2       1.1822E-4
0.0078  10:40:07        8.4972E+1       2.4523E+2       6.5842E+1       2.3335E+2       1.7632E-4
0.0098  10:40:07        8.4996E+1       2.4509E+2       6.5761E+1       2.3329E+2       1.3042E-4
0.0117  10:40:07        8.4996E+1       2.4509E+2       6.5761E+1       2.3329E+2       9.8697E-5
0.0137  10:40:07        8.4996E+1       2.4509E+2       6.5761E+1       2.3329E+2       1.3896E-4
0.0156  10:40:07        8.4922E+1       2.4525E+2       6.5740E+1       2.3328E+2       2.0774E-4
0.0176  10:40:07        8.4848E+1       2.4541E+2       6.5718E+1       2.3327E+2       1.9020E-4
0.0195  10:40:07        8.4848E+1       2.4541E+2       6.5718E+1       2.3327E+2       1.7708E-4
0.0215  10:40:07        8.4848E+1       2.4541E+2       6.5718E+1       2.3327E+2       1.9203E-4
0.0234  10:40:07        8.4917E+1       2.4531E+2       6.5737E+1       2.3323E+2       2.8460E-4
0.0254  10:40:07        8.5125E+1       2.4499E+2       6.5792E+1       2.3313E+2       3.3309E-4
0.0273  10:40:07        8.5125E+1       2.4499E+2       6.5792E+1       2.3313E+2       3.0763E-4
0.0293  10:40:07        8.5125E+1       2.4499E+2       6.5792E+1       2.3313E+2       2.7621E-4
0.0312  10:40:07        8.5125E+1       2.4499E+2       6.5792E+1       2.3313E+2       3.0900E-4
0.0332  10:40:07        8.5181E+1       2.4506E+2       6.5904E+1       2.3313E+2       3.0610E-4
0.0352  10:40:07        8.5181E+1       2.4506E+2       6.5904E+1       2.3313E+2       2.4113E-4
0.0371  10:40:07        8.5181E+1       2.4506E+2       6.5904E+1       2.3313E+2       1.9828E-4
0.0391  10:40:07        8.5181E+1       2.4506E+2       6.5904E+1       2.3313E+2       2.1582E-4
0.0410  10:40:07        8.5103E+1       2.4505E+2       6.5694E+1       2.3317E+2       2.0118E-4
0.0430  10:40:07        8.5076E+1       2.4505E+2       6.5624E+1       2.3318E+2       1.2295E-4
0.0449  10:40:07        8.5076E+1       2.4505E+2       6.5624E+1       2.3318E+2       9.1987E-5
0.0469  10:40:07        8.5076E+1       2.4505E+2       6.5624E+1       2.3318E+2       1.0373E-4
0.0488  10:40:07        8.4966E+1       2.4521E+2       6.5744E+1       2.3316E+2       1.3957E-4
0.0508  10:40:07        8.4856E+1       2.4537E+2       6.5865E+1       2.3313E+2       1.0373E-4
0.0527  10:40:07        8.4856E+1       2.4537E+2       6.5865E+1       2.3313E+2       3.4646E-5
0.0547  10:40:07        8.4856E+1       2.4537E+2       6.5865E+1       2.3313E+2       7.8109E-5
0.0566  10:40:07        8.4902E+1       2.4530E+2       6.5819E+1       2.3313E+2       9.8545E-5
```

Figure 3.6. SNL Text File Raw Data

A Matlab program was created to read the raw data and filter the data by removing any rows having ROP, RPM, or WOB values less than 0. After filtering, another sub-code was programmed to split the data based on WOB increment for each particular test. An example of the filtered and separated test data is shown in Figure 3.7, which shows the WOB, torque, applied RPM, and ROP for the 5-bladed rigid test configuration at 80 RPM with distinct colors representing compartmentalized data depending on WOB increments.

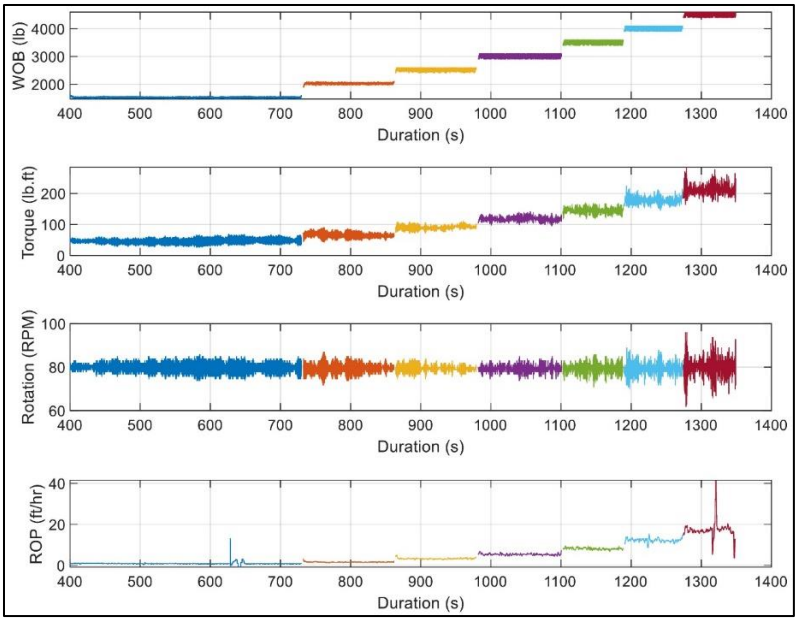

Figure 3.7. Compartmentalized WOB Increments for 5-Bladed Bit Rigid Test at 80 RPM

For each duration of the WOB increment, the applied WOB and RPM and measured ROP and torque were averaged for data visualization and analysis as shown in Table 3.3 for the rigid configuration test with the 4-bladed PDC bit.

Table 3.3. Averaged Filtered Data for 4-Bladed PDC Bit Rigid Configuration at 80 RPM

WOB (lbf)	RPM	ROP (ft/hr)	Torque (lb-ft)
1511	79.67	0.71	49.39
2012	79.98	2.01	79.97
2514	79.75	3.89	111.84
3014	79.51	7.44	159.46
3518	79.50	13.51	215.10
4014	80.40	21.82	271.63
4509	80.57	29.10	317.61
5017	80.04	35.19	363.97

Since the average incremental WOB for each test configuration was different, a labeling level was used to facilitate the analysis and comparison of the different drilling configurations. Table 3.4 and

Table 3.5 show the WOB level labeling for the 4 and 5-bladed bits respectively, where level 1 represents the lowest applied WOB for a particular test and level 8, depending on the test, represents the highest WOB that has been applied.

Table 3.4. Level Labeling of WOB Increments for the 4-Bladed Test Configurations

Levels	RPM	WOB (lbf)				
		R	TC	FW	AC	CAT
1	80	1511	1482	1641	1728	1793
2		2012	1969	2137	1931	2071
3		2514	2416	2637	2165	2334
4		3014	2889	3132	2385	2549
5		3518	3373	3635	2659	2788
6		4014	3893	4142	2993	3055
7		4509	4383	4650	-	-
8		5017	4913	5153	-	-
1	120	1517	1497	1661	1842	1554
2		2019	2031	2164	2089	1877
3		2523	2521	2663	2313	2169
4		3017	3025	3165	2625	2461
5		3522	3487	3672	2936	2761
6		4030	3988	4169	3166	3072
7		4537	4454	4670	-	-
8		5031	4947	5182	-	-
1	160	1542	1470	1682	1521	1557
2		2055	1950	2170	1779	1792
3		2553	2469	2672	2089	2088
4		3057	2981	3166	2365	2398
5		3550	3443	3675	2718	2735
6		4064	3937	4164	2996	3015
7		4562	4418	4673	-	-
8		5067	4904	5155	-	-

Table 3.5. Level Labeling of WOB Increments for the 5-Bladed Test Configurations

Levels	RPM	WOB (lbf)				
		R	TC	FW	AC	CAT
1	80	1114	1645	1661	1777	1767
2		1529	2058	2157	2236	1996
3		2029	2563	2659	2444	2290
4		2530	3073	3158	2730	2541
5		3032	3553	3660	3032	2862
6		3535	4086	4163	3377	3145

7		4031	4588	4664	-	-
8		4523	5175	5159	-	-
1	120	1465	1583	1657	1458	1562
2		1966	2031	2160	1779	1836
3		2469	2529	2668	2090	2134
4		2969	3049	3165	2388	2457
5		3476	3534	3661	2741	2733
6		3964	4046	4161	3073	3004
7		4470	4545	4678	-	-
8		4968	5101	5162	-	-
1	160	1527	1592	1662	1844	1538
2		2028	1992	2172	2026	1696
3		2533	2438	2681	2278	2029
4		3025	3000	3169	2621	2351
5		3526	3448	3675	2926	2723
6		4026	3967	4177	-	3022
7		4535	4438	4672	-	-
8		5031	4971	5183	-	-

3.1.4 Drilling configuration comparison

To get a better comparison and understanding of the test configurations, three WOB levels are selected, which include a low WOB level “W1”, an intermediate WOB level “W2”, and a high WOB level “W3”. The rigid drillstring configuration was selected as the base case to determine the effect of drillstring vibrations on bit performance. As such, the WOB levels selection for the comparison between the rigid and other configurations were selected based on the minimum difference in WOB. For instance, in Table 3.6, level 1 of WOB for rigid and axial compliance cannot be paired together because the WOB difference is greater than 200 lbs, therefore level 2 will be considered as W1 or the lowest applied WOB. For W2, level 3 of rigid will be paired with level 5 of axial compliance and for W3, level 4 of rigid will be paired with level 6 of axial compliance.

Table 3.6. Example of WOB Selection for Dynamic Comparison Using 4-Bladed Bit Data

RPM	Levels	R	AC	WOB Difference
		WOB (lbf)	WOB (lbf)	

80.0	1	1511.2	1727.7	216.5
	2	2012.0	1931.1	80.9
	3	2513.9	2165.4	348.5
	4	3013.8	2385.4	628.4
	5	3518.0	2659.4	858.5
	6	4014.1	2993.0	1021.1
	7	4509.0	-	-
	8	5016.6	-	-

The same procedure was followed to compare the rigid drilling dynamics to the other drilling configurations. The selected WOB levels of investigation for the rigid configuration for both bits compared to torsional compliance (TC), flywheel (F), axial compliance (AC), and combined axial-torsional (CAT) are listed in Table 3.7,

Table 3.8,

Table 3.9 and

Table 3.10, respectively.

Table 3.7. WOB Levels for R Vs TC Configuration Comparison for 4 and 5-Bladed PDC Bits

RPM	**WOB levels**	**4-Bladed PDC Bits**			**5-Bladed PDC Bits**		
		WOB (lbf)		**WOB Difference (lbf)**	**WOB (lbf)**		**WOB Difference (lbf)**
		R	**TC**		**R**	**TC**	
80	W1	1511	1482	29	2029	2058	29
	W2	2514	2416	98	3535	3553	18
	W3	5017	4913	104	4523	4588	66
120	W1	2523	2521	2	2469	2529	60
	W2	3017	3025	8	3476	3534	59
	W3	4537	4454	83	4470	4545	75
160	W1	1542	1470	72	2028	1992	36
	W2	3057	2981	76	3025	3000	25
	W3	4562	4418	145	5031	4971	61

Table 3.8. WOB Levels for R Vs FW Configuration Comparison for 4 and 5-Bladed PDC Bits

RPM	**WOB levels**	**4-Bladed PDC Bits**			**5-Bladed PDC Bits**		
		WOB (lbf)		**WOB Difference (lbf)**	**WOB (lbf)**		**WOB Difference (lbf)**
		Rigid	**FW**		**Rigid**	**FW**	
80	W1	1511	1641	130	2029	2157	128
	W2	3518	3635	117	3032	3158	126

	W3	5017	5153	136	3535	3660	125
120	W1	1517	1661	145	1465	1657	192
	W2	3017	3165	148	3476	3661	186
	W3	4537	4670	133	4968	5162	193
160	W1	1542	1682	140	1527	1662	136
	W2	4064	4164	100	3025	3169	144
	W3	5067	5155	88	4535	4672	137

Table 3.9. WOB Levels for R Vs AC Configuration Comparison for 4 and 5-Bladed PDC Bits

RPM	**WOB levels**	**4-Bladed PDC Bits**			**5-Bladed PDC Bits**		
		WOB (lbf)		**WOB Difference (lbf)**	**WOB (lbf)**		**WOB Difference (lbf)**
		Rigid	**AC**		**Rigid**	**AC**	
80	W1	2012	1931	81	2530	2444	87
	W2	2514	2659	146	3032	3032	1
	W3	3014	2993	21	3535	3377	158
120	W1	2019	2089	70	1465	1458	7
	W2	2523	2625	102	1966	2090	124
	W3	3017	2936	81	2969	3073	103
160	W1	1542	1521	22	2028	2026	1
	W2	2055	2089	35	2533	2621	87
	W3	3057	2996	61	3025	2926	99

Table 3.10. WOB Levels for R Vs CAT Configuration Comparison for 4 and 5-Bladed PDC Bits

RPM	**WOB levels**	**4-Bladed PDC Bits**			**5-Bladed PDC Bits**		
		WOB (lbf)		**WOB Difference (lbf)**	**WOB (lbf)**		**WOB Difference (lbf)**
		Rigid	**CAT**		**Rigid**	**CAT**	
80	W1	2012	2071	59	2029	1996	33
	W2	2514	2549	35	2530	2541	11
	W3	3014	3055	41	3032	3145	113
120	W1	1517	1554	38	1465	1562	97
	W2	2523	2461	62	2469	2457	12
	W3	3017	3072	55	2969	3004	35
160	W1	1542	1557	15	1527	1538	11
	W2	2055	2088	34	2028	2029	1
	W3	3057	3015	42	3025	3022	3

3.1.5 Analysis of drilling dynamics

The vibrations that occur during a field drilling operation are random, to help quantify these vibrations, the dynamic response during drilling is evaluated using the Power Spectral Density (PSD) to determine the dominant frequency of the vibrations during drilling.

A signal's spectral content may be described mathematically using the concept of PSD, it indicates how the power of a signal is spread in the frequency domain. In PSD analysis, the "power" stands for the mean-square value of the studied signal, while the "spectral" stands for the distribution of a signal across a range of frequencies. A single Hertz (Hz) bandwidth is used as the unit of density to standardize the PSD's magnitude. For example, a WOB measurement signal having a unit of lbf will have a PSD unit of lbf^2/Hz. PSD has traditionally been employed to measure a system's vibration characteristics.

Due to measurement difficulties, the downhole measured data for each configuration were not consistently measured, for example, the torsional displacement measurement was only active in the torsional compliance test configuration. Thus, several parameters were used to determine the PSD of the axial and torsional vibrations for different configurations. The dominant axial frequencies (f_A) of each drillstring configuration are determined by converting the time domain response of the downhole WOB (VRS-WOB) and the measured center position displacement transducer (CPDT). The torsional dominant frequencies (f_T) of each configuration are determined using the downhole measured RPM (VRS-RPM), downhole measured torque (VRS-Torque), torsional displacement transducer (TPDT), and the torsional acceleration (T-Acc). Table 3.11 summarizes the time-based parameters used in performing the PSD analysis and determining the dominant axial and torsional frequencies.

Table 3.11. Drilling Parameters Used for Determining the Torsional and Axial Frequencies

Axial Frequencies	VRS WOB
	CPDT
Torsional Frequencies	VRS RPM
	VRS TQ
	TPDT
	T-Acc

For a given WOB increment and RPM, the time for each frequency domain was set to be 10 seconds from the starting time of drilling. The vibration data is extremely noisy; thus, the gaussian-weighted

moving average is utilized to average the data by taking the median across 5 element sliding window.

Figure 3.8 shows an example of determining the axial frequency using the VRS WOB measurements at 80 RPM for the rigid and flywheel drillstring configuration at different WOB intervals. At a lower WOB interval (W1) the axial frequency of rigid is 6.5 Hz and 5.25 Hz for the flywheel. For higher WOB interval (W3) the axial 3.5 Hz for both rigid and flywheel. Note that 1.25 Hz was not selected because it corresponds to the drillstring rotational frequency.

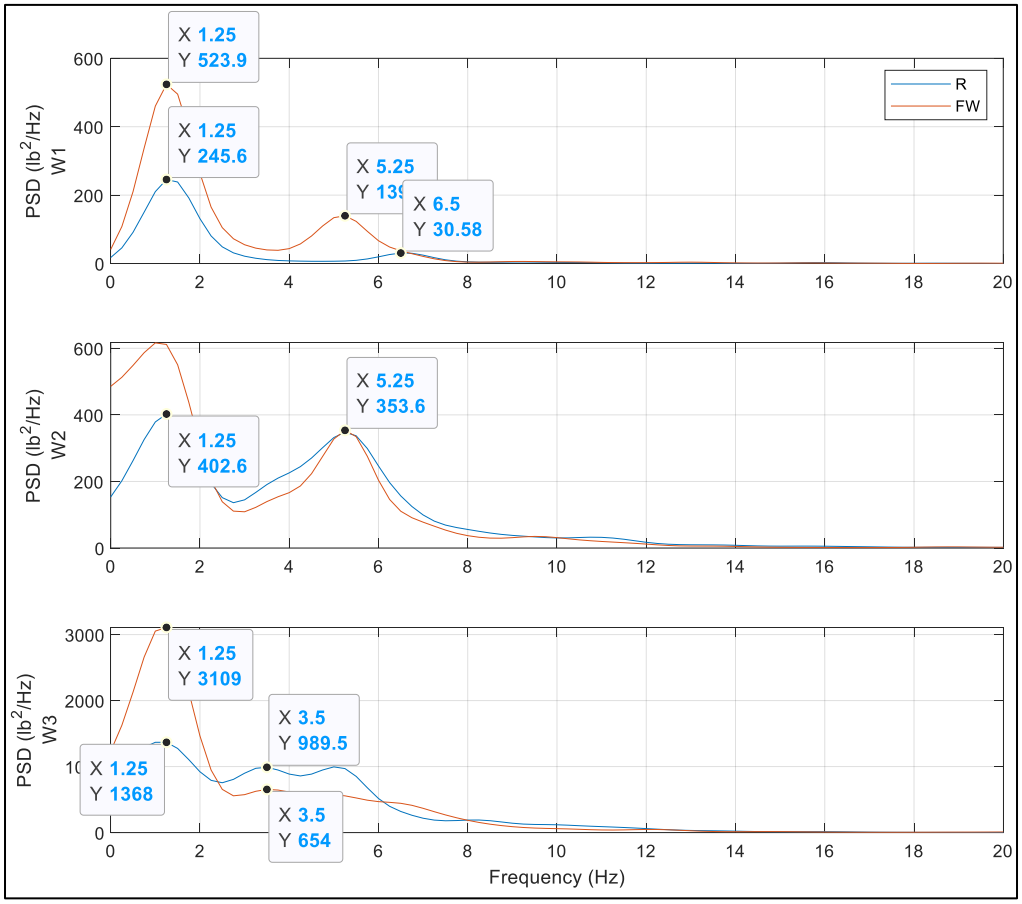

Figure 3.8. PSD Axial Frequency Response Comparison of R and FW Configuration at 80 RPM for the 4-Bladed Bit Test

3.2 Drillstring Vibration Modelling

One of the main sources of drillstring vibrations is the bit-rock interaction. The objective of this section is to evaluate several bit-rock interaction models and test their capability of predicting bit dynamics using the rigid test configuration. To reach this objective, a lumped mass parameter approach was used to model the drillstring equation of motion.

3.2.1 Drillstring equation of motion

The SNL-HRDF drillstring is modeled utilizing a lumped mode approximation method which represents the drillstring as a damper and spring system (Figure 3.9).

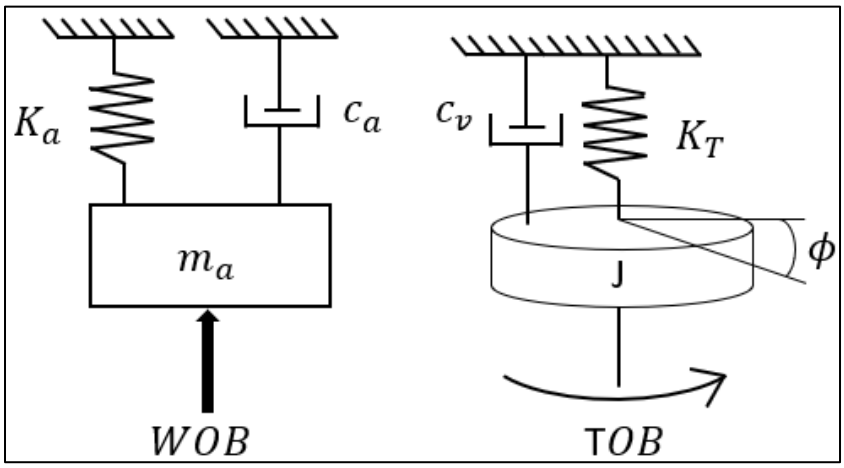

Figure 3.9. Lumped Drillstring Axial and Torsional Motion Model.

The axial equation of motion (EOM) is formulated below,

$$m_a\ddot{x} + c_a\dot{x} + k_a x = F_a \tag{49}$$

By assuming that the drill pipes and the drill collars correspond to continuous shafts with uniform cross-section and density, expressions for drillstring mass (m_a), and the axial stiffness (k_a) are derived from Richard et al. (2007). The drillstring mass m_a (kg) is calculated using the equation,

$$m_a = \frac{\rho\pi\left(OD_{dc}^2 - ID_{dc}^2\right)L_{dc}}{4} \tag{50}$$

Where ρ is the drillstring density which is about 7900 kg/m^3 for steel, OD_{dc} is the outside drill pipe diameter with a value of 3 inches, ID_{dc} is the inside drill pipe diameter with a value of 2.27 inches, and L_{dc} is 10 ft which is the length of the drillstring.

The axial stiffness k_a (N/m) is calculated using the equation,

$$k_a = \frac{E\pi\left(OD_{dc}^2 - ID_{dc}^2\right)}{4L_{dc}} \tag{51}$$

Where E is 210 GPa which is the Youngs modulus of steel.

The damping axial motion c_a $(N\ m/s)$ is calculated using the damping coefficient formula and the axial EOM (Equation 51), where ζ is the damping ratio with a value of 0.1 because the system vibration decreases with time.

$$c_a = 2\zeta\sqrt{k_a/m_a} \tag{52}$$

The axial force F_a is given by the equation below,

$$F_a = F_0 - WOB \tag{53}$$

The stationary quantity (F_0) is the applied WOB in kg and WOB is a function of bit interaction with the rock formation. Instead of solely employing a predetermined function, the WOB is determined by the features of the bit's interaction with the formation in coupled axial and torsional models.

The torsional EOM is formulated below,

$$J_T\ddot{\phi} + c_T\dot{\phi} + k_T\left(\phi - \dot{\phi}_{rt} \times t\right) = -TOB \tag{54}$$

Where J_T (kg m^2) represents the drillstring mass moment of inertia, derived by Richard et al. (2007) as shown below,

$$J_T = \frac{\rho\pi\left(OD_{dc}^4 - ID_{dc}^4\right)L_{dc}}{32} \tag{55}$$

The viscous damping coefficient c_T (N m s) is calculated using the damping coefficient formula and the torsional EOM as

$$c_T = 2\zeta\sqrt{k_T/J_T} \tag{56}$$

The torsional stiffness k_T (N m/rad) is calculated using the equation formulated by Richard et al. (2007) as

$$k_T = \frac{G\pi\left(OD_{dc}^4 - ID_{dc}^4\right)}{32 \times L_{dc}} \tag{57}$$

Where G is the shear modulus denoted by $G = \frac{E}{2(1+\nu)}$, and ν is 0.3 which is the steel Poisson's ratio. The value of G is 80.77 GPa.

In a coupled axial and torsional model, TOB is a function of cutting conditions and W. In an uncoupled torsional model, the TOB is a function of the bit cutting and friction processes.

A summary of the system EOM parameters is tabulated in Table 3.12

Table 3.12. SNL Drillstring EOM Parameters

EOM	Parameter	Value	Unit
Axial	m_a	46.94	kg
	c_a	338.2	$N\ m/s$
	k_a	134313001	N/m
Torsional	J_T	0.0536	kg m^2
	c_T	209.82	$N\ m\ s$
	k_T	58962	$N\ m/rad$

3.2.2 Bit-rock interaction friction parameters

The rigid mode of configuration at 80 RPM for lower and higher WOB increments of 1500 lbs and 5000 lbs is compared with the BRI models which include, one coupled axial and torsional model

(Christoforou & Yigit, 2003), and three uncoupled torsional models (Huang et al., 2018; Navarro-López & Cortés, 2007; Sampaio et al., 2007).

Several constants in these models such as frictional factors, bit factors, speed factors, cutting force factors, etc. do not have a suitable method of derivation (section-2.2), therefore while simulating the following BRI models, these constants were adjusted to match the SNL testing data.

The bit-rock interaction models are integrated into the axial and torsional EOM. For example, in the coupled axial and torsional BRI model in Christoforou and Yigit (2003), the TOB is given by,

$$\mathrm{TOB} = (WOB)\mathrm{R_b} \times \left[\mu(\dot{\phi}) + \zeta\sqrt{\delta_c/R_b}\right] \tag{58}$$

Where μ and ζ are the friction process and cutting process at the bit. The bit radius is given by R_b

The bit interaction with the rock formation in the axial EOM is given by,

$$WOB = \begin{cases} k_c(x-s) & if\ x \geq s, \\ 0 & if\ x < s, \end{cases} \tag{59}$$

The continuous function of the friction process is given by,

$$\mu(\dot{\phi}) = \mu_0(tanh\phi + \frac{\alpha\dot{\phi}}{1+\beta\dot{\phi}^{2\gamma}} + \nu\dot{\phi}) \tag{60}$$

Where k_c is the contact stiffness in N/m given by Yigit and Christoforou (1994) as,

$$k_c = \frac{4}{3}\sqrt{r_h}E \tag{61}$$

The Young modulus (E) of Sierra White Granite is 210×10^9 Pa.

The formation surface elevation (s) is given by,

$$s = s_0 sin(n_b\phi) \tag{62}$$

Where n_b is the bit factor with a value of 1 and ϕ = Drill collar angular displacement in radians. The value of s_0 is found to be 5×10^{-6} m.

The depth of cut δ_c in meters is given by,

$$\delta_c = \frac{2\pi ROP}{\omega_d} \tag{63}$$

The applied WOB (F_0) is 6728 N for W1 and 22266 N for W3. The average bit speed (ω_d) is 8.378 radians/second.

ROP is a function of applied WOB, and the average bit speed is given by,

$$ROP = c_1 F_0 \sqrt{\omega_d} + c_2 \tag{64}$$

The constants c_1 and c_2 were derived using regression analysis, using the rigid configuration data, ROP was plotted against $F_0\sqrt{\omega_b}$. Figure 3.10 shows the following graph, c_1 has a value of 1E-18 and c_2 is 3.1908

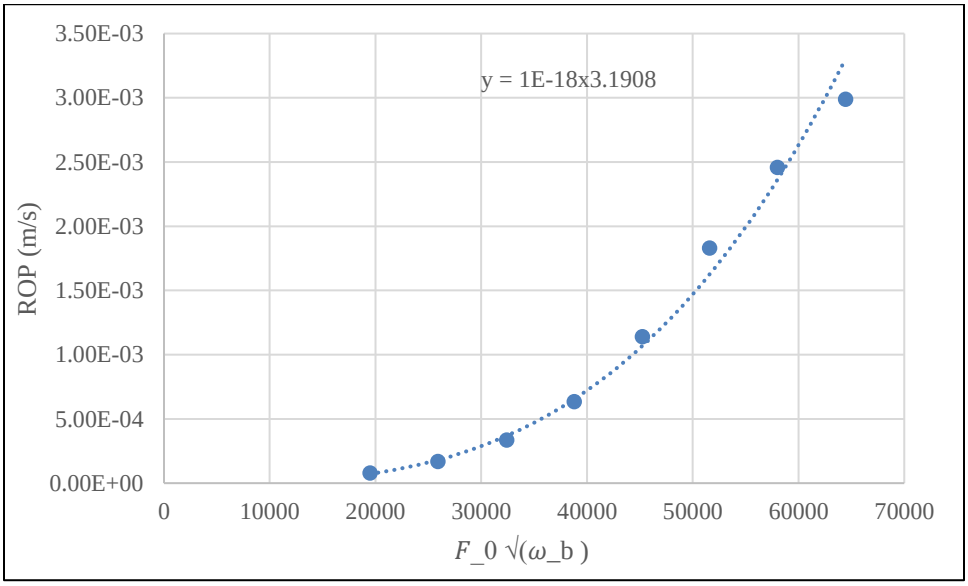

Figure 3.10. ROP Vs $F_0\sqrt{\omega_b}$ for Rigid 4-Blade at 80 RPM

Table 3.13 shows the frictional constants used in the above equations to contour the downhole TOB testing data to the BRI model.

Table 3.13. Christoforou and Yigit (2003) Constants for Rigid 4-Blade at 80 RPM for W1 and W8

Paper	Constants	WOB (lbs)

		1500	5000
Christoforou and Yigit (2003)	ξ	1	0.2
	μ_0	0.2	0.2
	α	2	2
	γ	1	1
	β	1	1
	ν	1	1

For uncoupled torsional bit-rock interaction models, the TOB is integrated into the torsional EOM. For example, in Navarro-López and Cortés (2007), the TOB is given by,

$$TOB = T_{ab}(\dot{\varphi}_{\mathrm{b}}) + T_{fb}(x) \tag{65}$$

Where T_{ab} is the viscous damping torque and T_{fb} represents the friction modeling of the bit-rock contact. The term *x* is the system state vector. The viscous damping torque is defined as $T_{ab} = c_b \times \dot{\theta}_b$, c_b is the bit damping coefficient which was set to 0.01 (N m s/rad). The frictional BRI torque was defined as a piecewise function accounting for stick, sliding, and transition between stick to slip mode written as:

$$T_{fb}(x) = \begin{cases} T_{eb}(x), & if\ |\dot{\varphi}| < D_v, |T_{eb}| \le T_{sb}\ (stick), \\ T_{sb} sgn\big(T_{eb}(x)\big), & if\ |\dot{\varphi}| < D_v, |T_{eb}| > T_{sb}\ (stick - slip), \\ f_b(\dot{\varphi}_b) sgn(\dot{\varphi}_b), & if\ |\dot{\varphi}| \ge D_v\ (sliding) \end{cases} \tag{66}$$

where D_v has a value of 10^{-6} and represents the zero-velocity band, T_{eb} is the required static reaction torque to move the bit, T_{sb} is the drilling torque defined in terms of static friction μ_{sb}, bit radius R_b, and applied WOB as:

$$T_{sb} = \mu_{sb} F_0 R_b \tag{67}$$

For the sliding mode, a combination of static and Coulomb friction was adopted with a velocity decaying function in the form of:

$$f_b(\dot{\varphi}_{\mathrm{b}}) = R_b F_0 \mu_b(\dot{\varphi}_{\mathrm{b}}) \tag{68}$$

Where $\mu_b(\dot{\varphi}_\mathrm{b})$ is defined as the bit dry friction given by,

$$\mu_b(\dot{\varphi}_\mathrm{b}) = [\mu_{cb} + (\mu_{sb} - \mu_{cb})e^{-\frac{\gamma_b}{\upsilon_f|\dot{\varphi}_b|}}] \tag{69}$$

In the above equation, γ_b is the friction model parameter and υ_f is the constant velocity with a value of 1 for unit consistency.

The required static reaction torque to move the bit is defined as a function of the bit and drillstring motion following:

$$T_{eb}(x) = c_t(\dot{\varphi}_r - \dot{\varphi}_b) + k_t(\varphi_r - \varphi_b) - T_{ab}(\dot{\varphi}_b) \tag{70}$$

Table 3.14 shows the frictional constants used in the above equations.

Table 3.14. Navarro-López and Cortés (2007) Constants for Rigid 4-Blade at 80 RPM for W1 and W8

Paper	**Constants**	**WOB (lbs)**	
		1500	**5000**
Navarro-López and Cortés (2007)	μ_{sb}	0.5	0.2
	μ_{cb}	0.014	0.016
	γ_b	0.5	0.4

The TOB in the uncoupled torsional bit-rock interaction model of Huang et al. (2018) is given by,

$$TOB = T_{bc} + T_{fb} \tag{71}$$

Where T_{fb} represents the friction modeling of the bit-rock contact which is the same as Navarro-López and Cortés (2007) and T_{bc} represents torque due to the cutting action in terms of the intrinsic specific energy of rock ϵ defined as,

$$T_{bc} = \frac{1}{2} \times \epsilon \times \bar{R}_b^2 \times n \times d \tag{72}$$

Where *n* is the number of radial blades of the PDC bit, and *d* is the depth of cut.

The depth of cut is calculated using the ROP and drilling starting and ending time for each WOB increment given by,

$$d = \frac{ROP}{t_{start} - t_{stop}} \tag{73}$$

The value of d is 1.25×10^{-7} m for 1500 lbs and 5000 lbs, the value of d is 7.11×10^{-5} m.

The equivalent radius of the PDC bit ($\bar{R}_b$) is given by,

$$\bar{R}_b = \int_0^{R_b} \frac{2\pi r}{\pi R_b^2} \times r \times dr = \frac{2}{3} \times R_b \tag{74}$$

where R_b is defined as the actual radius of the PDC bit which is 0.09525 m.

The intrinsic specific energy of the rock (Є) is 2×10^8 Pa.

Table 3.15 shows the frictional constants used in the modeling comparison of Huang's model.

Table 3.15. Huang et al. (2018) Constants for Rigid 4-Blade at 80 RPM for W1 and W8

Paper	Constants	WOB (lbs)	
		1500	5000
Huang et al. (2018)	μ_{sb}	0.001	0.001
	μ_{cb}	0.045	0.07
	γ_b	0.04	0.04

The TOB in the uncoupled torsional bit-rock interaction model of Sampaio et al. (2007) is given by,

$$TOB = \mu_{bit} F_0 \left(\tanh(\omega_b) + \frac{\alpha_1 \omega_b}{1 + \alpha_2 \omega_b^2} \right) \tag{75}$$

Here μ_{bit} is a function of the bit's cutting characteristics and α_1, α_2 are the rock property constants.

Table 3.16 shows the frictional constants used in the simulation.

Table 3.16. Sampaio et al. (2007) Constants for Rigid 4-Blade at 80 RPM for W1 and W8

Paper	Constants	WOB (lbs)	
		1500	5000
Sampaio et al. (2007)	α_1	1	0.6
	α_2	10	10
	μ_{bit}	6.5×10^{-5}	6.5×10^{-5}

The TOB on the bit-rock interaction model is defined as a function of bit axial velocity, depth of cut (DOC), and WOB in Trindade and Sampaio (2005) as shown below,

$$\text{TOB} = \text{a}_4 DOC + a_5, DOC = \frac{ROP}{\Omega}, ROP = -a_1 + a_2 WOB + a_3 \Omega \tag{76}$$

Where a_1, a_2, a_3, a_4, and a_5 are friction model parameters, Ω is the bit angular velocity.

Trindade and Sampaio (2005) regularization of TOB using a nonlinear equation, as shown below,

$$TOB = (-a_1 + a_2 WOB) a_4 \frac{\Omega^3}{(\Omega^2 + \epsilon^2)^2} + a_3 a_4 \frac{\Omega^3}{(\Omega^2 + \epsilon^2)^{\frac{3}{2}}} + a_5 \frac{\Omega}{(\Omega^2 + \epsilon^2)^{\frac{1}{2}}} \tag{77}$$

Here, the coulomb friction is represented by ϵ. To acquire the values for a_1, a_2, and a_3, $ROP = -a_1 + a_2 WOB + a_3 \Omega$ equation was used, and ROP Vs WOB data for rigid configuration at 80 RPM is plotted followed by linear regression (Figure 3.11).

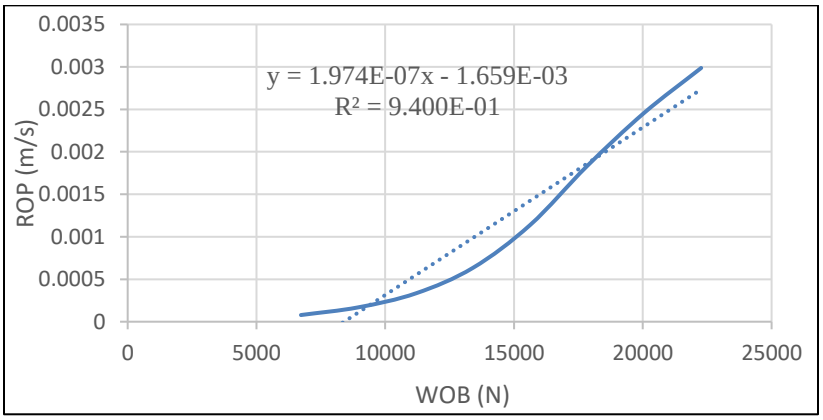

Figure 3.11. ROP Vs WOB of 4-Blade Rigid at 80 RPM

The value of a_2 from the trendline equation can be noted as 1.974×10^{-7}, and a_1, a_3 are written in an equation format shown as follows: $-1.659 \times 10^{-3} = -a_1 + a_3 \times RPM$

To find the values for a_4 and a_5, $\text{TOB} = \text{a}_4 DOC + a_5$ was used. TOB versus DOC for rigid data at 80 RPM was plotted followed by linear regression (Figure 3.12). The value of a_4 is 1153357 and a_5 is 100.

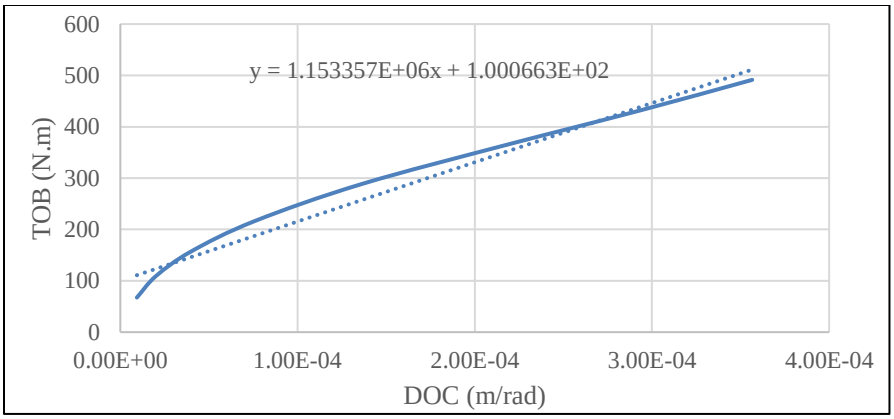

Figure 3.12. TOB Vs DOC of 4-Blade Rigid at 80 RPM

CHAPTER IV

4 RESULTS

The laboratory data is first analyzed to investigate the effect of drillstring vibration on drill bit dynamics using different drillstring compliant configurations for different bit designs. Secondly, the rigid drillstring configuration results are used to investigate bit-rock interaction models.

4.1 Time Domain Analysis of Drillstring Configurations

Four compliant drillstring configurations were tested at different operating conditions using two PDC bits. The rigid configuration is used as a controlled case to analyze the effect of each configuration on drill bit dynamics.

4.1.1 Rigid Vs torsional compliance

The measured drilling dynamics of the rigid and torsional compliance are compared for the 4-bladed bit at three WOB levels including low, medium, and high. For the 80 RPM test, the drilling data consisting of WOB, applied rotational speed (RPM), motor torque, ROP, and center position displacement are shown in Figure 4.1 for the rigid versus torsional compliance configurations for the three WOB levels. The first row of Figure 4.1 is the low WOB case, and the last row is the high WOB case. The applied WOB for the rigid configuration is slightly higher than the torsional configuration for each WOB level. At low WOB, an erratic rotational speed can be seen for both cases indicating difficulties engaging into the rock sample. As the WOB increases, a more stable

RPM can be seen for both configurations, with more stable RPM with torsional compliance. Overall, higher torque is generated with the rigid configuration, however, the torsional compliance provided a more stable torque compared to the rigid configuration. At low WOB, a higher ROP for torsional compliance is seen, as WOB increases, rigid configuration shows a higher ROP. CPDT indicates the drillstring axial movement and the level of axial vibrations, ROP is a function of CPDT (Figure 4.1).

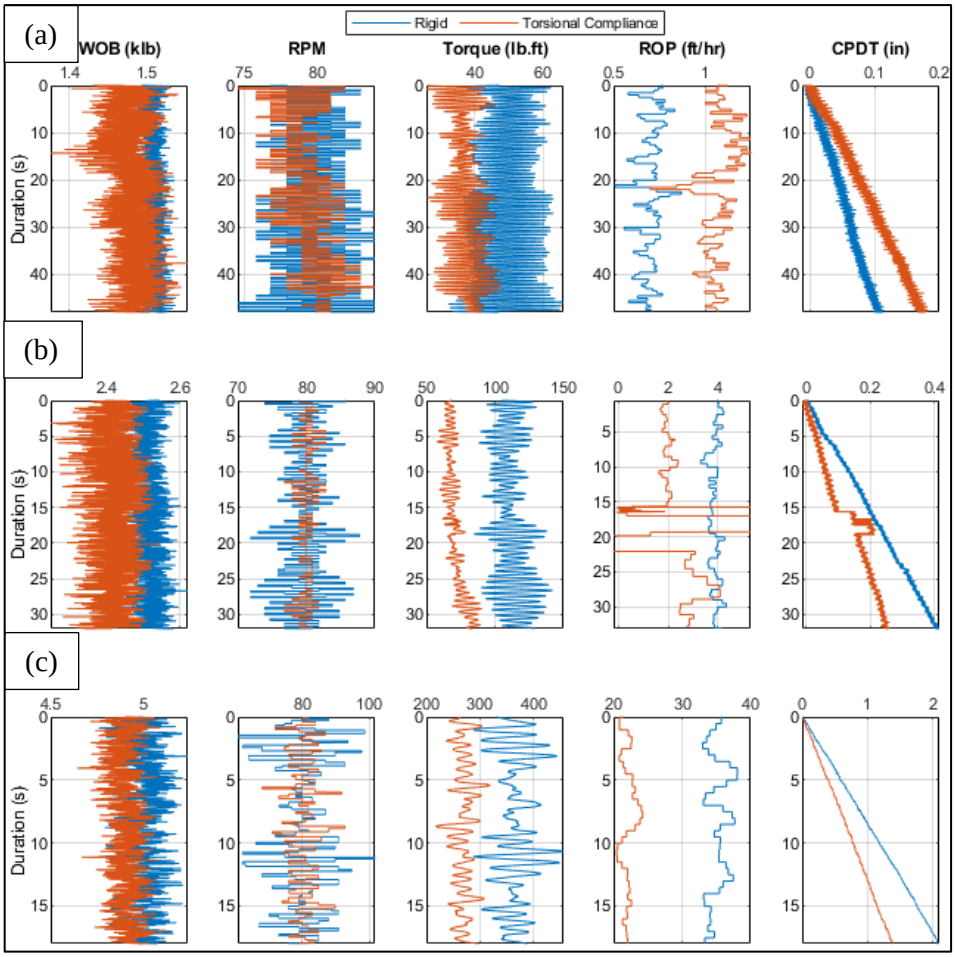

Figure 4.1. Rigid Vs TC Dynamics for 4-Bladed PDC Bit at 80 RPM (a) W1, (b) W2, and (c) W3

Figure 4.2 shows the dynamics of the 5-bladed PDC bit test at 80 RPM for low, intermediate, and high WOB levels. The applied WOB for torsional compliance is higher in all WOB levels compared to the rigid configuration. A comparatively stable RPM and torque can be seen at all WOB levels for torsional compliance configuration. At lower WOB, a similar ROP can be seen and as WOB

increases, the rigid configuration depicts a higher ROP. For CPDT the trend remains the same as the 4-bladed PDC bit.

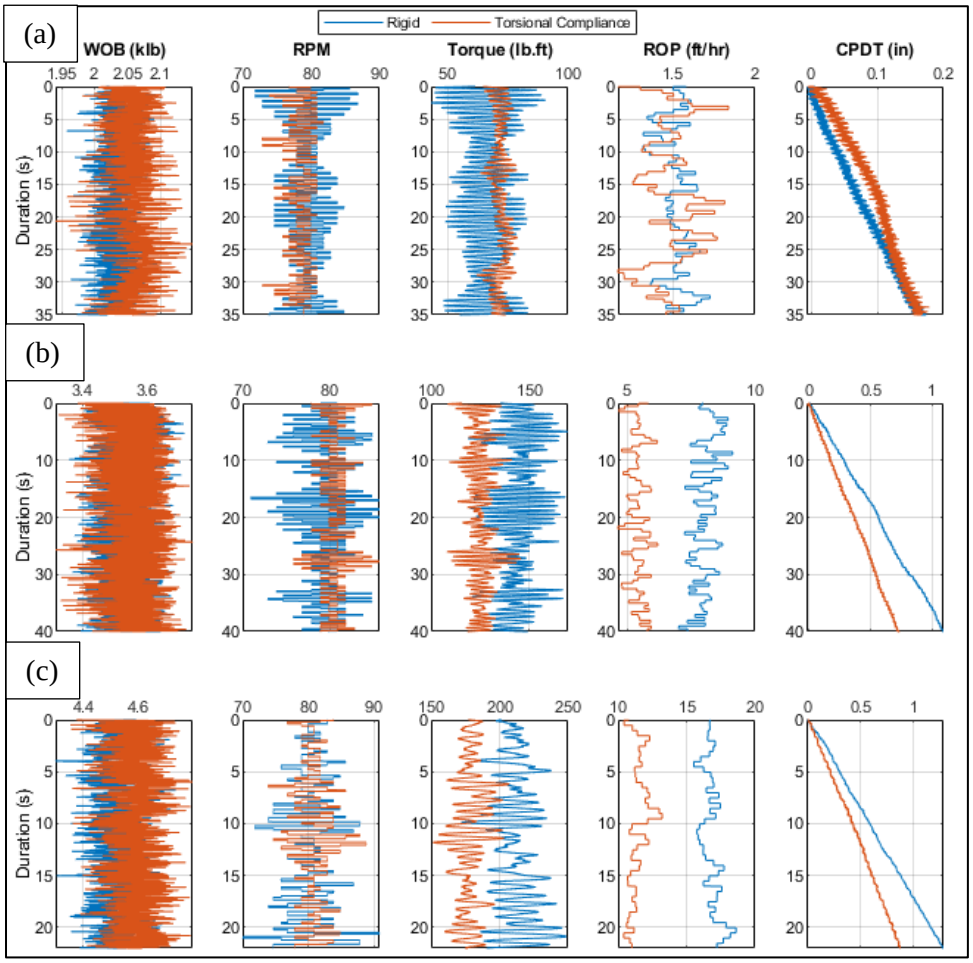

Figure 4.2. Rigid Vs TC Dynamics for 5-Bladed PDC Bit at 80 RPM (a) W1, (b) W2, and (c) W3

At higher rotational speeds, i.e., 120 and 160 RPM, the 4-bladed and 5-bladed bits show similar dynamics behavior, as shown in Appendix A, Figure A.1 and Figure A.2 for the 4-bladed bit, Figure A.3 and Figure A.4 for the 5-bladed bit.

4.1.2 Rigid Vs flywheel

The measured drillstring dynamics data is shown for rigid and flywheel configurations using the 4-bladed PDC bit at 80 RPM for the three WOB levels in Figure 4.3. An erratic WOB can be noticed for both flywheel and rigid at all WOB levels. The use of the flywheel provides a stable RPM and

torque at lower WOB levels, as WOB increases the fluctuations increase compared to the rigid configuration. As for ROP, at lower WOB, the flywheel has a higher ROP, at medium WOB, rigid has a higher ROP and at high WOB level, the ROP of both configurations are in the same range.

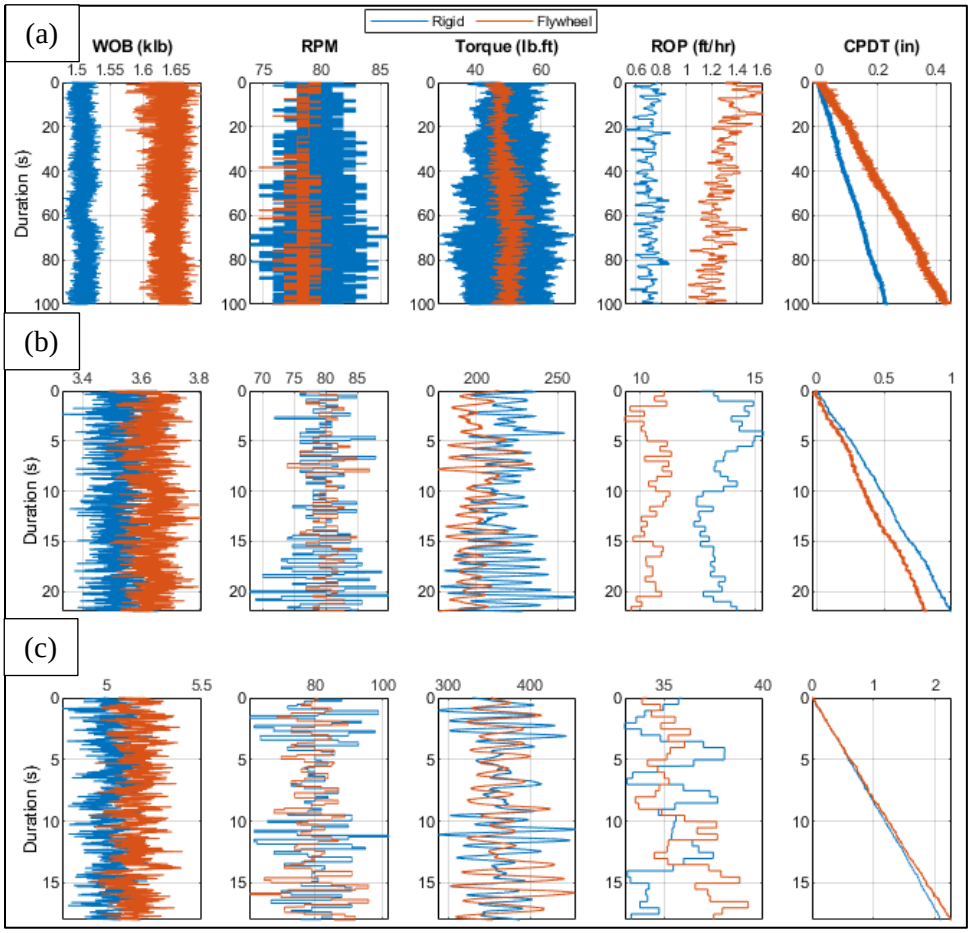

Figure 4.3. Rigid Vs FW Dynamics for 4-Bladed PDC Bit at 80 RPM (a) W1, (b) W2, and (c) W3

Figure 4.4 shows the dynamic results for the flywheel and rigid when a 5-bladed PDC bit is used at 80 RPM at the three WOB intervals. The WOB shows erratic behavior for both flywheel and rigid configurations and as WOB increases the difference decreases. Flywheel drillstring has smoother RPM and torque as compared to rigid drillstring.

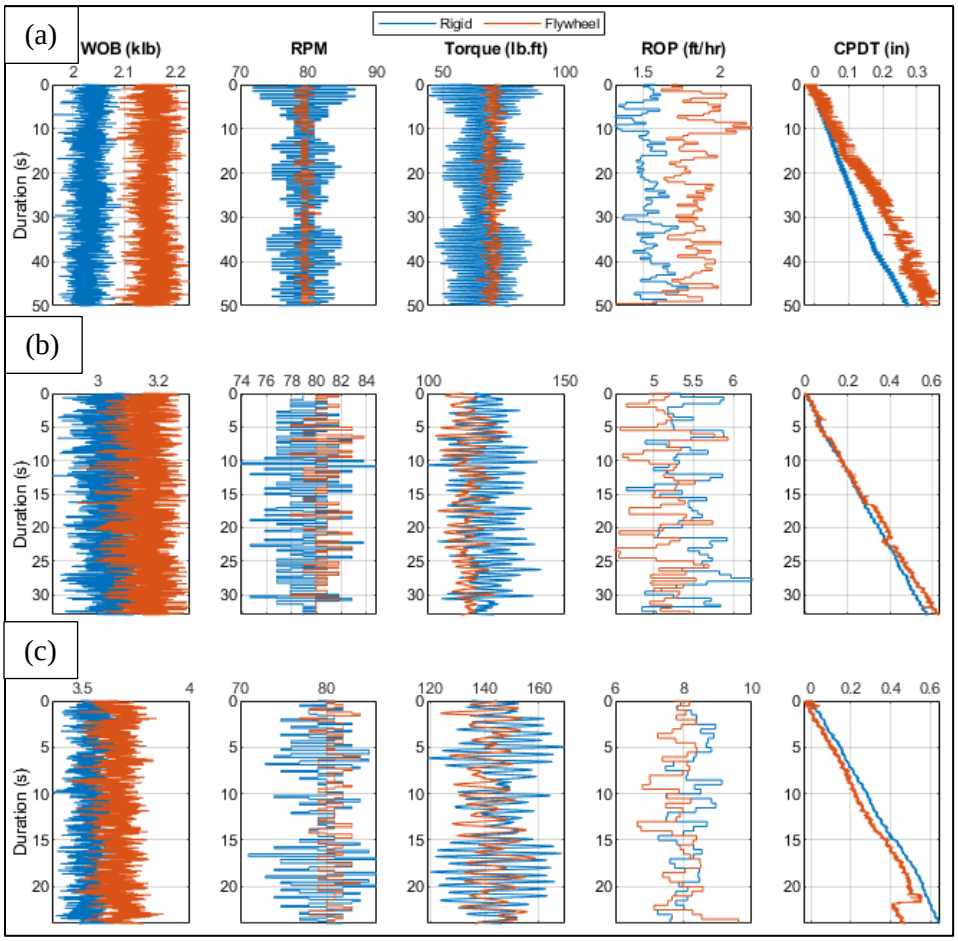

Figure 4.4. Rigid Vs FW Dynamics for 5-Bladed PDC Bit at 80 RPM (a) W1, (b) W2, and (c) W3

At higher rotational speeds, i.e., 120 and 160 RPM, the 4-bladed and 5-bladed bits show similar dynamics behavior, as shown in Appendix A, Figure A.6 and Figure A.7 for the 4-bladed bit and Figure A.8 and Figure A.9 for the 5-bladed bit.

4.1.3 Rigid Vs axial compliance

The drilling data for rigid and axial compliance configurations using the 4-bladed PDC bit at 80 RPM and three WOB levels for both rigid and axial compliance is shown in Figure 4.5. Reducing axial vibrations can cause severe fluctuations as shown in the WOB graph. The RPM shows an erratic fluctuation for the axial compliance in all WOB levels compared to the rigid configuration.

The torque depicts a decrease in fluctuation as WOB increases for axial compliance. Lower ROP can be seen for axial compliance in all three WOB levels.

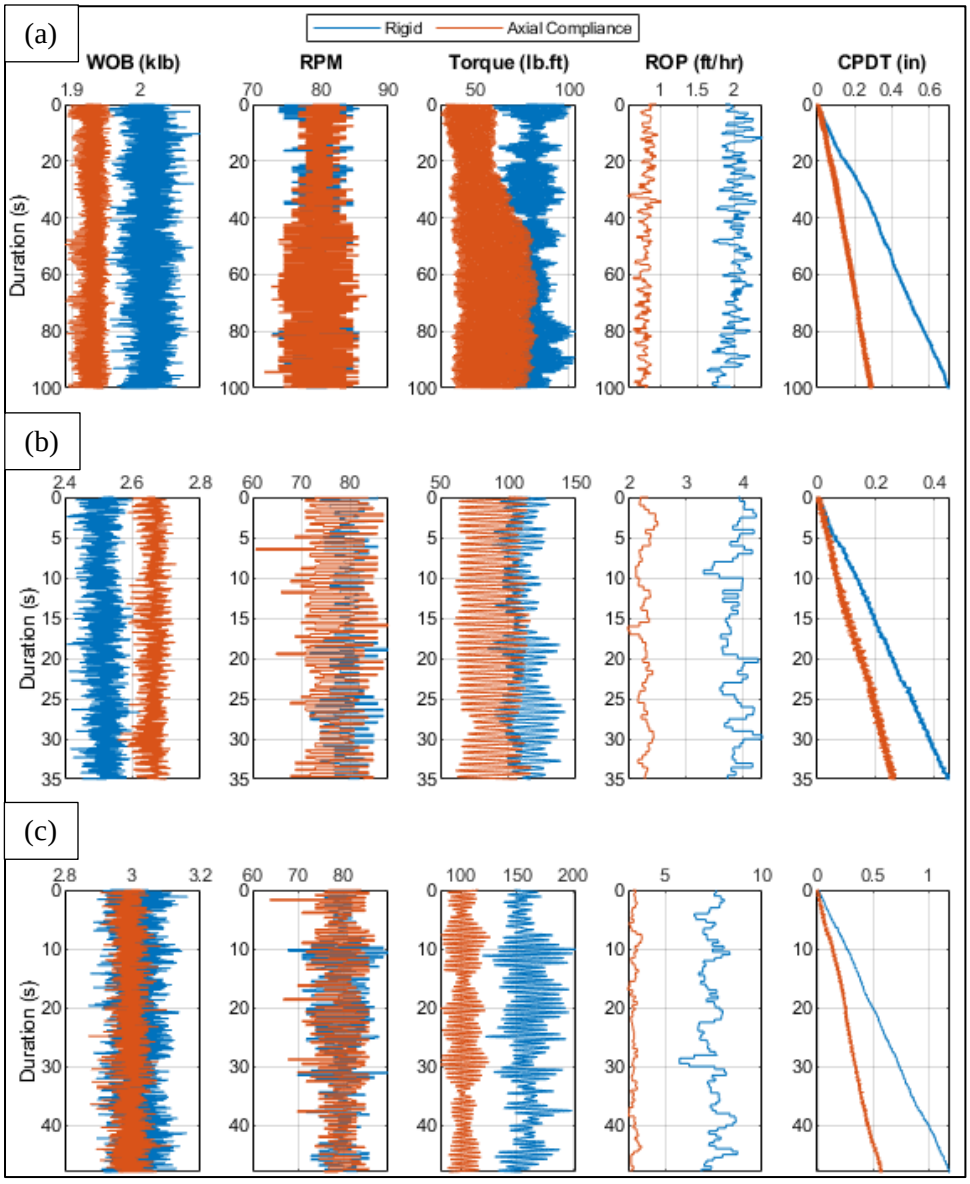

Figure 4.5. Rigid Vs AC Dynamics for 4-Bladed PDC Bit at 80 RPM (a) W1, (b) W2, and (c) W3

Figure 4.6 shows the dynamics of the testing results for rigid and axial compliance configurations utilizing the 5-bladed PDC bit at 80 RPM for all WOB levels. The WOB fluctuation is higher for axial compliance compared to the rigid drillstring as the WOB level increases. Similar behavior can be seen for RPM, torque, and ROP in the 4 and 5-bladed tests.

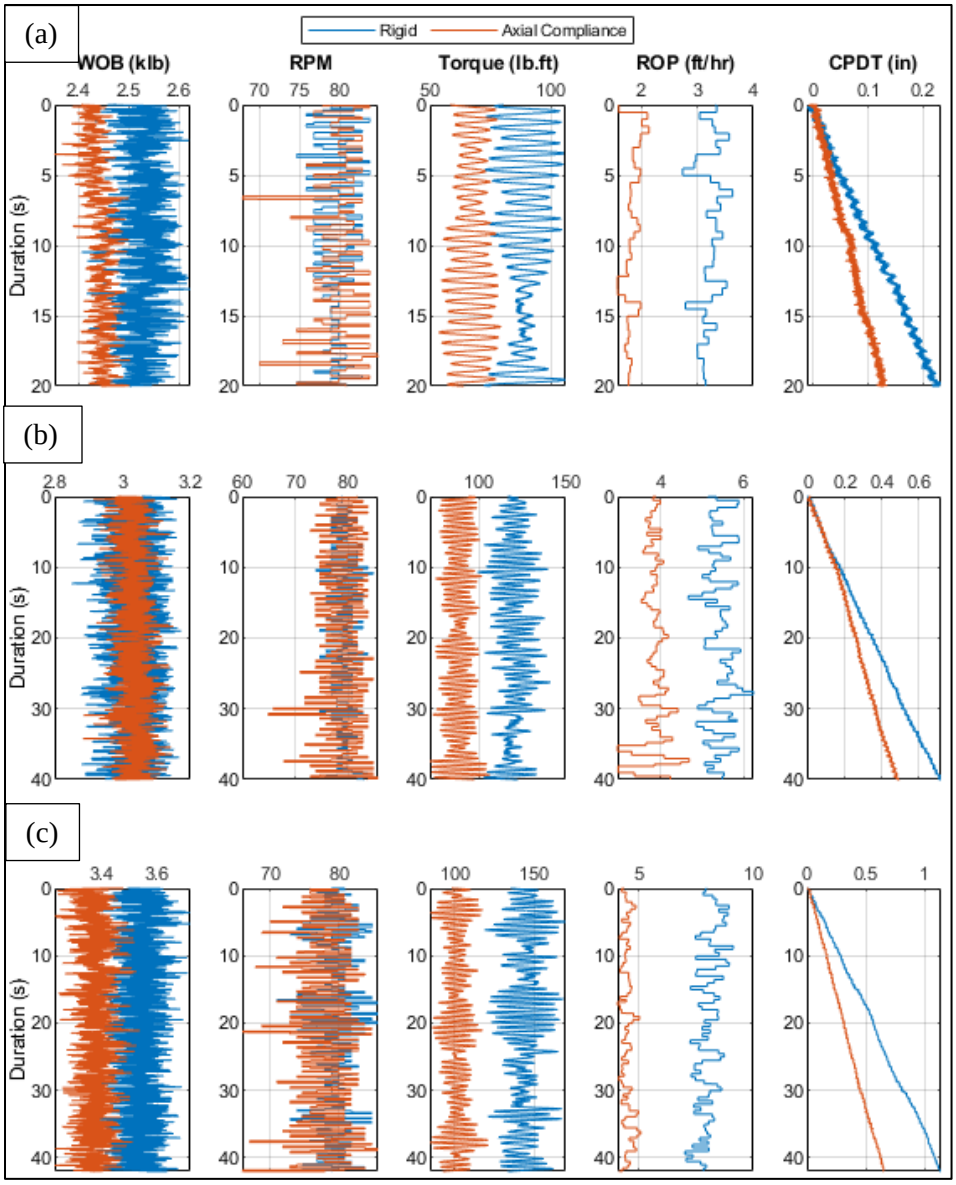

Figure 4.6. Rigid Vs AC Dynamics for 5-Bladed PDC Bit at 80 RPM (a) W1, (b) W2, and (c) W3

At higher rotational speeds, i.e., 120 and 160 RPM, the 4-bladed and 5-bladed bits show similar dynamics behavior, as shown in Appendix A, Figure A.10 and Figure A.11 for the 4-bladed bit, Figure A.12 and Figure A.13 for the 5-bladed bit.

4.1.4 Rigid Vs combined axial and torsional compliance

The combined axial and torsional compliance dynamics versus rigid for the 4-blade test is shown in Figure 4.7 at 80 RPM and three WOB levels. The WOB, RPM, and Torque depict erratic

behavior as the WOB level increases in the combined configuration as compared to the rigid drillstring. A reduction in ROP is seen for the combined configuration compared to the rigid drillstring.

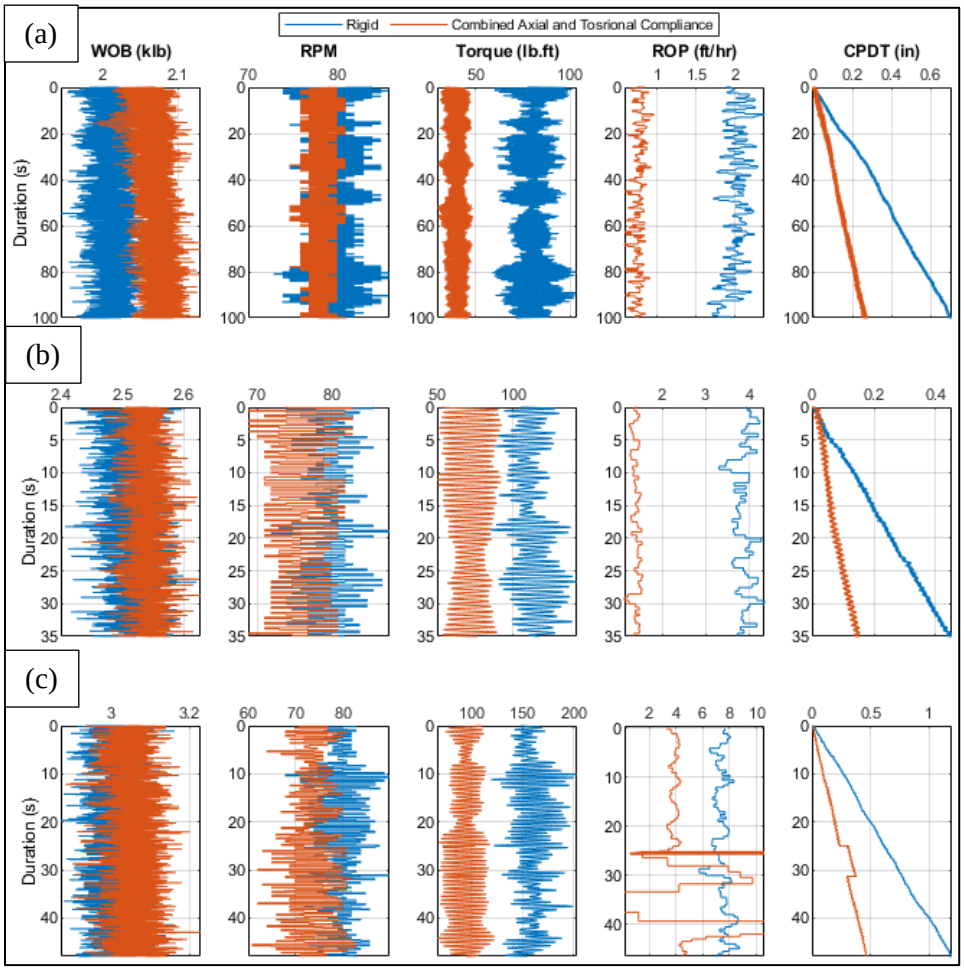

Figure 4.7. Rigid Vs CAT Dynamics for 4-Bladed PDC Bit at 80 RPM (a) W1, (b) W2, and (c) W3

The combined axial and torsional compliance dynamics versus the rigid for the 5-bladed test is shown in Figure 4.8 at 80 RPM and three WOB levels. As the WOB increases, the combined compliance shows lower erratic behavior compared to the rigid drillstring. The rotational speed and torque depict a similar outcome as the 4-bladed test. As the WOB increases, the ROP for combined configuration increases.

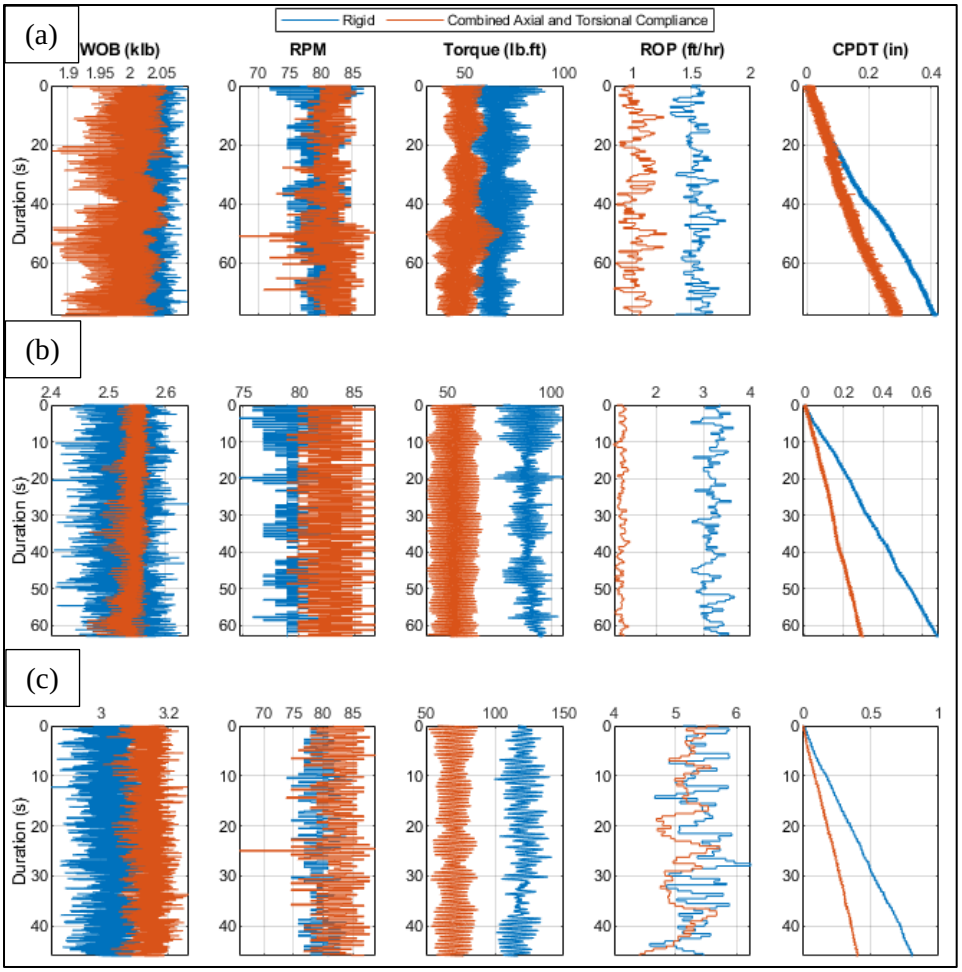

Figure 4.8. Rigid Vs CAT Dynamics for 5-Bladed PDC Bit at 80 RPM (a) W1, (b) W2, and (c) W3

At higher rotational speeds, i.e., 120 and 160 RPM, the 4-bladed and 5-bladed bits show similar dynamics behavior, as shown in Appendix A, Figure A.13 and Figure A.14 for the 4-bladed bit and Figure A.15 and Figure A.16 for the 5-bladed bit.

4.2 Frequency Domain Analysis of Drillstring Configurations

The Power Spectral Density (PSD) was used to convert the time domain drilling data to the frequency domain to determine the dominant axial and torsional frequencies of each test configuration at different operating conditions. The results of the effect of drillstring configurations on the axial and torsional frequencies are first presented for each bit. Then, a comparison of the

dominant frequencies is performed based on the drillstring configurations and the two different bits.

4.2.1 Frequency analysis of the 4-bladed PDC bit

For each drilling configuration, WOB level, and applied rotation speed, the PSD was calculated for several drilling parameters to identify the axial and torsional frequencies as shown in the methodology section (Figure 3.8). The analysis was done for all drilling configurations, where Table 4.1 summarizes the determined axial (f_A) and torsional (f_T) frequencies in hertz (Hz) for the 4-bladed PDC bit. The color scheme represents the time data used to identify each particular frequency as outlined in the methodology (Table 3.11).

Table 4.1. Axial and Torsional Frequencies for the 4-Bladed PDC Bit

Operating Speed	Configuration	W1		W2		W3	
		f_A	f_T	f_A	f_T	f_A	f_T
80 RPM	R	6.5	4	5.25	4.25	3.5	3.25
	FW	5.25	2.5	5.25	3.75	3.5	3.5
	TC	5.25	4	5.5	4	3.25	3.5
	AC	2.75	4	2.5	5.25	3	4
	CAT	3.75	2.5	2.5	3.75	5.25	2.5
120 RPM	R	5.75	5.75	3.75	3.75	3	7.75
	FW	3.75	3.75	3.75	3.75	4.25	5
	TC	4.25	1.5	4.25	1.25	3.25	1.25
	AC	4.25	4.25	3.75	5.75	3.75	3.75
	CAT	3.75	3.75	3.75	1.75	3.5	1.75
160 RPM	R	5.25	5.25	2.25	3.75	2.5	6.25
	FW	5.25	4.75	2.75	4	2.75	4
	TC	5.25	5.5	5.25	1.25	5.5	1.25
	AC	2.5	5.25	2.25	5.25	2.5	5.25
	CAT	2.75	5.25	2.75	5.25	2.75	5.25

For the rigid configuration in the axial direction at 80 RPM, Table 4.1 shows that as the WOB increases, the axial frequency decreases. At 120 RPM, the trend is reversed, as the WOB increases, the axial frequency decreases. At 160 RPM, the axial frequency decreases as WOB increases to

intermediate WOB from 5.25 Hz to 2.25 Hz and again increases at higher WOB to 2.5 Hz. For the torsional frequencies at 80 RPM, the rigid drillstring shows an increase in frequency moving from lower to intermediate WOB from 4 to 4.25 Hz and then decreasing to 3.25 Hz at a higher WOB level. At 120 RPM, as the WOB increases from low to intermediate, the torsional frequency decreases from 5.75 Hz to 3.75 Hz and increases to 5 Hz at a higher WOB level. A similar trend is followed at the 160 RPM test.

From the above result, it is hard to link a direct correlation between the frequencies of rigid configuration and other drillstring configurations. To compare the different drillstring configuration frequencies, the axial and torsional frequencies were averaged based on WOB levels and applied rotational speed and the percent difference for each configuration is calculated and compared to the rigid configuration as shown in Table 4.2

Table 4.2. Average Frequencies with Percent Difference of the 4-Bladed Bit Tests

Configuration	Average Frequencies		Percent Difference (%)	
	f_A	f_T	Axial	Torsional
R	2.4	2.8	-	-
FW	2.3	2.2	3.4	25.7
TC	2.6	1.5	-9.6	87.2
AC	1.7	2.7	38.5	2.9
CAT	1.9	2.0	22.8	38.6

Comparing the average axial and torsional frequencies of the rigid with other configurations, a clear comparison can be made. The axial frequency for the flywheel decreases by 0.1 Hz (3.4%) and the torsional frequency decreases by 0.6 Hz (25.7%) compared to the rigid drillstring, this is due to the added weight of the flywheel resulting in an increased rotary moment of inertia. The axial frequency of torsional compliance increases by 0.4 Hz (-9.6%) and is reduced by 1.3 Hz (87.2%) in the torsional direction compared to the rigid configuration, this is because suppressing the drillstring in one direction arouses vibration in the other direction. Similarly for axial compliance configuration, a decrease of 0.7 Hz (38.5%) is seen in the axial direction and a negligible decrease

of 0.1 Hz (2.9%) is seen in the torsional direction when compared to the rigid drillstring. For the combined configuration a decrease of 0.5 Hz (22.8%) is seen in the axial direction and 0.8 Hz (38.6%) in the torsional direction.

4.2.2 Frequency analysis of the 5-bladed PDC bit

A similar procedure was followed for the 5-blade PDC bit frequency analysis. Table 4.3 shows the identified axial and torsional frequencies for 5-bladed PDC bit tests for all configurations.

Table 4.3. Axial and Torsional Frequencies for 5-Bladed PDC Bit

Operating Speed	Configuration	W1		W2		W3	
		f_A	f_T	f_A	f_T	f_A	f_T
80 RPM	R	2.5	5.25	2.5	6.75	0.5	6
	FW	2.5	6.25	2.25	4.75	0.25	0.75
	TC	3.75	1.25	4.5	0.25	3.5	3.25
	AC	1.5	2.5	1	4	0.75	3.5
	CAT	1.25	1.5	1.25	1.5	1.25	1.5
120 RPM	R	5.75	3.75	1.75	0.5	1.75	4.5
	FW	5.75	3.75	0.75	0.5	1.75	4.75
	TC	4.25	1.75	4.25	2.25	5.25	2.25
	AC	1.75	1.75	1.75	2.25	1.75	2.25
	CAT	1.75	2.25	1.75	2.25	1.75	2.25
160 RPM	R	2.5	2.5	0.5	2.75	0.75	3.75
	FW	2.5	2.5	0.5	2.5	0.75	3.25
	TC	2.5	2.5	2.5	2.75	2.5	3.25
	AC	2.5	3	2.5	5.5	2.5	5.25
	CAT	2.5	5.25	2.5	5.25	0.25	5.5

Similar to the 4-bladed bit analysis, the axial f_A and torsional f_T frequencies were averaged per configuration as shown in Table 4.4 and the rigid configuration was compared with the other configurations.

Table 4.4. Average Frequencies with Percent Difference of the 5-Bladed Bit Tests

Configuration	Average Frequencies		Percent Difference (%)	
	f_A	f_T	Axial	Torsional
R	1.2	2.2	-	-

FW	1.1	1.8	8.8	23.3
TC	2.1	1.2	-43.9	83.3
AC	1.0	1.9	15.6	19.2
CAT	0.9	1.7	29.8	31.2

The axial and torsional frequencies of the flywheel show decreases of 0.1 Hz (8.8%) and 0.4 Hz (23.3%) compared to the rigid drillstring. The torsional compliance shows an increase of 0.9 Hz (-43.9%) in the axial direction and a decrease of 1 Hz (83.3%) in the torsional direction. The axial compliance shows a decrease of 0.2 Hz (15.6%) in the axial direction and 0.3 Hz (19.2%) in the torsional direction, the decreases are insignificant. For the combined compliance, the axial frequency shows a decrease of 0.3 Hz (29.8%) and 0.5 Hz (31.2%) in the torsional direction compared to the rigid drillstring. Overall, the configurations don't depict a significant frequency decrease compared to the rigid configuration.

4.2.3 Effect of bit design on the axial and torsional vibrations

The calculated average axial and torsional frequencies were used to study the effect of bit design on drill bit vibrations. Table 4.5 shows the average axial and torsional vibration frequency for each bit and the percentage difference between the 4 and 5-bladed bit designs.

Table 4.5. Average Frequencies with Percent Difference of 4 and 5-Bladed PDC Bits

Dynamics	**4-Blade**		**5-Blade**		**Percent Difference (%)**	
	f_A	**f_T**	**f_A**	**f_T**	**Axial**	**Torsional**
R	2.4	2.8	1.2	2.2	51.0	18.8
FW	2.3	2.2	1.1	1.8	53.4	17.1
TC	2.6	1.5	2.1	1.2	21.0	17.0
AC	1.7	2.7	1.0	1.9	41.3	29.8
CAT	1.9	2.0	0.9	1.7	53.7	14.2

In comparison to the 4-bladed PDC bits, the remainder of the configurations in 5-bladed PDC bits show a comparable shift in frequencies in both the axial and torsional directions. The percentage decrease indicates a reduction in frequencies from 4-bladed to 5-bladed PDC bit. The rigid

configuration reduces 51% in the axial direction and 18.8% in the torsional direction when using a 5-balded PDC bit for the test. In the flywheel configuration, a 53.4% reduction in the axial and 17.1% in the torsional direction when comparing the 4-bladed to the 5-bladed bits. In the torsional compliance configuration, a 21% reduction in the axial direction and 17% in the torsional direction when comparing the 4-bladed to the 5-bladed bits. In the axial compliance configuration, a 41.3% reduction in the axial direction and a 29.8% reduction in the torsional direction when comparing the 4-bladed to the 5-bladed bits. In the combined axial and torsional compliance, a 53.7% reduction in the axial direction and a 14.2% reduction in the torsional direction when comparing the 4-bladed to the 5-bladed bits.

4.3 Evaluation of Bit-Rock Interaction Models

The rigid test configuration was selected to evaluate the bit-rock interaction models since the intention in this section is to evaluate the external forces acting on the drill bit rather than the drillstring vibration compliance. The evaluation considers the ability of each model in predicting the measured downhole WOB and torque at a low and high range of WOB, i.e., 1500 lbs and 5000 lbs.

Using Christoforou and Yigit (2003) model, the equation of motion (Equations 49 and 54) was solved numerically at WOB of 1500 and 5000 lbs and a rotation speed of 80 RPM. Figure 4.9 shows the coupled bit-rock interaction for the rigid 4-bladed PDC bit data at 80 RPM and low WOB of 1500 lbs. In the first graph (a) the WOB represents the applied WOB for the test, DWOB represents the downhole WOB reading and MWOB represents the model WOB result. The model WOB differs by about 200 lbs from the downhole WOB data. In the second graph (b), STQ represents the surface torque applied during the test, MTOB represents the model TOB and DTOB is the downhole TOB reading from the test. The third graph (c) is a zoomed-in version of graph (b) to examine the MTOB and DTOB. The MTOB matches the DTOB data with fewer vibrations. In the

fourth graph (d), RPM, MRPM, and DRPM represent the applied, model, and downhole rotational speeds. The fifth graph (e) is a zoomed-in version of the fourth graph (d) to observe the rotational speeds. The model RPM does not show a lot of variation compared to DRPM and applied RPM; it is nearly constant.

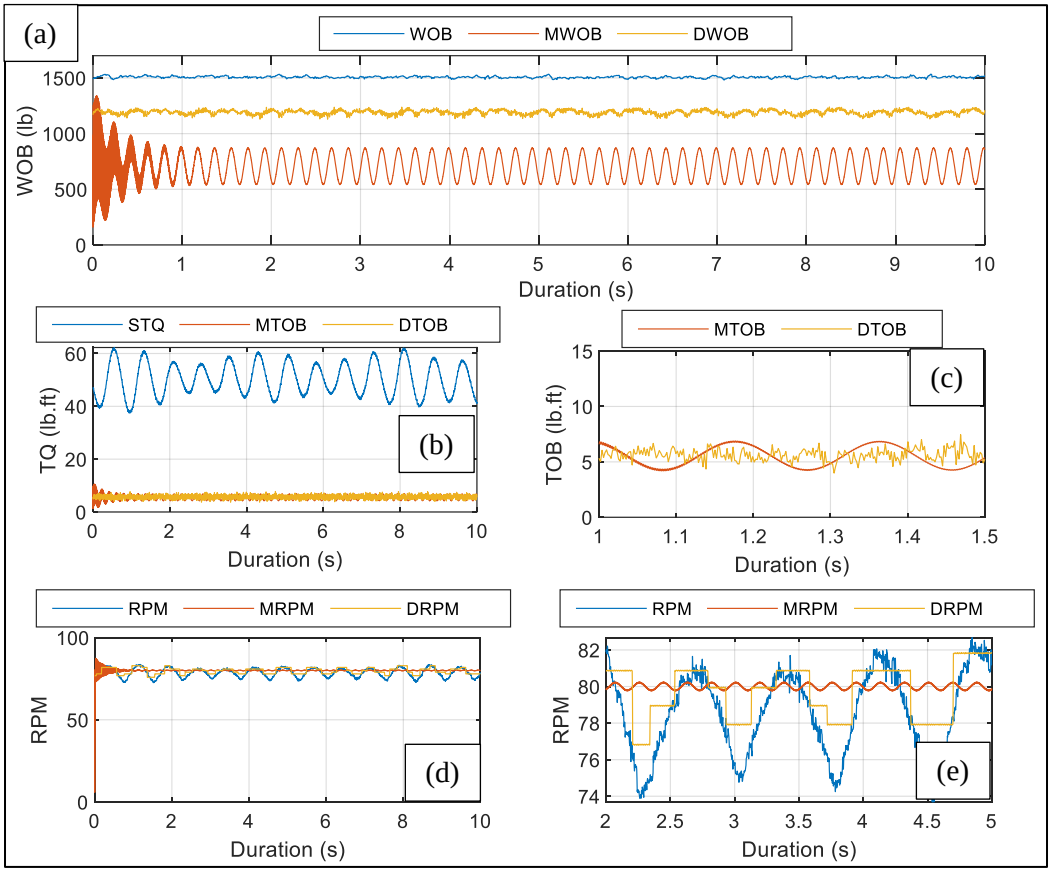

Figure 4.9. Christoforou and Yigit (2003) Model Comparison for 4-Blade Rigid at 80 RPM and W1

Figure 4.10 shows Christoforou and Yigit (2003) BRI model compared with the rigid configuration at 80 RPM and high WOB (W8). Similar results can be seen, the MWOB does not match the DWOB data with a difference of 900 lbs. The MTOB data matches the DTOB data but with reduced vibrations and DRPM shows some fluctuations at the start but becomes constant after 1 second.

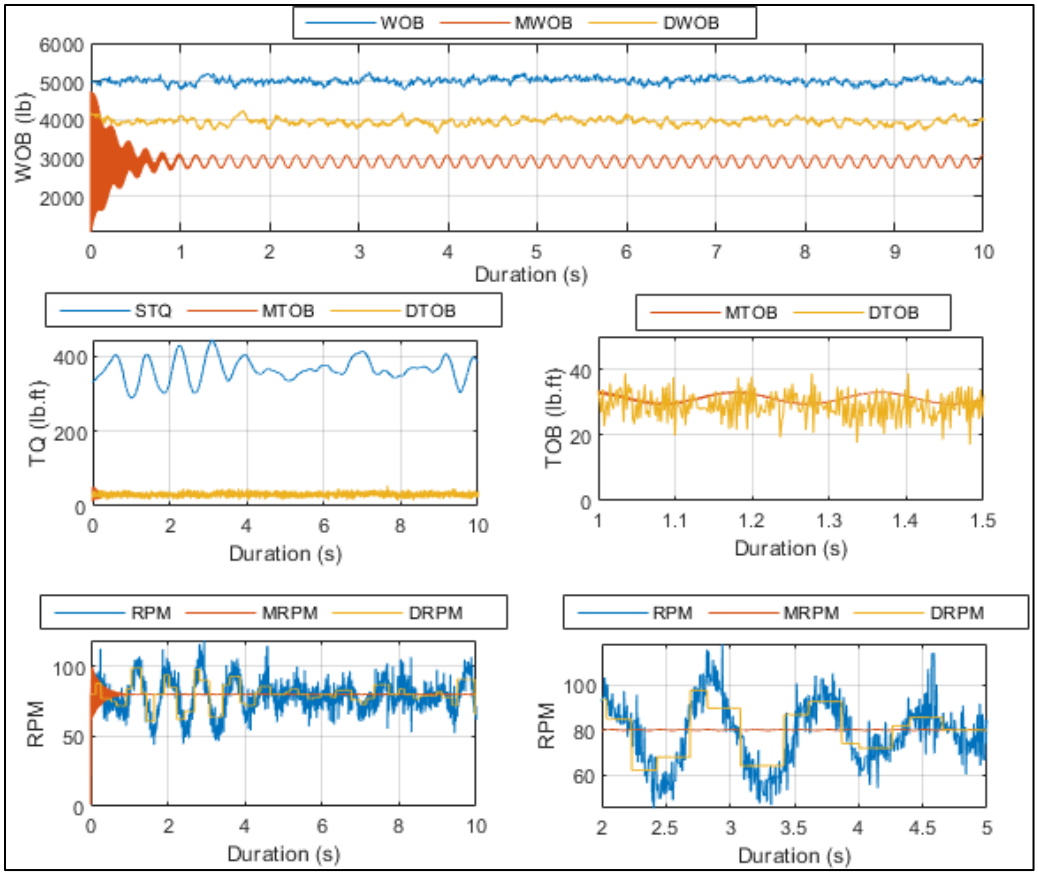

Figure 4.10. Christoforou and Yigit (2003) Model Comparison for 4-Blade Rigid at 80 RPM and W8

The BRI modeling comparison of Navarro-López and Cortés (2007) for rigid at 80 RPM and W1 is shown in Figure 4.11. Since the model is uncoupled torsional mode, there is no MWOB. The model generates a lot of noise for MTOB and MRPM compared to the testing data.

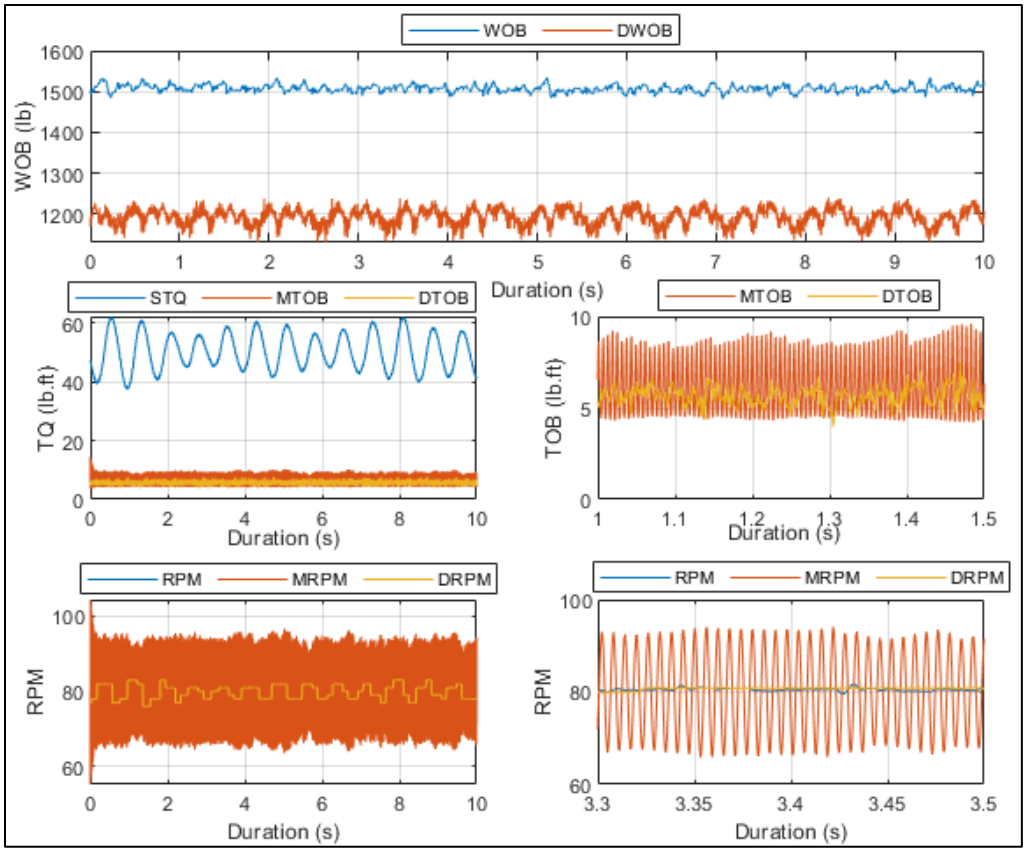

Figure 4.11. Navarro-López and Cortés (2007) Model Comparison for 4-Blade Rigid at 80 RPM and W1

Figure 4.12 shows Navarro-López and Cortés (2007) model comparison at W8. At higher WOB, the modeling torque aligns accurately with the testing downhole torque data, but a lot of fluctuation can be seen in MRPM compared to DRPM. The model is very sensitive to RPM and bit constants.

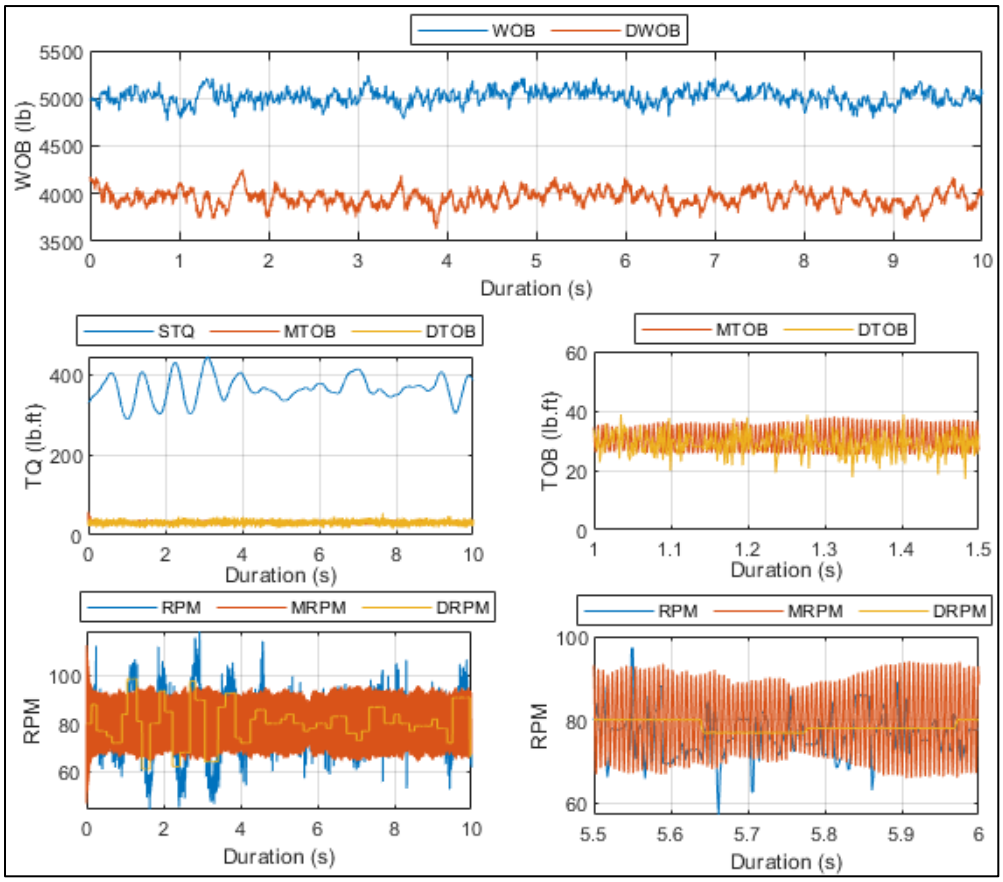

Figure 4.12. Navarro-López and Cortés (2007) Model Comparison for 4-Blade Rigid at 80 RPM and W8

The next model is Huang et al. (2018), Figure 4.13 shows the uncoupled torsional BRI for rigid at 80 RPM and W1. Similar to Navarro's model, a significant variation can be seen in MRPM compared to the applied and measured downhole RPM. The DTOB and MTOB coincide adequately. The model is comparatively more sensitive when a lower WOB is applied.

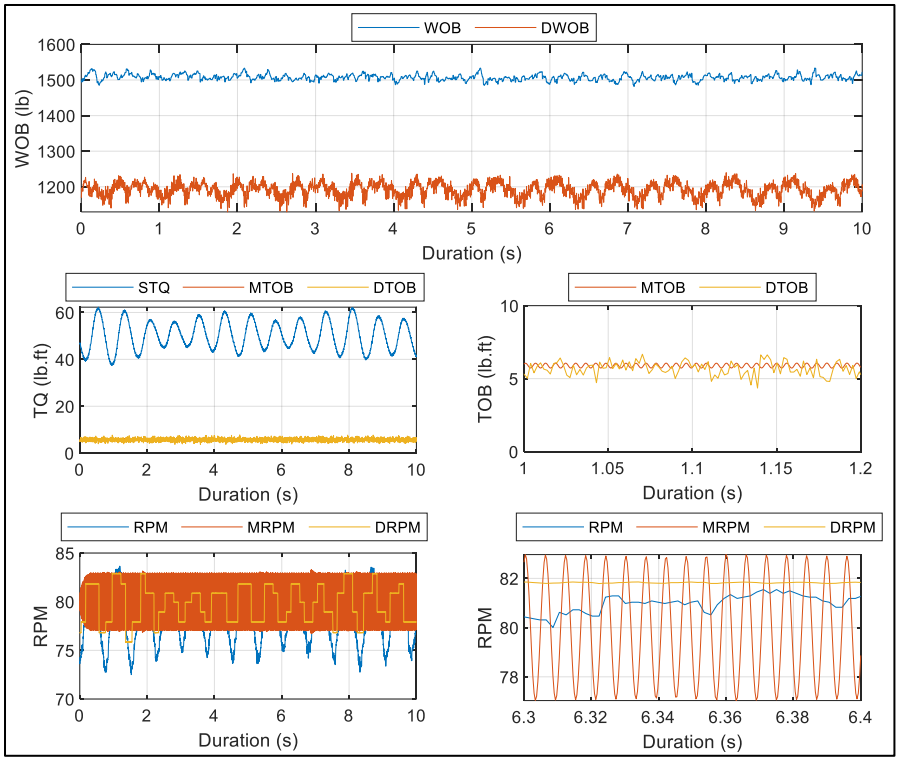

Figure 4.13. Huang et al. (2018) Model Comparison for 4-Blade Rigid at 80 RPM and W1

Figure 4.14 shows Huang et al. (2018) BRI model comparison at W8. A difference can be seen from lower to higher WOB, the MTOB and MRPM are almost steady with minor fluctuations.

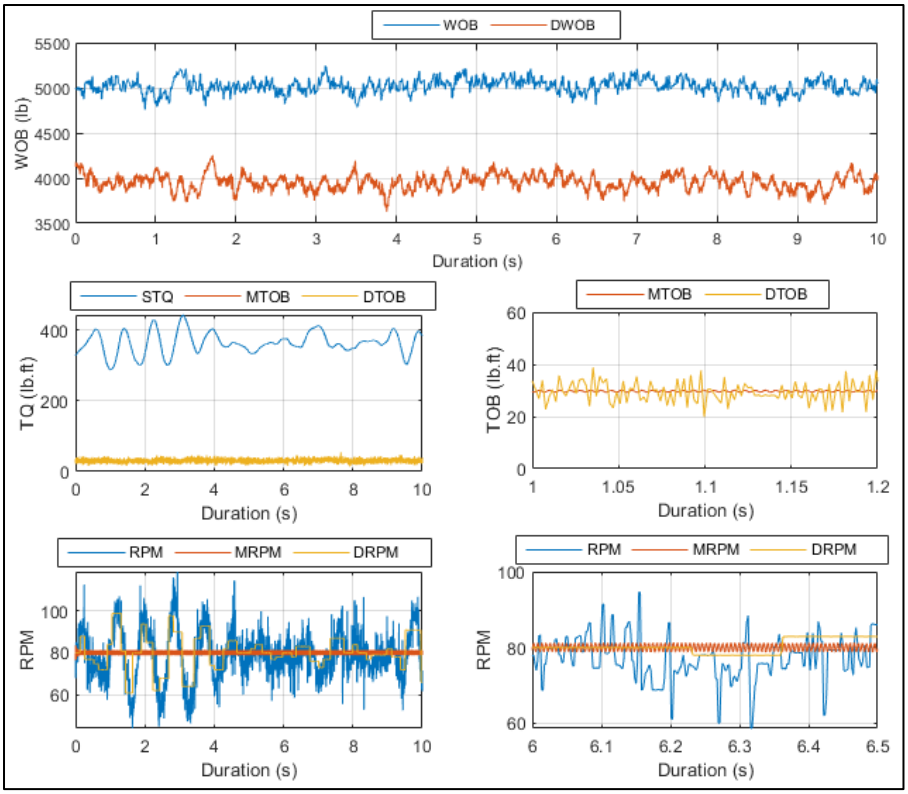

Figure 4.14. Huang et al. (2018) Model Comparison for 4-Blade Rigid at 80 RPM and W8

Figure 4.15 shows Sampaio et al. (2007) uncoupled torsional BRI model at 80 RPM and W1. MTOB shows minor fluctuation compared to DTOB and MRPM has a substantially larger variation compared to the applied and downhole RPM.

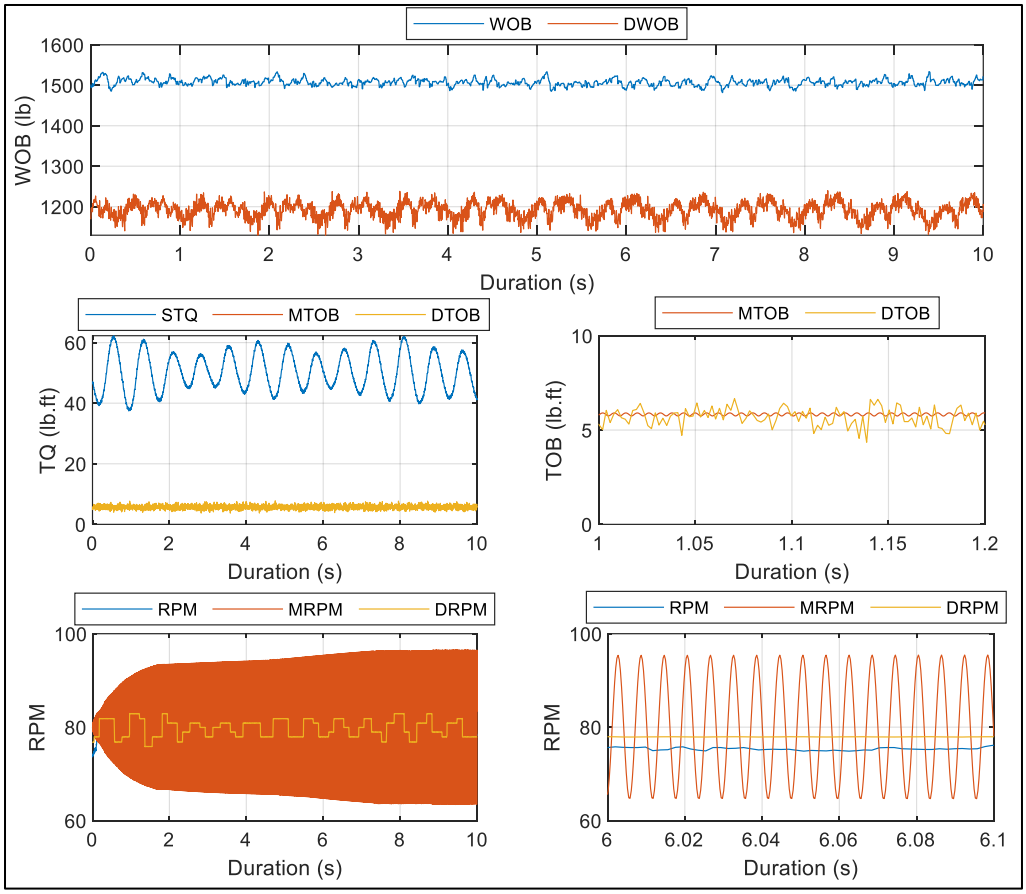

Figure 4.15. Sampaio et al. (2007) Model Comparison for 4-Blade Rigid at 80 RPM and W1

Figure 4.16 shows Sampaio et al. (2007) BRI interaction modeling comparison for W8. The model TOB again shows minor fluctuation compared to DTOB and the model RPM has lower variation compared to the applied RPM and DRPM. The model is sensitive to lower WOB compared to higher WOB levels.

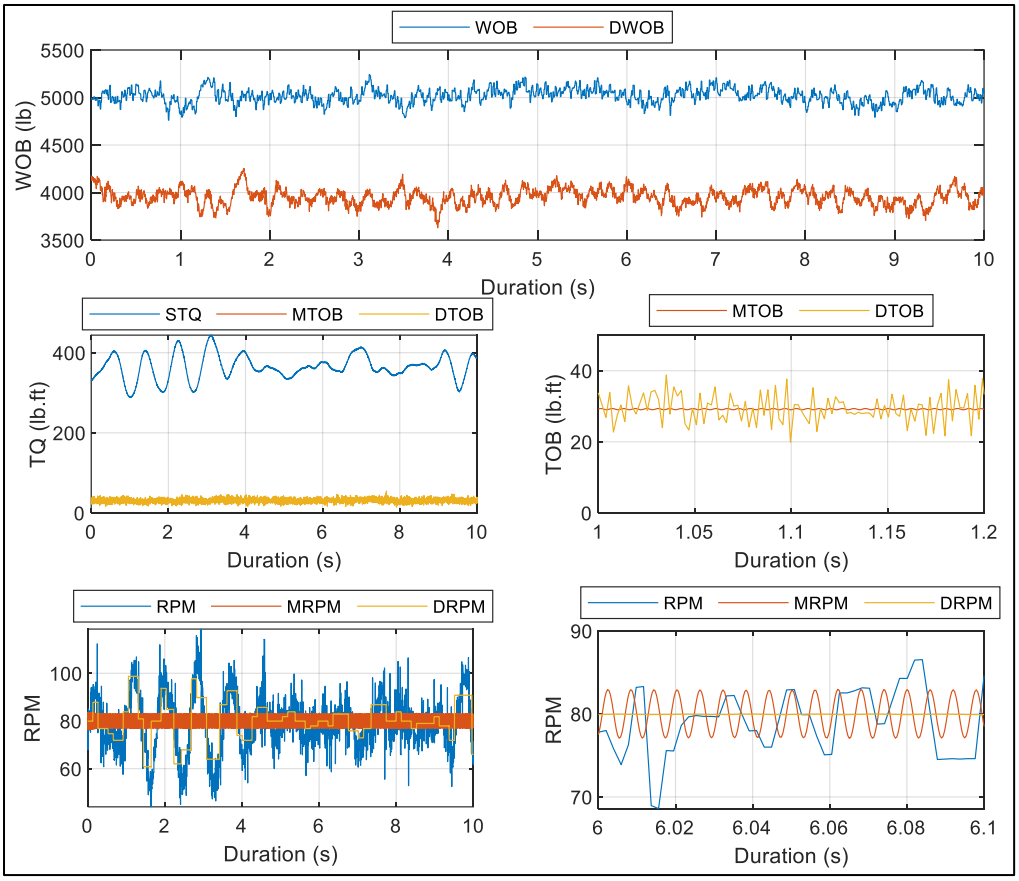

Figure 4.16. Sampaio et al. (2007) Model Comparison for 4-Blade Rigid at 80 RPM and W8

CHAPTER V

5 DISCUSSION

Understanding and overcoming the effect of vibration can eliminate issues related to drillstring dynamics and can optimize drilling performance. Drill bit performance is influenced by drillstring harmonics, which is a function of the drillstring design.

5.1 Effect of Drillstring Vibration on Drill Bit Dynamics

The objective of performing a time domain analysis on four different drillstring configurations and comparing it with the rigid testing data is to understand the effect of drillstring dynamics and how each configuration affected the bit performance. The rigid configuration, without imposed vibration, is used as a testing standard in this work. The addition of the flywheel to the drillstring shows a reduction in the natural frequencies of a laboratory drillstring. The flywheel worked as an energy storage device and helps to provide a steady RPM, minimizing the dramatic decrease in speed caused by stick-slip vibrations and providing energy to the drillstring when it is required to overcome stick-slip. From the visual representation of drillstring dynamics, torsional compliance also provides a stable RPM. Reducing axial vibration causes significant fluctuation in WOB as compared to the rigid configuration, this fluctuation or variation can potentially result in a bit-bounce. In a laboratory context, combining axial and torsional compliance provides an equivalent field drillstring design. The combined configuration showed increased fluctuations in WOB, RPM, and torque compared to the rigid drillstring. As for time domain analysis, there is

no clear signature of bit dynamics, and it is difficult to analyze the effect of each drillstring configuration. However, from a drilling performance point of view, the rigid configuration showed the highest average ROP compared to other configurations followed by the flywheel configuration. The lowest average ROP was generated by the combined and axial compliance configurations.

The purpose of performing frequency analysis is to study the change of dominant frequency in each drillstring tests configurations and the two different bits, which is also used to prove the fact that conventional laboratory drillstring designs are having higher frequencies in both torsional and axial directions compared to the drillstring used on the field.

The results demonstrate that in both the 4 and 5-bladed PDC tests, the four drillstring configurations show a decrease in the axial and torsional frequencies except for the torsional compliance configuration test which showed a slight increase in the axial frequency when compared to the rigid configuration. The combined axial and torsional compliance is the closest to an actual field drillstring, therefore comparing the field drillstring configuration (CAT) to the laboratory drillstring (R), a noticeable 22.8% frequency decrease can be seen in the axial direction and a 38.6% decrease in the torsional direction using the 4-balded PDC bit. For the 5-bladed PDC bit, the axial frequency decrease is 29.8% and 31.2% in the torsional direction. Therefore, the average frequency decrease of combined compliance in both the 4 and 5-bladed PDC tests is 26.3% in the axial direction and 35% in the torsional direction.

In comparison to the 4-bladed PDC bit, the remainder of the 5-bladed PDC bit configurations exhibits a drastic reduction in frequency in both the axial and torsional directions. This is due to the increased number of cutters in the 5-bladed PDC bit, the applied axial load is comparatively reduced on each cutter compared to the 4-bladed PDC bit. Table 5.1 shows the frequency decrease in the combined configuration when using the 4-bladed versus the 5-bladed PDC bits. The use of the 5-bladed PDC bit in hard rock reduces axial vibrations by 53.7% in the axial direction and 14.2% in the torsional direction.

Table 5.1. Average Frequencies with Percent Difference of CAT Using 4 and 5-Bladed PDC Bit

Configuration	4-Blade		5-Blade		Percent Difference (%)	
	f_A	f_T	f_A	f_T	Axial	Torsional
CAT	1.9	2.0	0.9	1.7	53.7	14.2

5.2 Bit-Rock Interaction Modelling Comparison

The sensitivity analysis of various bit-rock interaction models showed that the coupled axial and torsional model of Christoforou and Yigit (2003) and the uncoupled torsional model of Navarro-López and Cortés (2007) depict a good fit for TOB data compared to other models. The uncoupled torsional models of Huang et al. (2018) and Sampaio et al. (2007) show very minimal fluctuations in model TOB and have erratic rotational speed at lower WOB levels, this is because the models are extremely sensitive towards the frictional law constants. None of the models were able to accurately predict the laboratory testing data, they are either very erratic or very stable.

CHAPTER VI

6 CONCLUSIONS

Understanding and overcoming the effect of vibration can eliminate issues related to drillstring dynamics and can optimize drilling performance. Drill bit performance is influenced by drillstring harmonics, which is a function of the drillstring design, each test drilling configuration affects bit performance differently. For a realistic bit performance evaluation in laboratory settings, considering the natural vibration frequencies for a specific drillstring design will ensure the compatibility of the drill bit with the selected bottom hole assembly. The most typical way to test drill bits in laboratories is with a rigid configuration, which does not accurately represent the performance and field conditions that are encountered in field applications.

The combined axial and torsional compliance, mimicking field drillstring, showed an average frequency decrease of 26.3% in the axial direction and 35% in the torsional direction compared to the rigid laboratory drillstring. The 5-bladed PDC bit in hard rock showed lower axial and torsional vibrations by 53.7% and 14.2% respectively, compared to the 4-bladed bit design.

The bit-rock interaction models comparison showed that most models are very sensitive to drilling operating parameters. The use of such models to optimize drilling operating parameters to avoid drillstring vibration might not reflect the actual conditions seen in the field.

REFERENCES

Aarsnes, U. J. F., & Van De Wouw, N. (2019). Axial and torsional self-excited vibrations of a distributed drill-string. *Journal of Sound and Vibration*, *444*, 127-151. https://doi.org/10.1016/j.jsv.2018.12.028

Al Sairafi, F. A., Al Ajmi, K. E., Yigit, A. S., & Christoforou, A. P. (2016, 2016). Modeling and Control of Stick Slip and Bit Bounce in Oil Well Drill Strings.

Aldred, W. D., & Sheppard, M. C. (1992, 1992). Drillstring Vibrations: A New Generation Mechanism and Control Strategies.

Ashley, D. K., McNary, X. M., & Tomlinson, J. C. (2001, 2001). Extending BHA Life with Multi-Axis Vibration Measurements.

Barnett, L., Al Dushaishi, M. F., & Mubarak Hussain Khan, M. F. (2022). Experimental investigation of drillstring torsional vibration effect on rate of penetration with PDC bits in hard rock. *Geothermics*, *103*, 102410. https://doi.org/10.1016/j.geothermics.2022.102410

Belokobyl'skii, S. V., & Prokopov, V. K. (1982). Friction-induced self-excited vibrations of drill rig with exponential drag law. *Soviet Applied Mechanics*, *18*(12), 1134-1138. https://doi.org/10.1007/bf00882226

Brett, J. F. (1992). The Genesis of Bit-Induced Torsional Drillstring Vibrations. *SPE Drilling Engineering*, *7*(03), 168-174. https://doi.org/10.2118/21943-pa

Christoforou, A. P., & Yigit, A. S. (2003). Fully coupled vibrations of actively controlled drillstrings. *Journal of Sound and Vibration*, *267*(5), 1029-1045. https://doi.org/10.1016/s0022-460x(03)00359-6

Depouhon, A., Denoël, V., & Detournay, E. (2015). Numerical simulation of percussive drilling. *International Journal for Numerical and Analytical Methods in Geomechanics*, *39*(8), 889-912. https://doi.org/10.1002/nag.2344

Dunayevsky, V. A., & Abbassian, F. (1998). Application of Stability Approach to Bit Dynamics. *SPE Drilling & Completion*, *13*(02), 99-107. https://doi.org/10.2118/30478-pa

Elsayed, M., & Raymond, D. (1999). *Measurement and analysis of Chatter in a Compliant Model of a Drillstring Equipped With a PDC Bit*.

Elsayed, M. A., & Raymond, D. W. (2002). *Analysis of Coupling Between Axial and Torsional Vibration in a Compliant Model of a Drillstring Equipped With a PDC Bit* https://doi.org/10.1115/ETCE2002/STRUC-29002

Garcia-Gavito, D., & Azar, J. J. (1994). Proper Nozzle Location, Bit Profile, and Cutter Arrangement Affect PDC-Bit Performance Significantly. *SPE Drilling & Completion*, *9*(03), 167-175. https://doi.org/10.2118/20415-pa

Glowka, D. A. (1987). *Development of a method for predicting the performance and wear of PDC (polycrystalline diamond compact) drill bits*. https://dx.doi.org/10.2172/5591640

Hareland, G., Nygaard, R., Yan, W., & Wise, J. L. (2009). Cutting Efficiency of a Single PDC Cutter on Hard Rock. *Journal of Canadian Petroleum Technology*, *48*(06), 60-65. https://doi.org/10.2118/09-06-60

Hohl, A., Kulke, V., Kueck, A., Herbig, C., Reckmann, H., & Ostermeyer, G.-P. (2020, 2020). The Nature of the Interaction Between Stick/Slip and High-Frequency Torsional Oscillations.

Huang, Z., Xie, D., Xie, B., Zhang, W., Zhang, F., & He, L. (2018). Investigation of PDC bit failure base on stick-slip vibration analysis of drilling string system plus drill bit. *Journal of Sound and Vibration*, *417*, 97-109. https://doi.org/10.1016/j.jsv.2017.11.053

Kamel, J. M., & Yigit, A. S. (2014). Modeling and analysis of stick-slip and bit bounce in oil well drillstrings equipped with drag bits. *Journal of Sound and Vibration*, *333*(25), 6885-6899. https://doi.org/10.1016/j.jsv.2014.08.001

Kapitaniak, M., Vaziri Hamaneh, V., Páez Chávez, J., Nandakumar, K., & Wiercigroch, M. (2015). Unveiling complexity of drill–string vibrations: Experiments and modelling. *International Journal of Mechanical Sciences*, *101-102*, 324-337. https://doi.org/https://doi.org/10.1016/j.ijmecsci.2015.07.008

Kapitaniak, M., Vaziri, V., Páez Chávez, J., & Wiercigroch, M. (2018). Experimental studies of forward and backward whirls of drill-string. *Mechanical Systems and Signal Processing*, *100*, 454-465. https://doi.org/10.1016/j.ymssp.2017.07.014

Katz, S., & Chilingarian, G. V. (1996). Wave propagation in petroleum engineering@ Modern applications to drillstring vibrations, measurement-while-drilling, swab-surge, and geophysics. *Journal of Petroleum Science and Engineering*.

Khulief, Y. A., Al-Sulaiman, F. A., & Bashmal, S. (2007). Vibration analysis of drillstrings with self-excited stick–slip oscillations. *Journal of Sound and Vibration*, *299*(3), 540-558. https://doi.org/https://doi.org/10.1016/j.jsv.2006.06.065

Kriesels, P. C., Keultjes, W. J. G., Dumont, P., Huneidi, I., Owoeye, O. O., & Hartmann, R. A. (1999, 1999). Cost Savings through an Integrated Approach to Drillstring Vibration Control.

Leine, R. I., Van Campen, D. H., & Keultjes, W. J. G. (2002). Stick-slip Whirl Interaction in Drillstring Dynamics. *Journal of Vibration and Acoustics*, *124*(2), 209-220. https://doi.org/10.1115/1.1452745

Li, Z., & Guo, B. (2007). Analysis of Longitudinal Vibration of Drill String in Air and Gas Drilling.

Manzatto, L., & Trindade, M. (2011). *Analysis of stability and performance of an oil well drilling operation subject to stick-slip using non-collocated linear velocity control*.

Mendil, C., Kidouche, M., Doghmane, M. Z., Benammar, S., & Tee, K. F. (2021). Rock–bit interaction effects on high-frequency stick-slip vibration severity in rotary drilling systems. *Multidiscipline Modeling in Materials and Structures*, *17*(5), 1007-1023. https://doi.org/10.1108/mmms-10-2020-0256

Miyazaki, K., Ohno, T., Karasawa, H., & Imaizumi, H. (2019). Performance of polycrystalline diamond compact bit based on laboratory tests assuming geothermal well drilling. *Geothermics*, *80*, 185-194. https://doi.org/10.1016/j.geothermics.2019.03.006

Monteiro, H. L. S., & Trindade, M. A. (2017). Performance analysis of proportional-integral feedback control for the reduction of stick-slip-induced torsional vibrations in oil well drillstrings. *Journal of Sound and Vibration*, *398*, 28-38. https://doi.org/10.1016/j.jsv.2017.03.013

Navarro-López, E. M., & Cortés, D. (2007). Avoiding harmful oscillations in a drillstring through dynamical analysis. *Journal of Sound and Vibration*, *307*(1-2), 152-171. https://doi.org/10.1016/j.jsv.2007.06.037

Navarro-Lopez, E. M., & Suarez, R. (2004). Practical approach to modelling and controlling stick-slip oscillations in oilwell drillstrings.

Raymond, D. W., Elsayed, M. A., Polsky, Y., & Kuszmaul, S. S. (2008). Laboratory Simulation of Drill Bit Dynamics Using a Model-Based Servohydraulic Controller. *Journal of Energy Resources Technology*, *130*(4), 043103. https://doi.org/10.1115/1.3000142

Raymond, D. W., Scott S. Kuszmaul, Elton K. Wright, & Elsayed., M. A. (2005). Controllable Damper Demonstrates Improved Stability for PDC Bits Drilling Hard-Rock Formations. *GRC Transactions*, *29*.

Real, F. F., Batou, A., Ritto, T. G., Desceliers, C., & Aguiar, R. R. (2018). Hysteretic bit/rock interaction model to analyze the torsional dynamics of a drill string. *Mechanical Systems and Signal Processing*, *111*, 222-233. https://doi.org/10.1016/j.ymssp.2018.04.014

Ren, F., & Wang, B. (2017). Modeling and analysis of stick-slip vibration and bit bounce in drillstrings. *Journal of Vibroengineering*, *19*(7), 4866-4881. https://doi.org/10.21595/jve.2017.18529

Richard, T., Germay, C., & Detournay, E. (2004). Self-excited stick–slip oscillations of drill bits. *Comptes Rendus Mécanique*, *332*(8), 619-626. https://doi.org/https://doi.org/10.1016/j.crme.2004.01.016

Richard, T., Germay, C., & Detournay, E. (2007). A simplified model to explore the root cause of stick–slip vibrations in drilling systems with drag bits. *Journal of Sound and Vibration*, *305*(3), 432-456. https://doi.org/10.1016/j.jsv.2007.04.015

Ritto, T. G., Aguiar, R. R., & Hbaieb, S. (2017). Validation of a drill string dynamical model and torsional stability. *Meccanica*, *52*(11-12), 2959-2967. https://doi.org/10.1007/s11012-017-0628-y

Ritto, T. G., & Sampaio, R. (2012). Stochastic drill-string dynamics with uncertainty on the imposed speed and on the bit-rock parameters. *International Journal for Uncertainty Quantification*, *2*(2).

Ritto, T. G., Soize, C., & Sampaio, R. (2009). Non-linear dynamics of a drill-string with uncertain model of the bit–rock interaction. *International Journal of Non-Linear Mechanics*, *44*(8), 865-876. https://doi.org/10.1016/j.ijnonlinmec.2009.06.003

Sampaio, R., Piovan, M. T., & Venero Lozano, G. (2007). Coupled axial/torsional vibrations of drill-strings by means of non-linear model. *Mechanics Research Communications*, *34*(5), 497-502. https://doi.org/https://doi.org/10.1016/j.mechrescom.2007.03.005

Sotomayor, G. P. G., Placido, J. C., & Cunha, J. C. (1997, 1997). Drill String Vibration: How to Identify and Suppress.

Spanos, P. D., Chevallier, A., Politis, N., & Payne, M. (2003). Oil and gas well drilling: a vibrations perspective. *The Shock and Vibration Digest*, *35*(2), 85-103.

Srivastava, S., & Teodoriu, C. (2019). An extensive review of laboratory scaled experimental setups for studying drill string vibrations and the way forward. *Journal of Petroleum Science and Engineering*, *182*, 106272. https://doi.org/https://doi.org/10.1016/j.petrol.2019.106272

Trindade, M. A., & Sampaio, R. (2005). Active control of coupled axial and torsional drill-string vibrations. Proceedings of 18th COBEM International Congress of Mechanical Engineering, Ouro Preto, MG, in CD-ROM,

Tucker, R. W., & Wang, C. (2003). Torsional Vibration Control and Cossert Dynamics of a Drill-Rig Assembly. *Meccanica*, *38*(1), 145-161. https://doi.org/10.1023/a:1022035821763

Westermann, H., Gorelik, I., Rudat, J., Moritz, C., Neubauer, M., Wallaschek, J., & Höhn, O. (2015). A New Test Rig for Experimental Studies of Drillstring Vibrations. *SPE Drilling & Completion*, *30*(02), 119-128. https://doi.org/10.2118/176019-pa

Wiercigroch, M., Nandakumar, K., Pei, L., Kapitaniak, M., & Vaziri, V. (2017). State Dependent Delayed Drill-string Vibration: Theory, Experiments and New Model. *Procedia IUTAM*, *22*, 39-50. https://doi.org/10.1016/j.piutam.2017.08.007

Yigit, A., & Christoforou, A. (1998). Coupled torsional and bending vibrations of drillstrings subject to impact with friction. *Journal of Sound and Vibration*, *215*(1), 167-181.

Yigit, A. S., & Christoforou, A. P. (1994). On the impact of a spherical indenter and an elastic-plastic transversely isotropic half-space. *Composites Engineering*, *4*(11), 1143-1152. https://doi.org/https://doi.org/10.1016/0961-9526(95)91288-R

Yigit, A. S., & Christoforou, A. P. (2000). COUPLED TORSIONAL AND BENDING VIBRATIONS OF ACTIVELY CONTROLLED DRILLSTRINGS. *Journal of Sound and Vibration*, *234*(1), 67-83. https://doi.org/10.1006/jsvi.1999.2854

Yigit, A. S., & Christoforou, A. P. (2006). Stick-Slip and Bit-Bounce Interaction in Oil-Well Drillstrings. *Journal of Energy Resources Technology*, *128*(4), 268-274. https://doi.org/10.1115/1.2358141

Zhu, X., & Liu, W. (2013). The effects of drill string impacts on wellbore stability. *Journal of Petroleum Science and Engineering*, *109*, 217-229. https://doi.org/10.1016/j.petrol.2013.08.004

APPENDIX A. DRILLSTRING TIME DOMAIN ANALYSIS

Rigid Vs Torsional Compliance:

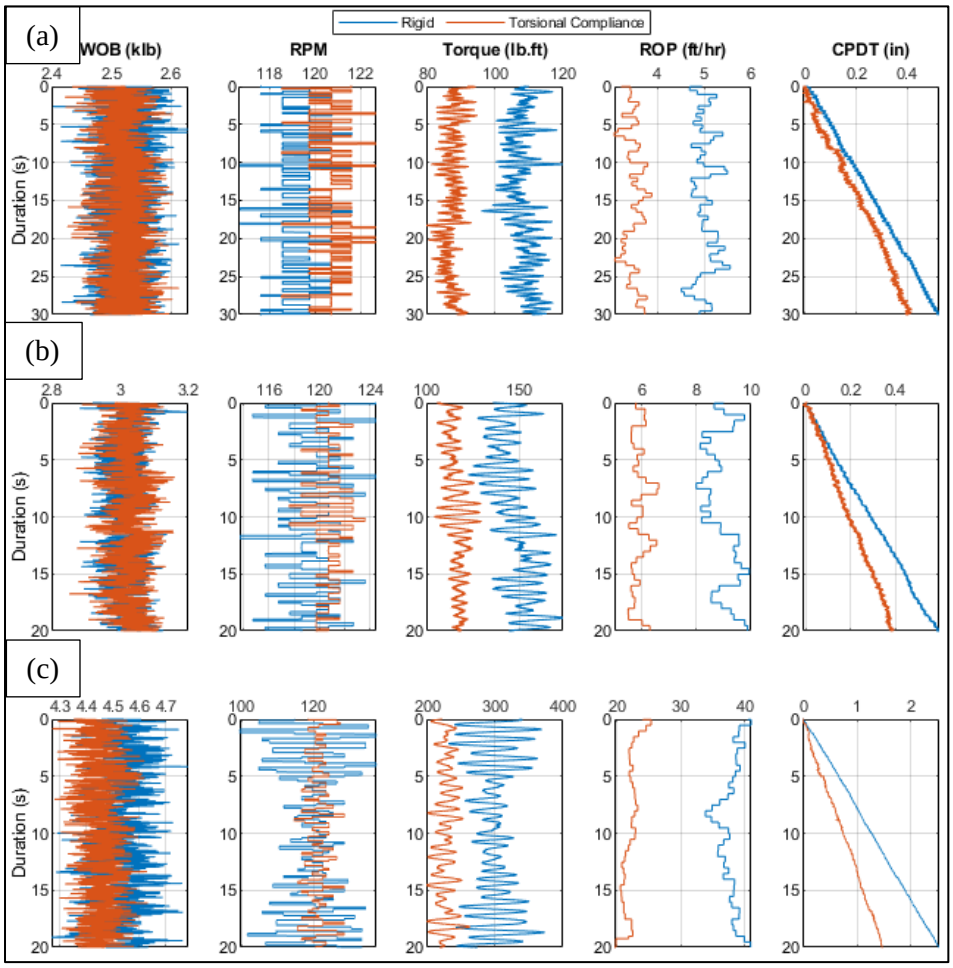

Figure A.1. Rigid Vs TC Dynamics for 4-Bladed PDC Bit at 120 RPM (a) W1, (b) W2, and (c) W3

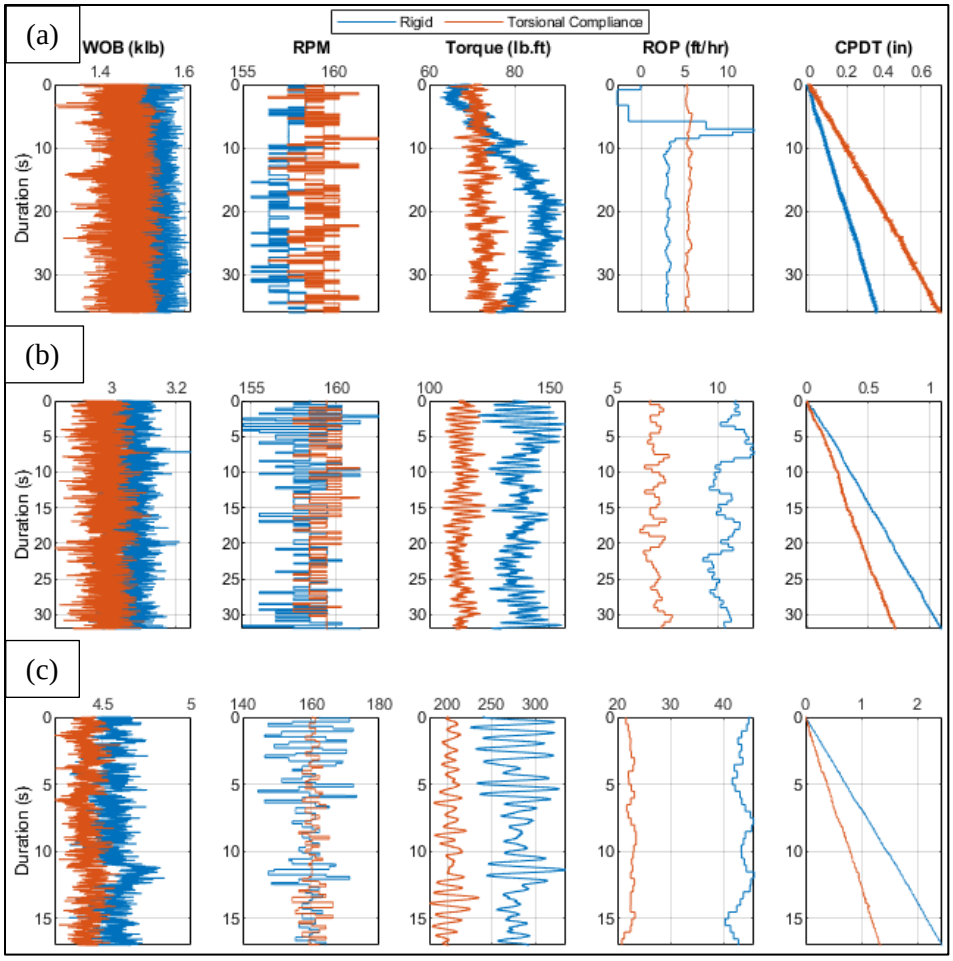

Figure A.2. Rigid Vs TC Dynamics for 4-Bladed PDC Bit at 160 RPM (a) W1, (b) W2, and (c) W3

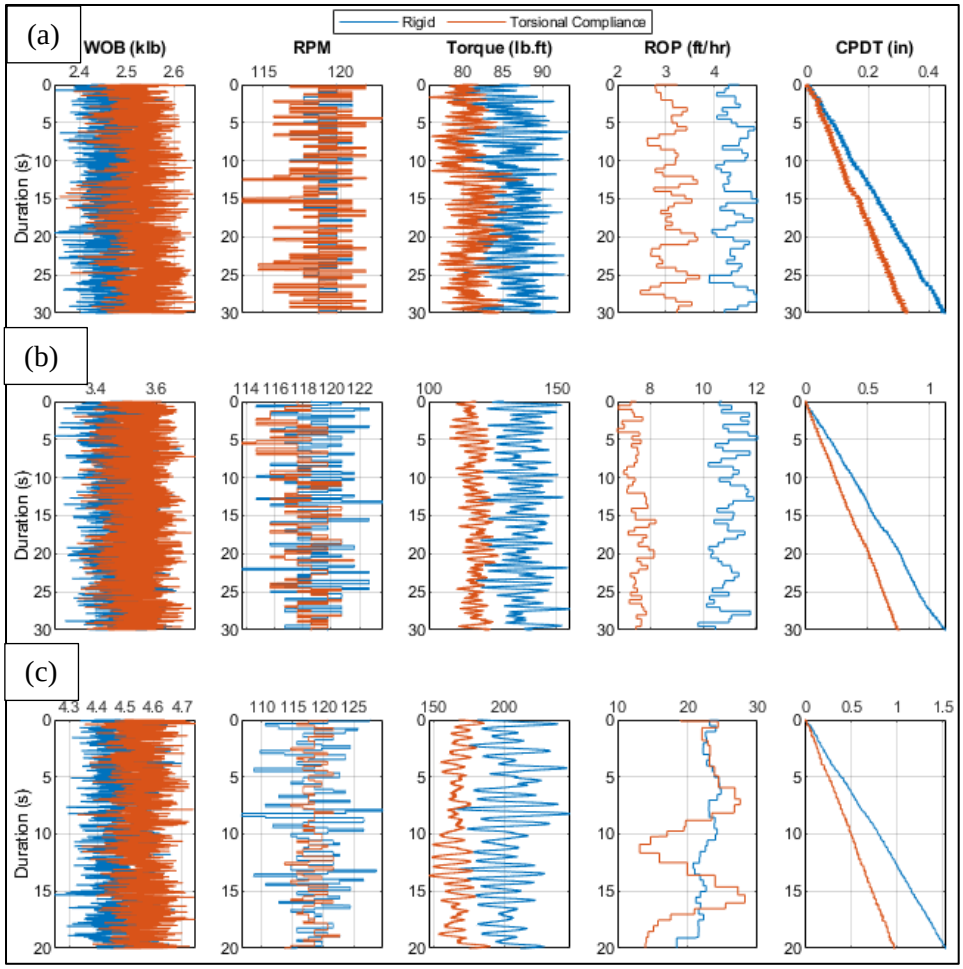

Figure A.3. Rigid Vs TC Dynamics for 5-Bladed PDC Bit at 120 RPM (a) W1, (b) W2, and (c) W3

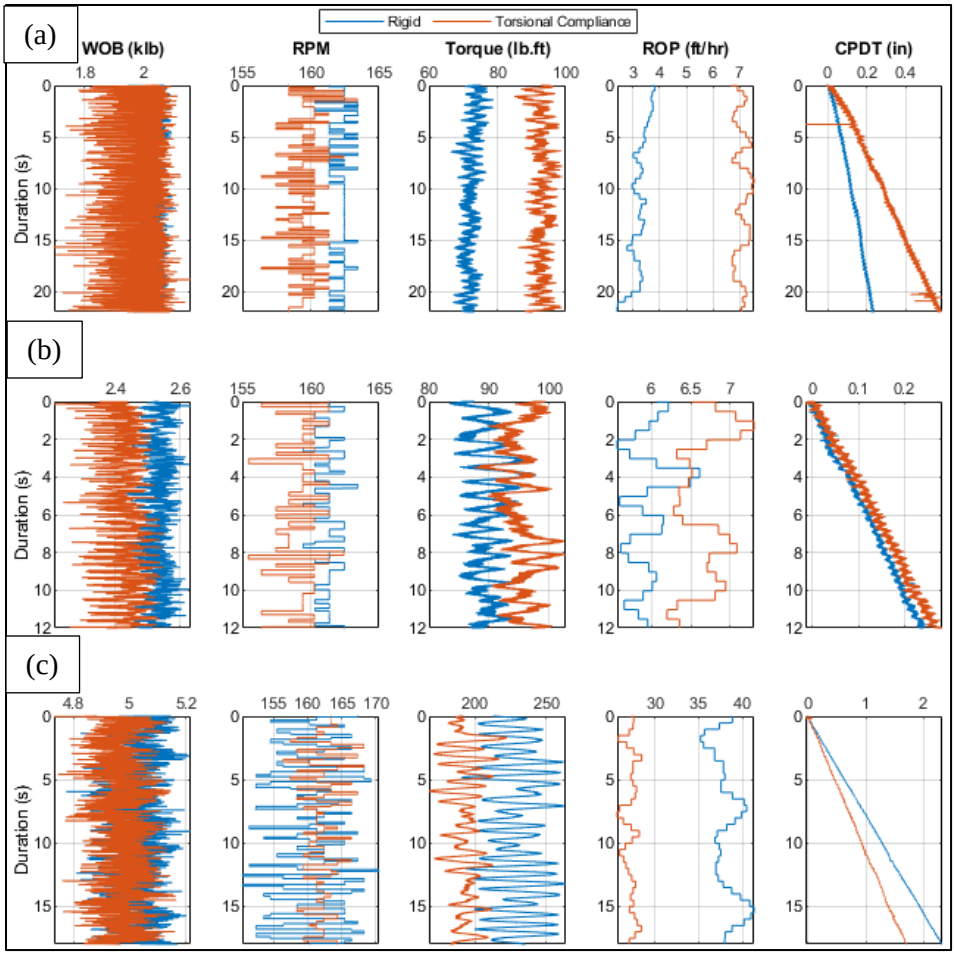

Figure A.4. Rigid Vs TC Dynamics for 5-Bladed PDC Bit at 160 RPM (a) W1, (b) W2, and (c) W3

Rigid Vs Flywheel

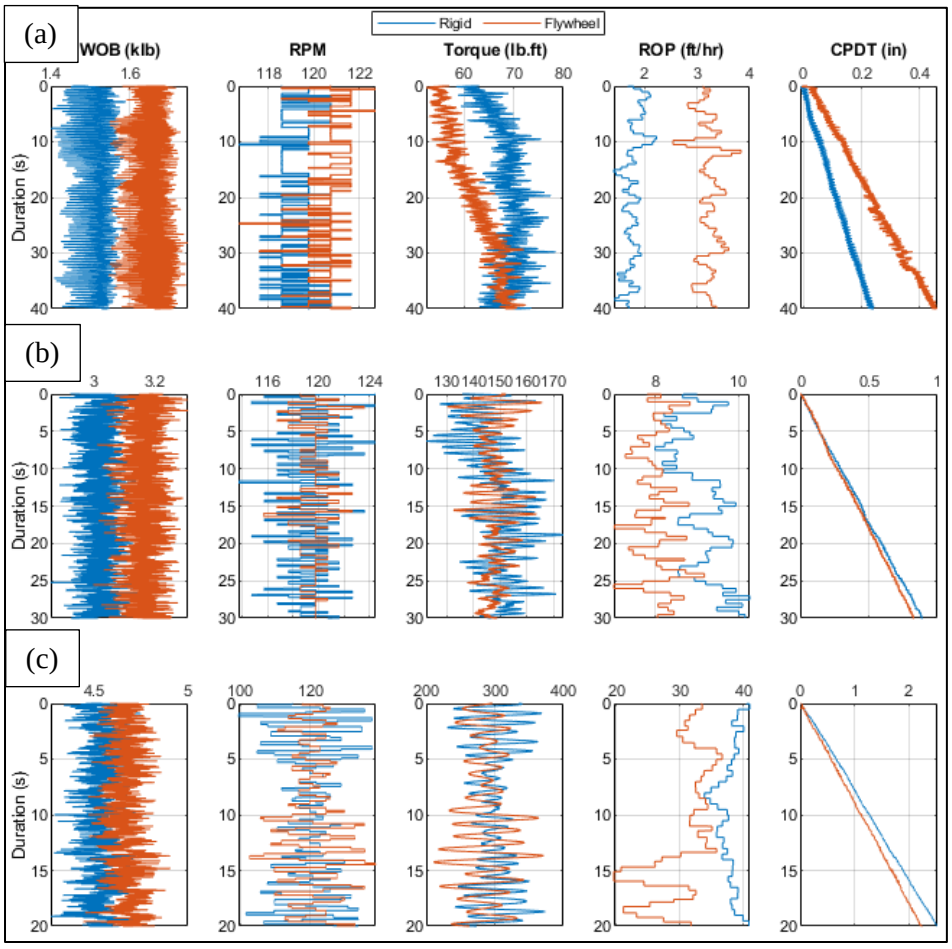

Figure A.5. Rigid Vs FW Dynamics for 4-Bladed PDC Bit at 120 RPM (a) W1, (b) W2, and (c) W3

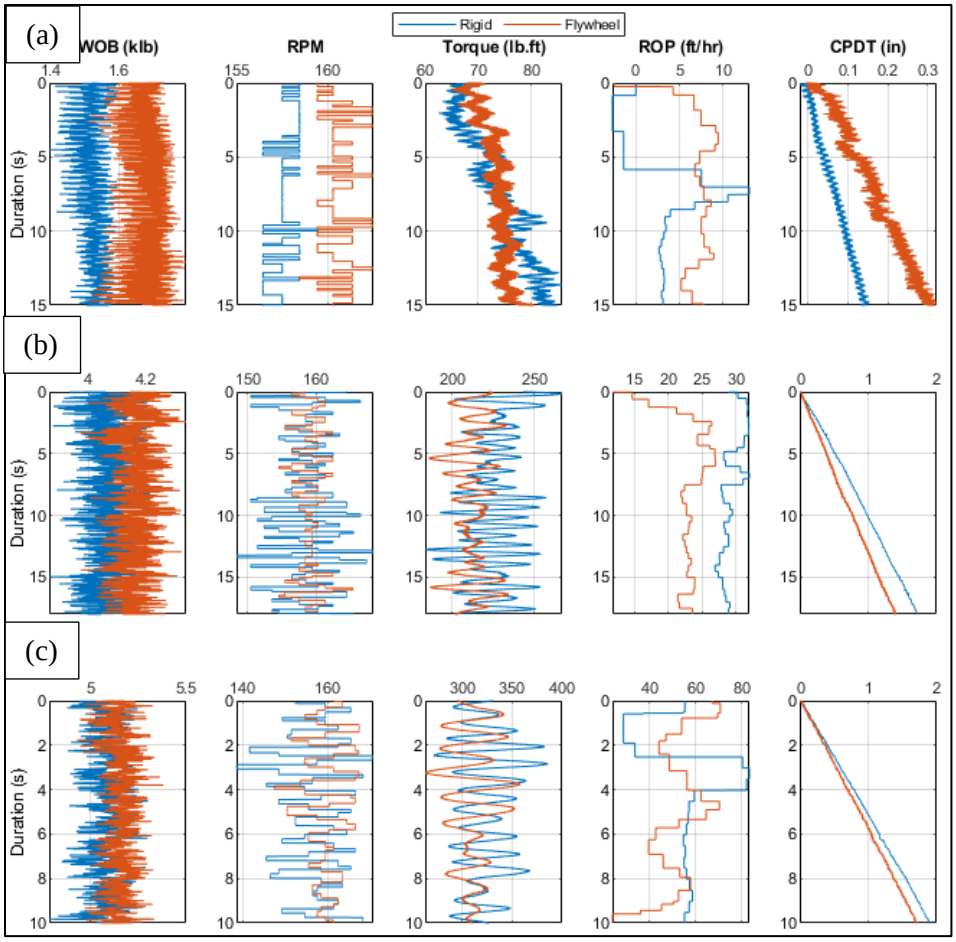

Figure A.6. Rigid Vs FW Dynamics for 4-Bladed PDC Bit at 160 RPM (a) W1, (b) W2, and (c) W3

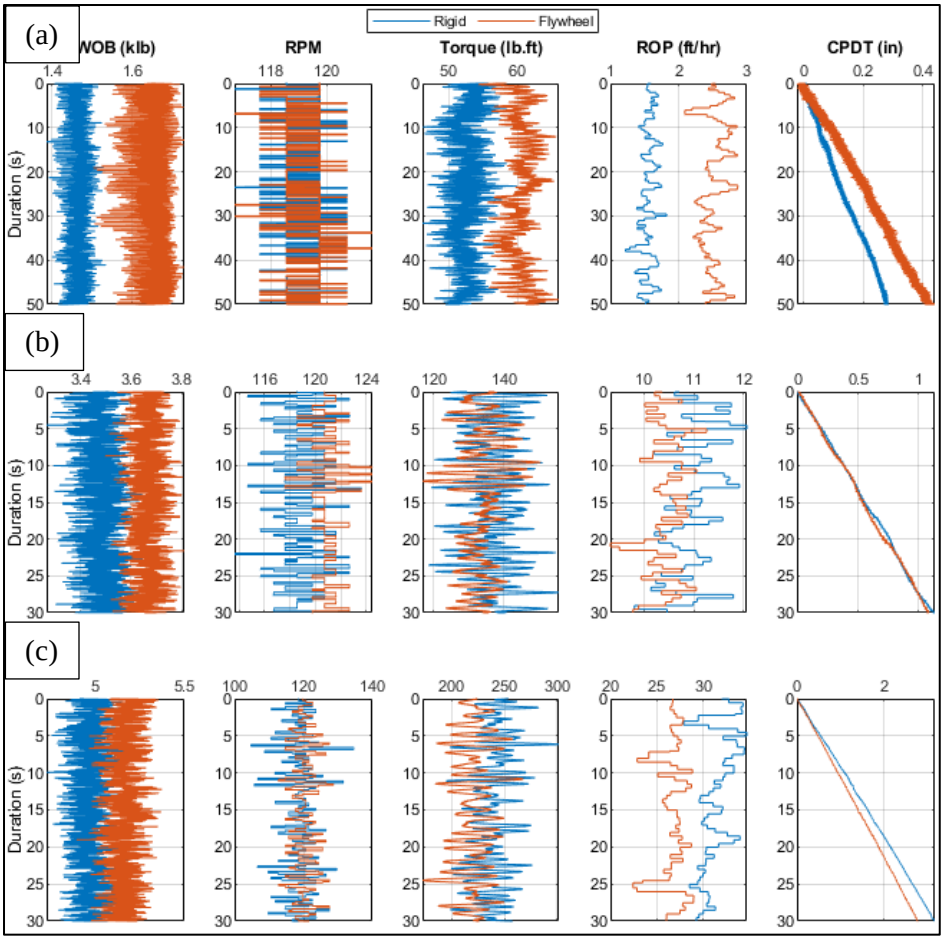

Figure A.7. Rigid Vs FW Dynamics for 5-Bladed PDC Bit at 120 RPM (a) W1, (b) W2, and (c) W3

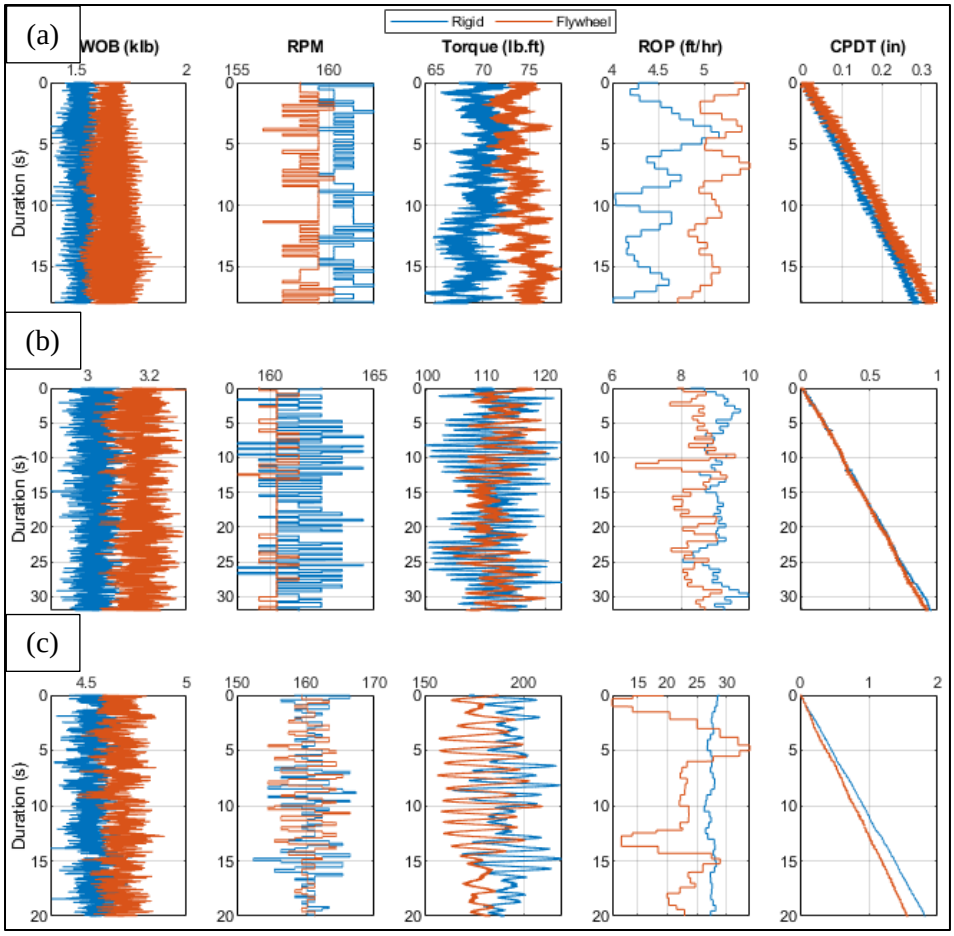

Figure A.8. Rigid Vs FW Dynamics for 5-Bladed PDC Bit at 160 RPM (a) W1, (b) W2, and (c) W3

Rigid Vs Axial Compliance

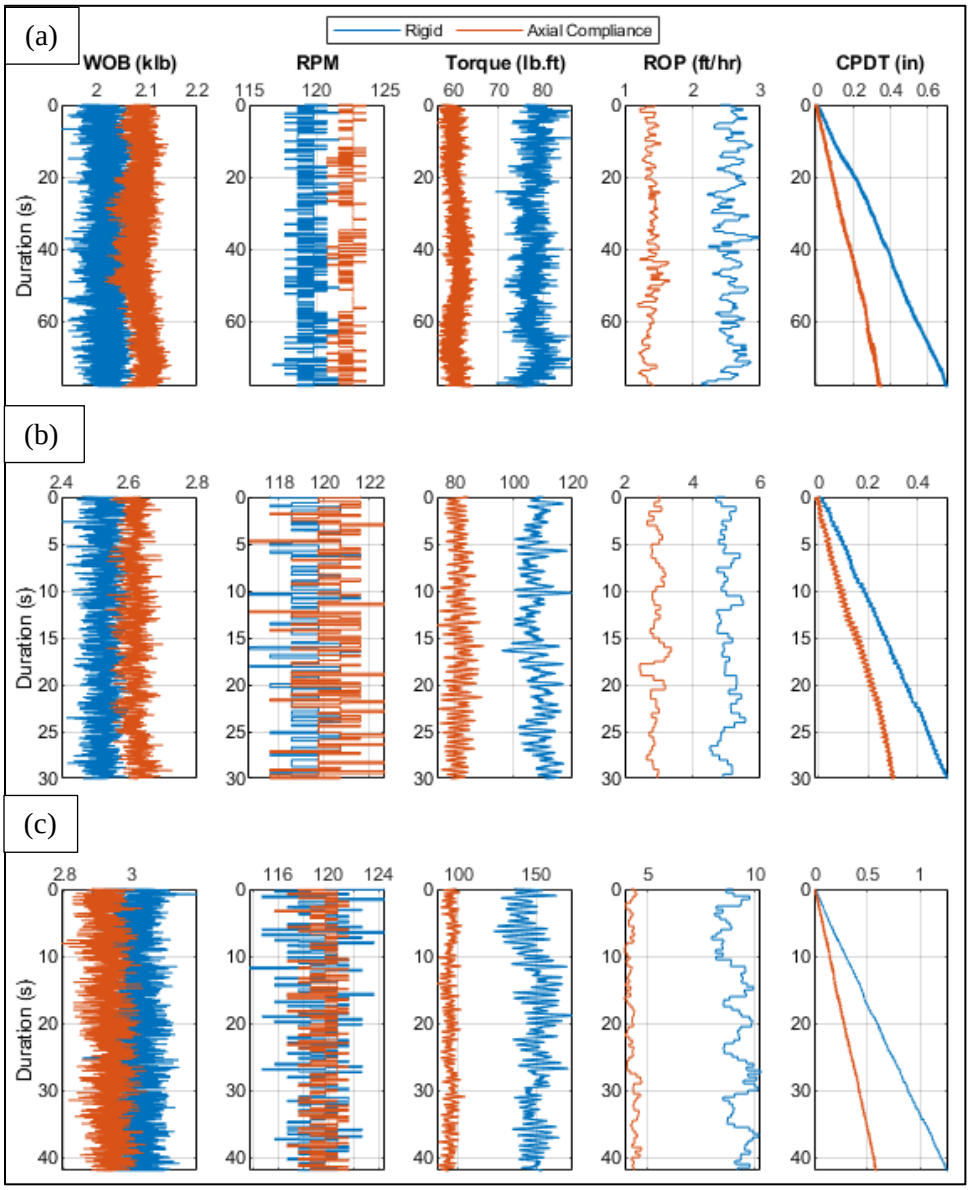

Figure A.9. Rigid Vs AC Dynamics for 4-Bladed PDC Bit at 120 RPM (a) W1, (b) W2, and (c) W3

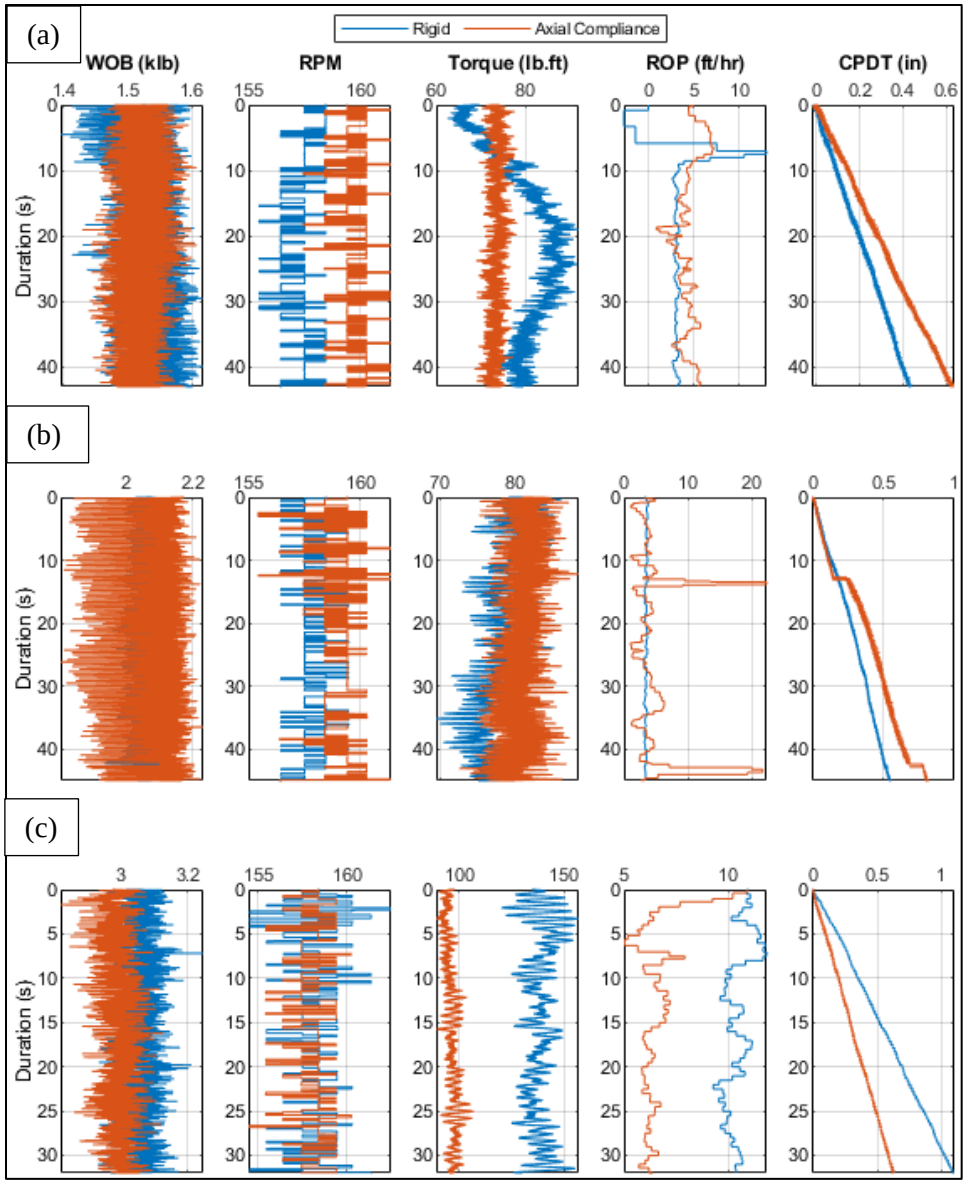

Figure A.10. Rigid Vs AC Dynamics for 4-Bladed PDC Bit at 160 RPM (a) W1, (b) W2, and (c) W3

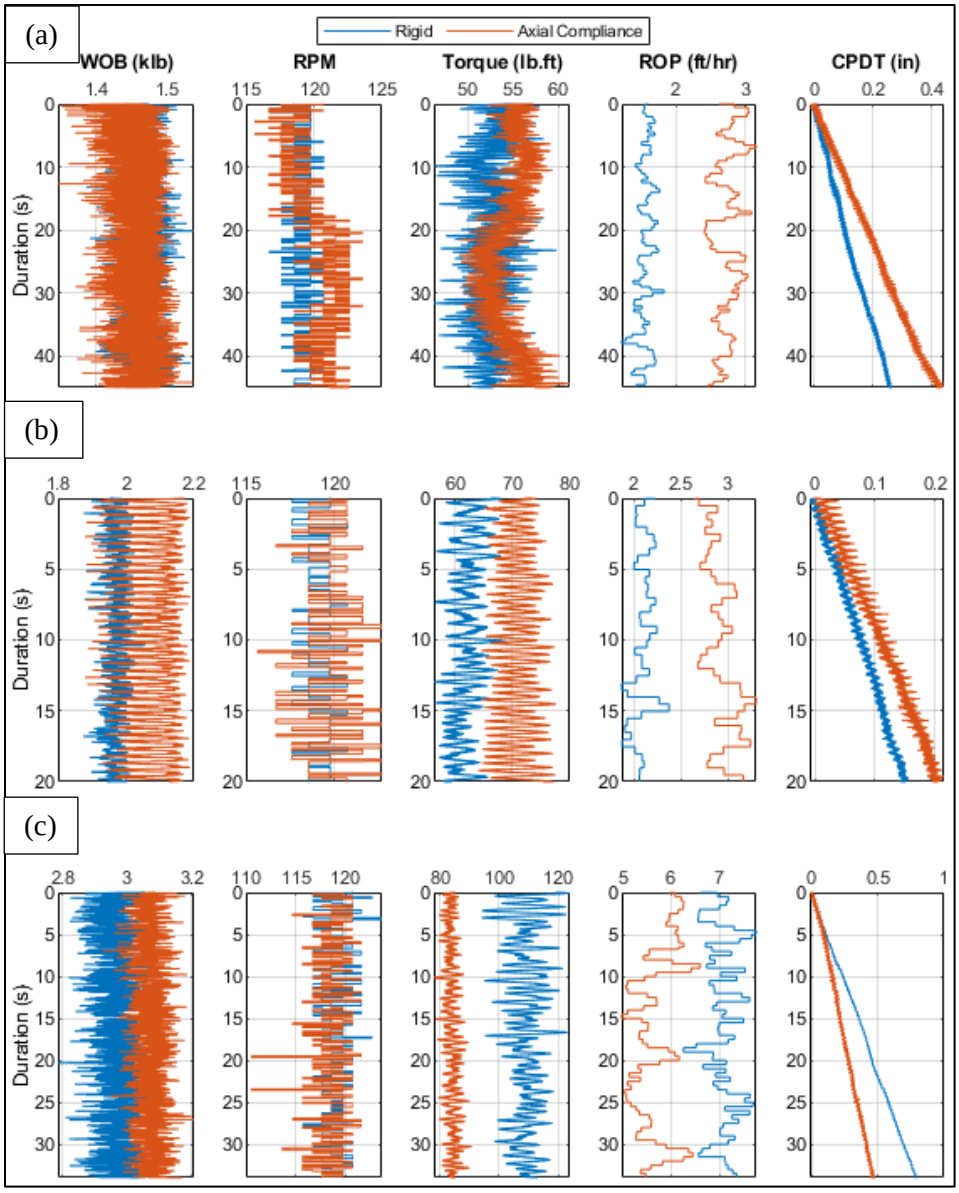

Figure A.11. Rigid Vs AC Dynamics for 5-Bladed PDC Bit at 120 RPM (a) W1, (b) W2, and (c) W3

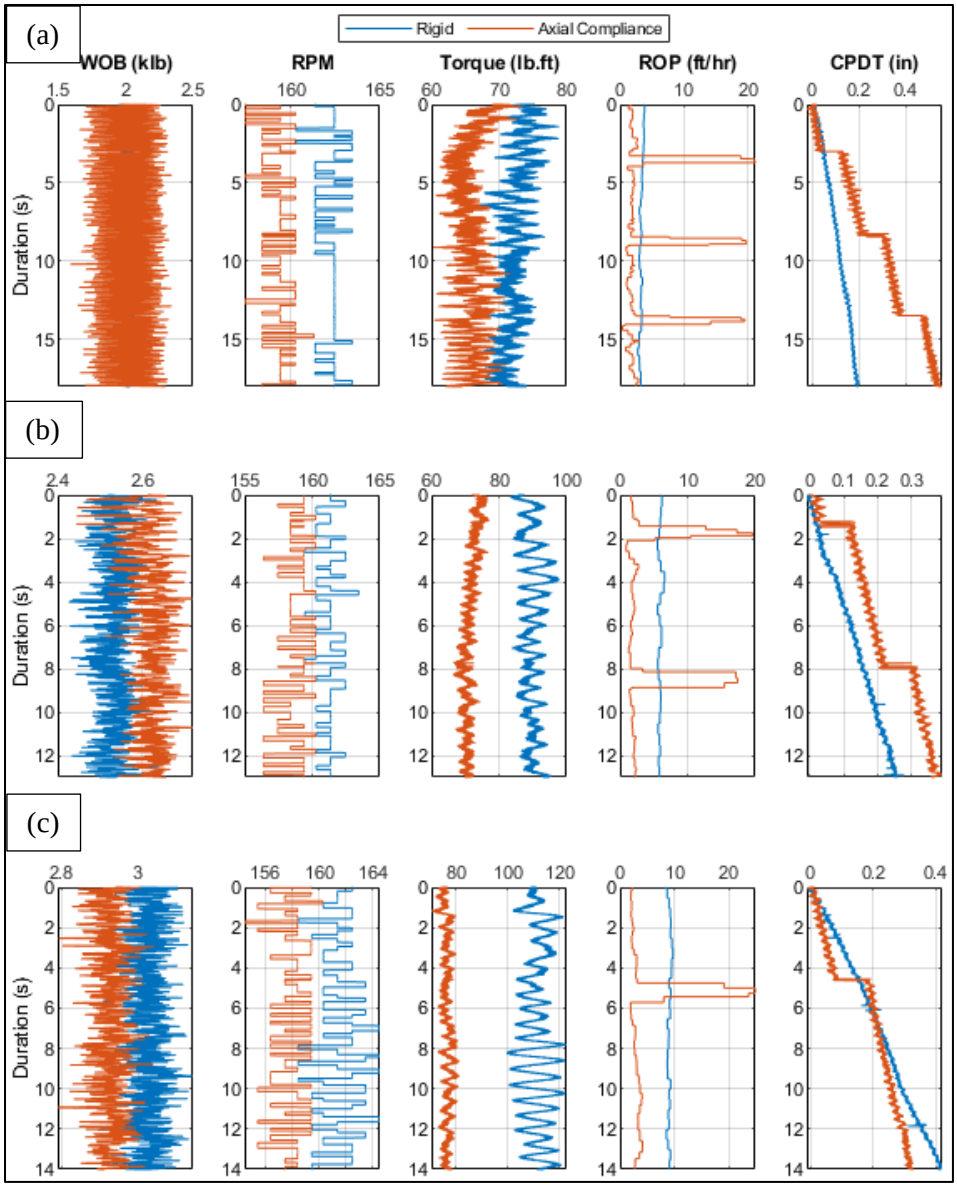

Figure A.12. Rigid Vs AC Dynamics for 5-Bladed PDC Bit at 160 RPM (a) W1, (b) W2, and (c) W3

Rigid Vs Combined Axial and Torsional Compliance

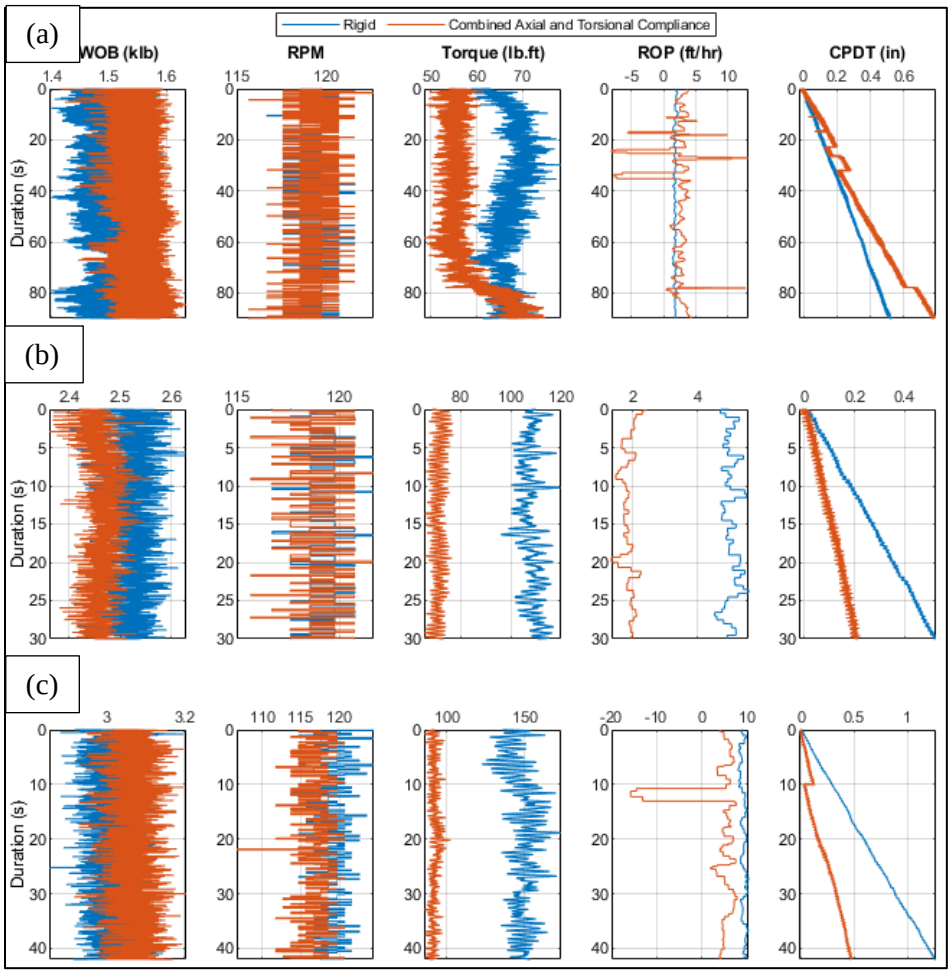

Figure A.13. Rigid Vs CAT Dynamics for 4-Bladed PDC Bit at 120 RPM (a) W1, (b) W2, and (c) W3

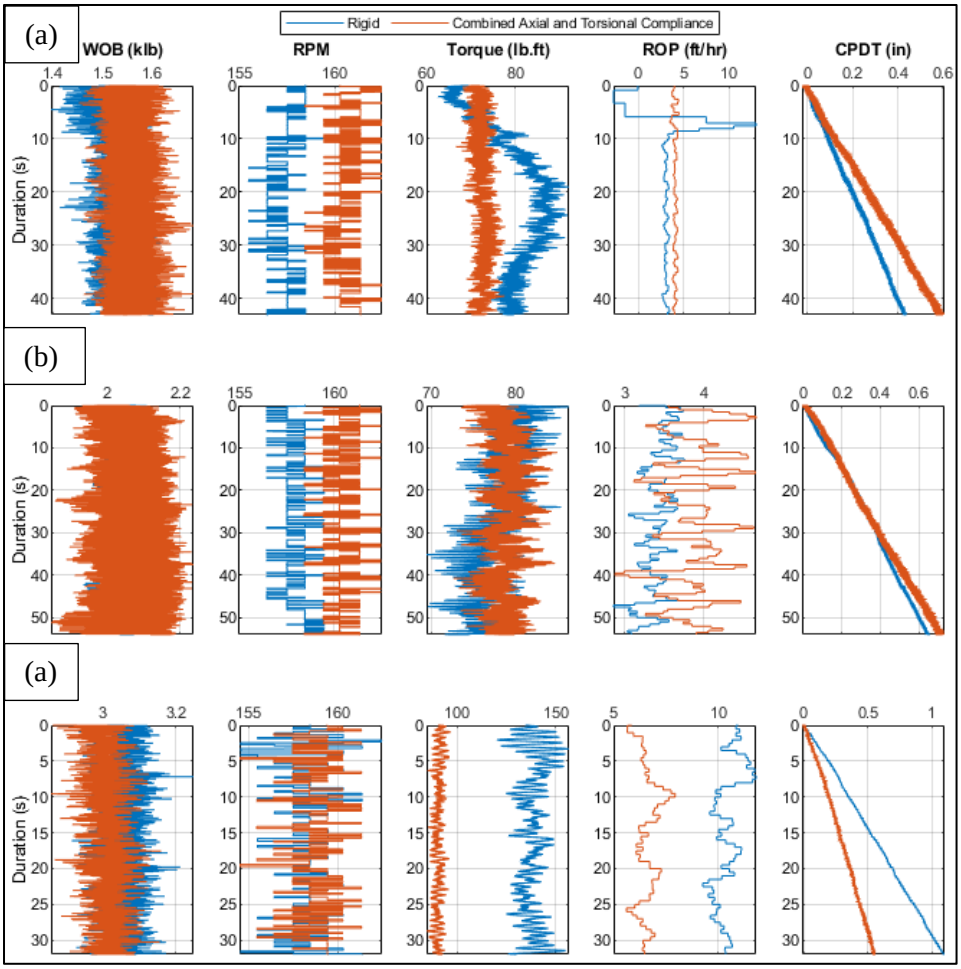

Figure A.14. Rigid Vs CAT Dynamics for 4-Bladed PDC Bit at 160 RPM (a) W1, (b) W2, and (c) W3

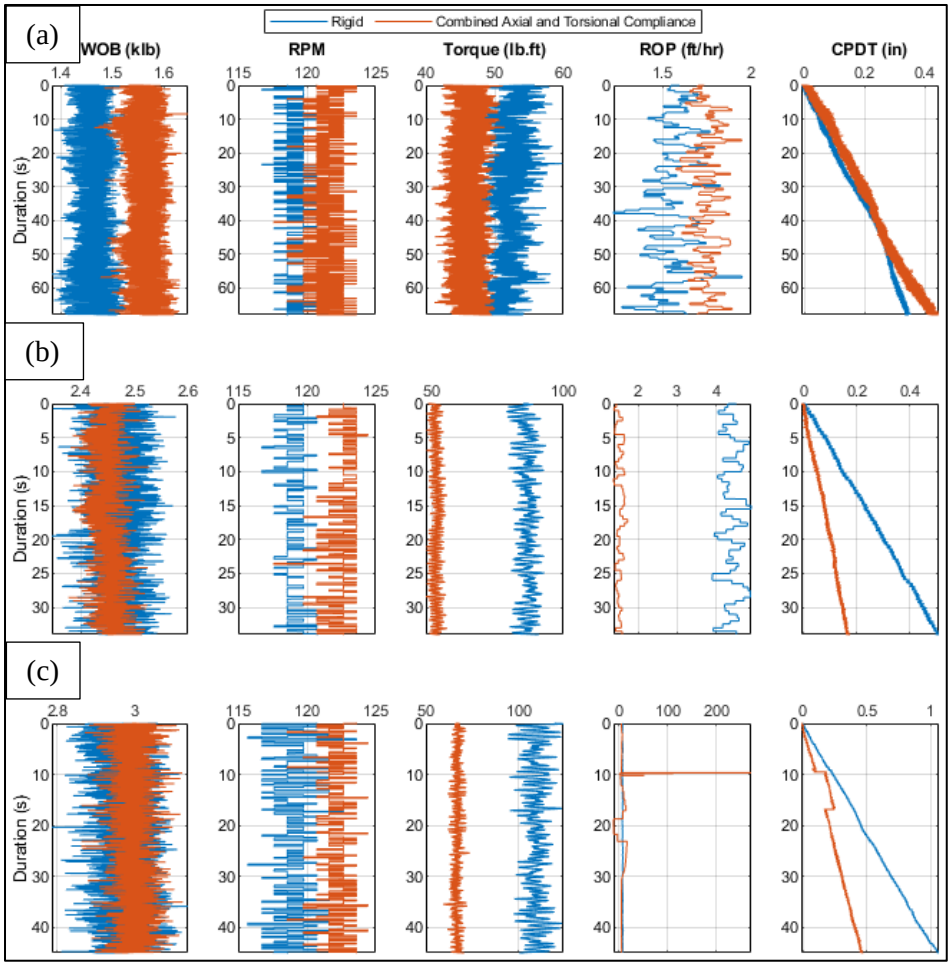

Figure A.15. Rigid Vs CAT Dynamics for 5-Bladed PDC Bit at 120 RPM (a) W1, (b) W2, and (c) W3

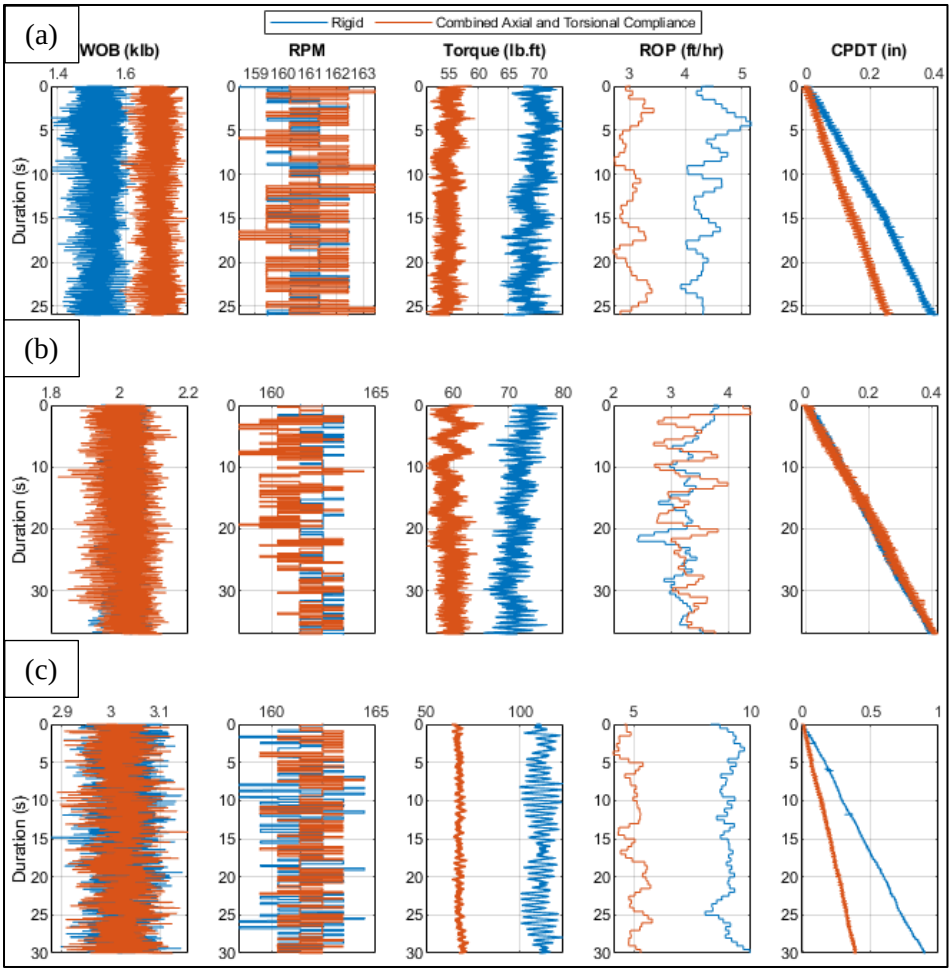

Figure A.16. Rigid Vs CAT Dynamics for 5-Bladed PDC Bit at 160 RPM (a) W1, (b) W2, and (c) W3

VITA

Mohammad Faraz Mubarak Hussain Khan

Candidate for the Degree of

Master of Science

Thesis: VIBRATIONAL ANALYSIS OF PDC BITS IN A LABORATORY COMPLIANT DRILLSTRING

Major Field: Petroleum Engineering

Biographical:

Education:

Completed the requirements for the Master of Science in Petroleum Engineering at Oklahoma State University, Stillwater, Oklahoma in December 2022.

Completed the requirements for the Bachelor of Science in Mechanical Engineering at Oklahoma State University, Stillwater, Oklahoma in December 2020.

Experience: 4 months Undergraduate Research Assistant at Oklahoma State University
1 month Petroleum Engineering Trainee at MB Petroleum Services
2 years Graduate Research Assistant at Oklahoma State University

Professional Memberships: Society of Petroleum Engineers
American Association of Drilling Engineers
Phi Kappa Phi Honor Society